On the spatial and temporal variability of upwelling in the southern Caribbean Sea and its influence on the ecology of phytoplankton and of the Spanish sardine (Sardinella aurita)

Digna Tibisay Rueda-Roa
University of South Florida, dignarueda@gmail.com

On the spatial and temporal variability of upwelling in the southern Caribbean Sea and its

influence on the ecology of phytoplankton and of the Spanish sardine (*Sardinella aurita*)

by

Digna T. Rueda-Roa

A dissertation submitted in partial fulfillment
of the requirements for the degree of
Doctor of Philosophy
College of Marine Science
University of South Florida

Major Professor: Frank E. Muller-Karger, Ph.D.
Mark Luther, Ph.D.
Ernst Peebles, Ph.D.
David Hollander, Ph.D.
Eduardo Klein, Ph.D.
Jeremy Mendoza, Ph.D.

Date of Approval:
June 18, 2012

Keywords: Ekman Transport, Ekman Pumping, hydroacoustics, CARIACO ocean time
series, Subtropical Underwater

DEDICATION

Dedicated to the health of the oceans! With the deep belief that the better we know the oceans, the better we can take care of them

I am very touched for the continued and unconditional support that my family has provided throughout my career. I am also deeply indebted for the continuous help and support of my extended family at the Institute for Marine Remote Sensing, especially to Frank Muller-Karger, Laura Lorenzoni, Inia Soto and Enrique Montes with whom I have shared a significant part of my career and personal life since I started my studies and research at USF. To all those especial people in my life I also dedicate this work.

.

ACKNOWLEDGEMENTS

TABLE OF CONTENTS

LIST OF TABLES

LIST OF FIGURES

GENERAL ABSTRACT

The Southern Caribbean Sea experiences a strong upwelling process along the coast from about 61°W to 75.5°W and 10-13°N. In this dissertation three aspects of this upwelling system are examined: (A) A mid-year secondary upwelling that was previously observed in the southeastern Caribbean Sea between June-July, when land based stations show a decrease in wind speed. The presence and effects of this upwelling along the whole southern Caribbean upwelling system were evaluated, as well as the relative forcing contribution of alongshore winds (Ekman Transport, ET) and wind-curl (Ekman Pumping, EP). (B) Stronger upwelling occurs in two particular regions, namely the eastern (63-65°W) and western (70-73°W) upwelling areas. However, the eastern area has higher fish biomass than the western area (78% and 18%, respectively, of the total small pelagic biomass of the southern Caribbean upwelling system). The upwelling dynamics along the southern Caribbean margin was studied to understand those regional variations on fish biomass. (C) The most important fishery in the eastern upwelling area off Venezuela is the Spanish sardine (*Sardinella aurita*). The sardine artisanal fishery is protected and only takes place up to ~10 km offshore. The effects of the upwelling cycle on the spatial distribution of *S. aurita* were studied. The main sources of data were satellite observations of sea surface temperature (SST), chlorophyll-*a* (Chl) and wind (ET and EP), *in situ* observations from the CARIACO Ocean Time-Series program, sardine

biomass from 8 hydroacoustics surveys (1995-1998), and temperature profiles from the World Ocean Atlas 2005 used to calculate the depth of the Subtropical Underwater core (traced by the 22°C isotherm). The most important results of the study were as follows:

(A) The entire upwelling system has a mid-year upwelling event between June-August, besides the primary upwelling process of December-April. This secondary event is short-lived (~5 weeks) and ~1.5°C warmer than the primary upwelling. Together, both upwelling events lead to about 8 months of cooler waters (<26°C) and 8-9.5 months of high Chl ($\geq$0.35 mg m^{-3}, averaged from the coast to 100 km offshore) in the region. Satellite nearshore wind (~25 km offshore) remained high in the eastern upwelling area (> 6 m s^{-1}) and had a maximum in the western area (~10 m s^{-1}) producing high offshore ET during the mid-year upwelling (vertical transport of 2.4 - 3.8 m^3 s^{-1} per meter of coastline, for the eastern and western areas, respectively). Total coastal upwelling transport was mainly caused by ET (~90%). However, at a regional scale, there was intensification of the wind curl during June as well; as a result open-sea upwelling due to EP causes isopycnal shoaling of deeper waters enhancing the coastal upwelling.

(B) The eastern and western upwelling areas had upwelling favorable winds all year round. Minimum / maximum offshore ET (from weekly climatologies) were 1.52 /d 4.36 m^3 s^{-1} per meter, for the western upwelling area; and 1.23 / 2.63 m^3 s^{-1} per meter, for the eastern area. The eastern and western upwelling areas showed important variations in their upwelling dynamics. Annual averages in the eastern area showed moderate wind speeds (6.12 m s^{-1}), shallow 22ºC isotherm (85 m), cool SSTs (25.24°C), and phytoplankton biomass of 1.65 mg m^{-3}. The western area has on average stronger wind speeds (8.23 m s^{-1}) but a deeper 22ºC isotherm (115 m), leading to slightly warmer SSTs

(25.53°C) and slightly lower phytoplankton biomass (1.15 mg m^{-3}). We hypothesize that the factors that most inhibits fish production in the western upwelling area are the high level of wind-induced turbulence and the strong offshore ET.

(C) Hydroacoustics values of *Sardinella aurita* biomass (sAsardine) and the number of small pelagics schools collected in the eastern upwelling region off northeast Venezuela were compared with environmental variables (satellite products of SST, SST gradients, and Chl –for the last two cruises-) and spatial variables (distance to upwelling foci and longitude-latitude). These data were examined using Generalized Additive Models. During the strongest upwelling season (February-March) sAsardine was widely distributed in the cooler, Chl rich upwelling plumes over the wide (~70km) continental shelf. During the weakest upwelling season (September-October) sAsardine was collocated with the higher Chl (1-3 mg m^{-3}) found within the first 10 km from the upwelling foci; this increases Spanish sardine availability (and possibly the catchability) for the artisanal fishery. These results imply that during prolonged periods of weak upwelling the environmentally stressed (due to food scarceness) Spanish sardine population would be closer to the coast and more available to the fishery, which could easily turn into overfishing. After two consecutive years of weak upwelling (2004-2005) Spanish sardine fishery crashed and as of 2011 has not recovered to previous yield; however during 2004 a historical capture peak occurred. We hypothesize that this Spanish sardine collapse was caused by a combination of sustained stressful environmental conditions and of overfishing, due to the increased catchability of the stock caused by aggregation of the fish in the cooler coastal upwelling cells during the anomalous warm upwelling season.

PREAMBLE

The Southern Caribbean Sea experiences a strong upwelling process along the coast from about 61°W to 75.5°W, 10-13°N, area that is called hereafter the 'southern Caribbean upwelling system'. This process had been characterized historically as following a simple seasonal cycle, with strong upwelling occurring between about December and April every year caused by the seasonal strengthening of the alongshore Trade Winds (Richards 1960, Herrera and Febres-Ortega 1975, Muller-Karger and Aparicio 1994, Muller-Karger *et al.* 2004). This upwelling process maintains a highly productive ecosystem in the region (e.g. Stromme and Saetersdal 1989). A preliminary study based on data from the CARIACO Ocean Time-Series program revealed substantial temporal variation in the upwelling observed in the southeastern Caribbean Sea. This led to a dissertation to study the spatial extent and the temporal variability of the upwelling dynamic along the entire southern Caribbean upwelling system. Satellite imagery was extensively used in this research because of its synoptic coverage and high temporal resolution. Satellite sea surface temperature was used as a proxy for upwelling, satellite chlorophyll-*a* was used as a proxy for phytoplankton biomass, and satellite marine wind products were used to calculate upwelling due to wind forcing. The research focused in three main topics, outlined below.

1

Mid-year upwelling:

During a preliminary study using 1996-1998 data from the CARIACO Ocean Time-Series (10.5°N, 64.67°W, http://www.imars.usf.edu/CAR/), a short, weak secondary upwelling pulse was found during June-August (Rueda-Roa 2000). Although previous hydrographic data had indications of this upwelling pulse, the observations were too short to provide evidence that this mid-year upwelling was part of the normal upwelling cycle of the southeastern Caribbean Sea. Wind data from coastal meteorological stations showed a decrease in the wind at the time of this secondary upwelling (Rueda-Roa 2000, Astor *et al.* 2003).

The upwelling phenomenon along the southern Caribbean Sea is a complex process that depends on a number of factors including the geostrophic adjustment of the Caribbean Current, the distance of the Caribbean Current to the continent, stratification of the water column, bathymetry, and the local and regional wind patterns. In this work we focus on the effect of changes in local and regional wind forcing to assess the contribution of Ekman transport and Ekman Pumping on the seasonality of the upwelling process, especially during the mid-year upwelling. The following objectives were proposed: (a) Establish whether the mid-year upwelling is part of the seasonal upwelling cycle of the southern Caribbean Sea; (b) characterize the mid-year upwelling and its effect on phytoplankton biomass; and (c) assess the relative contribution of local and regional along-shore winds and wind curl in forcing the upwelling process. The results of this study are presented in the first chapter of this dissertation.

Contrasting the eastern and western upwelling areas:

The results obtained in the study of the secondary upwelling showed that there are differences in the dynamics of upwelling in different parts of the southern Caribbean Sea. The two areas that experience the strongest SST fluctuations are also important fishery grounds: an eastern upwelling area located between 63°W and 65°W, and a western upwelling area between 70°W and 73°W. Acoustic fisheries surveys conducted in the southern Caribbean Sea between 61°W and 74.5°W estimated a total biomass of small pelagics of 1,580,000 tonnes (Stromme and Saetersdal 1989). More than 95% of that biomass was concentrated in the eastern and western upwelling areas (78% and 18% respectively). Due to the importance of upwelling to regional fisheries, the goal of this chapter was to study the differences in upwelling dynamics of the upwelling foci along the southern Caribbean Sea margin, with emphasis in the eastern and western upwelling areas. The results of this study are presented in the second chapter.

Upwelling cycle influence on the Spanish sardine spatial distribution

The Spanish sardine, *Sardinella aurita* (also called round sardinella), is one of the most important fish resources in the eastern upwelling area. Spanish sardine catch in this area of Venezuela represents nearly 90% of the total small pelagic fish catch for the Caribbean Sea (FAO-FIGIS, 1980-2011). Fishing activities only take place within ~10 km of the shore owing to the artisanal nature of this fishery, which is protected by Venezuelan law (Freón and Mendoza 2003, González *et al.* 2005, INAPESCA 2001). Following two consecutive years of weak upwelling (2004-2005) the Venezuelan Spanish sardine fishery crashed and, even as of June 2011, has not recovered to previous yields.

The economic and social problems that have arisen from the collapse of the Spanish sardine fishery in this area made clear the need for better fishery management strategies for this resource. For instance, what may be a reasonable level of exploitation during years with good recruitment may produce overfishing during years of unfavorable environmental conditions. The great economic and social importance of Spanish sardine fishery led to a joint study with Venezuelan fisheries experts to determine how the spatial distribution of Spanish sardine biomass is related to the upwelling annual cycle. A major goal was to clarify if Spanish sardine catchability is influenced by the upwelling cycle. The results of this study are presented in the third chapter.

Chapter four is a summary of the major findings of this dissertation, linking the observations and conclusions presented in the first three chapters.

Scientific manuscripts

The central part of this dissertation is formed by three multi-authored scientific papers that are going to be submitted for publication, in a slightly modified form, in international, peer-reviewed journals in the immediate future.

Chapter 1: Contribution of Ekman transport and pumping on the mid-year Southern Caribbean upwelling and on phytoplankton biomass, by D. Rueda-Roa, F. Muller-Karger and T. Ezer.

Chapter 2: Southern Caribbean Upwelling System: characterization of sea surface temperature, Ekman forcing and chlorophyll concentration, by D. Rueda-Roa and F. Muller-Karger.

Chapter 3: Spatial variability of Spanish sardine (*Sardinella aurita*) abundance related to the upwelling cycle in the southeastern Caribbean Sea, by D. Rueda-Roa, J. Mendoza and F. Muller-Karger.

D. Rueda-Roa and F. Muller-Karger are both affiliated with the University of South Florida, College of Marine Science, Institute of Marine Remote Sensing. T. Ezer is affiliated with the Old Dominion University, College of Science, Department of Ocean, Earth and Atmospheric Sciences. J. Mendoza is affiliated with the Universidad de Oriente, Instituto Oceanográfico de Venezuela, Department of Fisheries.

CHAPTER ONE

Contribution of Ekman transport and pumping on the mid-year southern Caribbean Sea upwelling and on phytoplankton biomass

1.1 Abstract

The Southern Caribbean Sea experiences a well-known seasonal cycle of strong coastal upwelling during December-April. Data from the CARIACO Ocean Time-Series, established in 1995 off northeastern Venezuela (10.50ºN, 64.66ºW), have revealed a secondary upwelling pulse in June-July, when wind speed over the area is decreasing. This study examined this secondary upwelling pulse and its effects on phytoplankton biomass, and evaluated the relative contribution of alongshore winds (Ekman Transport, ET) and wind-curl (Ekman Pumping, EP) in forcing this phenomenon. Historical sea level data dating back to 1948, and satellite-derived Sea Surface Temperature (SST from the AVHRR; 1994-2009) observations revealed that the mid-year upwelling is a normal feature of the annual upwelling cycle and that it occurs along the entire Southern Caribbean Sea (from 61 to 75.5°W). This mid-year upwelling is short-lived (~5 weeks) and ~1.5°C warmer than the primary upwelling; both processes combined lead to about 8 months of cooler waters (< 26°C) at the surface along this continental margin. Stronger upwelling occurs in two particular regions, the eastern (63-65°W) and western (70-73°W) upwelling areas. Chlorophyll-a concentrations observed by satellite (SeaWiFS) were

6

averaged from the coast to 100 km offshore (Chl_100km) and were compared with the values in the central Caribbean Sea (seasonal maximum 0.29 mg m^{-3}). High Chl_100km ($\geq$ 0.35 mg m^{-3}) were present during 8-9.5 months in the western and eastern upwelling areas, respectively. During June, when the Trade Winds in the south-eastern Caribbean Sea coast decreased, nearshore satellite wind data from QuikSCAT (~25 km offshore) remained high in the east region (> 6 m s^{-1}) and showed an intensification to the west (peak ~ 10 m s^{-1}). This strengthening produced high offshore ET during the mid-year upwelling (vertical transport of 2.4 - 3.8 m^3 s^{-1} per meter of coastline, for the east and west region, respectively). In the coastal area total coastal upwelling transport was mainly caused by ET (~90%); however, at a regional scale, the wind curl intensifies during June. Over the Caribbean Sea the wind curl exhibits a year-round pattern of positive/negative EP in the south/north Caribbean Sea that induces open-sea upwelling/downwelling. This pattern is intensified during June. As a result, EP enhances the coastal upwelling phenomenon by isopycnal shoaling on the waters feeding the mid-year coastal upwelling, which is in turn forced by the larger-scale traditional wind-driven Trade Wind blowing along the coast. Chl_100km and SST showed higher correlations with EP than with ET indicating the importance of this wind curl effect in the upwelling process of the southern Caribbean Sea.

1.2 Introduction

The continental margin of much of the southern Caribbean Sea, from Trinidad to Colombia (i.e. about 61-75.5°W, Figure 1.1), experiences pronounced seasonal upwelling from December to April caused by Ekman Transport (ET) driven by the Trade Winds

(Richards 1960, Herrera and Febres-Ortega 1975, Muller-Karger and Aparicio 1994, Muller-Karger *et al.* 2004). Off northeastern Venezuela, the CARIACO Ocean Time-Series program (10.50ºN, 64.66ºW; Figure 1.1) has studied decadal-scale variability in upwelling intensity and the impact of this process on productivity, nutrient cycling, and the sedimentation of particles to the bottom of the Cariaco Basin. CARIACO was established in November 1995, and has generated a time series of monthly or more frequent observations. The time series provided sufficient temporal resolution to detect a short-lived and less intense secondary upwelling event that occurs between June-July (Rueda-Roa 2000, Astor *et al.* 2003, Muller-Karger *et al.* 2004). Previous works (Fukuoka 1966, Okuda 1975, Febres-Ortega 1975) overlooked this upwelling pulse or treated it as an anomaly and not as a part of the seasonal upwelling cycle.

The mid-year upwelling coincides with a weakening in wind intensities at land-based meteorological stations located around northeastern Venezuela (Rueda-Roa 2000, Astor *et al.* 2003; Peterson and Haug 2006). This decrease in the local wind stress suggested that other mechanisms lead to the mid-year event. Here, in addition to the contribution of ET due to along-shore winds, we explored the contribution of cross-shelf wind speed gradients in the Caribbean Sea that cause Ekman Pumping (EP) due to curl in the wind stress (Gill 1982, Oey 1999). Another mechanism for upwelling can be variations in along-shelf currents (i.e. Caribbean Current) position and/or intensity that can cause dynamical uplift of colder nutrient-rich waters from the deep ocean onto the shelf (Tomczak 1998), However, this latter mechanism is usually associated with turbulent flow and therefore is not the likely cause of the mid-year upwelling, simply because the expression of the upwelling has an extremely well defined annual periodicity.

This remarkable periodicity suggests that we also can discard irregular events such as tropical storms, random coastal trapped waves, or random eddies as the cause. The upwelling phenomenon along the southern Caribbean Sea is a complex process that depends on a number of factors including the geostrophic adjustment of the Caribbean Current, the distance of the Caribbean Current to the continent, stratification of the water column, bathymetry, and the local and regional wind patterns. In this work we focus on the effect of changes in local and regional wind forcing to assess the contribution of Ekman transport and Ekman Pumping on the seasonality of the upwelling process, especially during the mid-year upwelling.

The upwelling along the southern Caribbean Sea brings waters rich in nutrients that produce important phytoplankton blooms and which in turn support significant fisheries (Stromme and Saetersdal, 1989; Cárdenas and Achury, 2002; Cárdenas, 2003). More than 60% of the marine fish catch within the Caribbean Sea occurs in these waters shared between Trinidad, Venezuela and Colombia (FAO 1980-2011). The ultimate importance of the mid-year upwelling in terms of the regional fisheries is that it serves to extend the high phytoplankton biomass season in the southern Caribbean Sea.

The objectives of this study were to: a) characterize the mid-year upwelling cycle off northeastern Venezuela; b) determine the spatial extent of the phenomenon along the southern Caribbean Sea margin; c) assess the relative contribution of along-shore winds and wind curl in forcing the upwelling process; d) assess the impact on the length of the phytoplankton productivity cycle. We used historical observations and satellite-derived products over the Caribbean Sea for our research, including Sea Surface Temperature (SST), Chlorophyll-a (Chl), and wind speed and direction.

We found that historical sea level records collected at the coast off northeastern Venezuela trace the mid-year upwelling back to 1948. We also found that this phenomenon occurs throughout the entire southern Caribbean upwelling system. Our analysis shows that while coastal meteorological stations display a decrease in wind intensity in June-July, satellite-derived near-shore winds reveal high wind during this period along the southern Caribbean Sea coast. Thus, there is Ekman Transport (ET) that continues after the primary upwelling season into August. The presence of high phytoplankton biomass in the upwelling system starts on December (due to the principal upwelling) and it is prolonged through August as a result of the mid-year upwelling pulse

1.3 Methods

1.3.1 Temperature

Historical temperature profiles collected monthly as part of the CARIACO Ocean Time-Series station at 10.50ºN, 64.66ºW were used (Figure 1.1 and Figure 1.2; see site details on the hydrography at this location in: Astor *et al.,* 2003; Muller-Karger *et al.,* 2001; Scranton *et al.* 2006 and Thunell *et al.* 2007).

High resolution (pixel size ~1 km^2) Sea Surface Temperature (SST) satellite images collected by the Advanced Very High Resolution Radiometer (AVHRR) were used to construct weekly SST means over the period 1994-2009 for the southern Caribbean Sea (8ºN-16ºN, 77ºW-58ºW). Images were collected using a ground-based L-band antenna located at the University of South Florida (St. Petersburg, Florida, U.S.A.). SST was derived using the Multi-Channel Sea Surface Temperature split-window techniques (Walton 1988; Strong and McClain 1984; McClain *et al.* 1983). The nominal

accuracy of AVHRR SST retrievals is in the range of ±0.3 to ±1.0 °C (Brown *et al.* 1985, Minnett 1991). AVHRR imagery contains false cold pixels as a result of cloud contamination; to improve data quality we implemented a cloud filter similar to that of Hu *et al.* (2009). This was based on a weekly climatology derived for each pixel. All daily values in the time series larger than 2 standard deviations above the climatology or 1.5 standard deviations below the climatology were discarded. These values were selected by trial and error and work well for the tropical SSTs in the Caribbean Sea where the upwelled waters produce the coolest seasonal SST signal in the area. The filtered daily images were then used to calculate new weekly composites and a new long-term weekly climatology.

SST time series were extracted from 172 points to analyze the variability of SST along the continental margin of the southern Caribbean Sea. These points were distributed along the continental margin, approximately 10 km from the coast, between Trinidad and the central coast of the Colombian Caribbean Sea (Figure 1.3). Each point represented an average of the SST in a 5x5 pixel box (~25 km^2) centered at each station.

Seasonal SST from the mid-Caribbean Sea basin (Figure 1.1) was contrasted (Figure 1.4) with seasonal SST from the continental margin along the two main upwelling regions of the Southern Caribbean Sea (the western upwelling area [70-72.5°W, 11.3-12.9°N] and the eastern upwelling area [63-65°W, 10-11°N], Figure 1.3).

We also examined SST in the Tropical Atlantic Ocean (30°S to 30°N and 10°W to 85°W) using lower resolution satellite imagery (~16 km^2 pixels, AVHRR Pathfinder daily gridded observations, level 3, version 5) from the Physical Oceanography

Distributed Active Archive Center (PO.DAAC.) at the NASA Jet Propulsion Laboratory, Pasadena, CA.
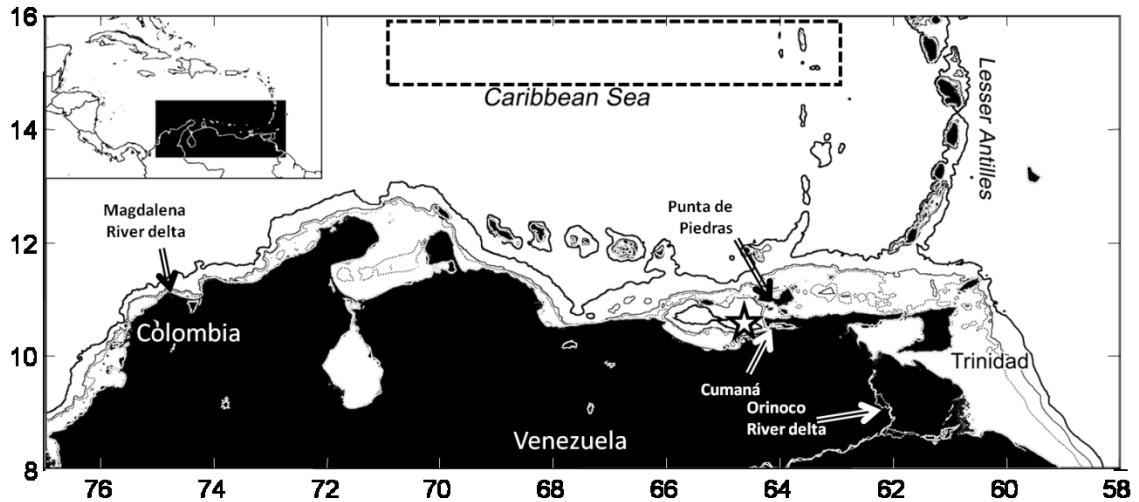
Figure 1.1. Map showing the study area in the southern Caribbean Sea (8-16ºN and 58-77º W). The 1000, 200 and 100 m isobaths are shown (black, dark gray and light gray lines, respectively). The star shows the location of the CARIACO Ocean Time-Series station (10.50ºN, 64.66ºW). Sea surface temperature (SST) time series were extracted and averaged from satellite data covering the central-eastern Caribbean Sea (dashed rectangle, 15-16 ºN and 63-71 ºW).

1.3.2 Wind

Synoptic surface ocean wind observations (spatial resolution 0.25 degree) for the period 1999-2008 from NASA's QuikSCAT satellite were obtained from PO.DAAC. Away from coastal zones, scatterometer wind retrievals were accurate to better than 2 m s^{-1} in speed and 20° in direction, similar to the accuracy of *in situ* buoy measurements (Freilich and Dunbar 1999). Due to contamination by radar backscatter from land in the antenna side lobes, there is at least a ~25 km gap between the QuikSCAT measurements and the coast (Hoffman and Leidner 2005).

QuikSCAT data were used to calculate long-term average wind patterns (Figures 1.5, 1.6 and 1.7), Ekman transport (ET) due to alongshore winds, and Ekman pumping (EP) due to the wind curl over the Caribbean Sea and the Tropical Atlantic Ocean (5-30°N and 10-85°W). Daily zonal and meridional QuikSCAT wind speed components (u, v) were used to estimate the wind stress components (τ_x, τ_y and τ_{xy}, Bakun 1973) using a drag coefficient which includes curve fits for low and high wind speeds (Oey *et al.* 2006 and 2007). To examine ET (m^2 s^{-1}, which is the same as m^3 s^{-1} per m of coast or Sv/1,000 km of coast) it was calculated the wind speed along a direction parallel to the coastline direction (Castelao and Barth 2006) to obtain the alongshore wind stress (Mendo *et al.* 1987) and the cross-shore ET (Chereskin 1995) at each QuikSCAT grid point closest to the coast (Figure 1.8). Positive/negative values are used to indicate offshore/onshore ET (upwelling/downwelling). EP (m s^{-1}) was calculated based on wind curl estimates (*curl_τ$_{xy}$*, Smith 1968) computed from weekly means of wind stress, using one pixel to the east/west and to the north/south from each QuikSCAT grid point. In the northern hemisphere, positive wind curl means counterclockwise vorticity that induces upward EP (upwelling). Total upwelling transport was calculated by adding the cross-shore ET plus the transport of EP integrated over 100 km offshore per meter of coast (EP100k, m^3 s^{-1}, Pickett and Paduan, 2003); we found that this distance includes most of the positive EP in this region.

1.3.3 Chlorophyll-a

We used high resolution (pixel resolution ~1 km^2) satellite chlorophyll-*a* (Chl), produced with the default NASA chlorophyll algorithm (O'Reilly *et al.*, 2000) from

images collected by the ocean color scanner Sea-viewing Wide Field-of-view Sensor (SeaWiFS). Data were downloaded for the study area from NASA and mapped to a uniform spatial grid using Matlab routines provided by NASA. Weekly averages of Chl, from Jan 1998 to Dec 2009, were calculated. Because chlorophyll is approximately log-normally distributed, we did all our calculations using log[Chl].

Riverine discharge can produce a very strong signal in the satellite derived Chl product because of its high concentrations of CDOM (Colored Dissolved Organic Matter). The SeaWiFS default Chl algorithm tends to fail in turbid coastal waters with high concentrations of CDOM, producing erroneous high estimates of pigment concentration (Carder *et al.* 1999). The southern Caribbean Sea waters are influenced by two large rivers (Orinoco and Magdalena, Figure 1.1) and several other small rivers. In order to separate the influence of upwelling from the freshwater discharge on Chl levels, we used a linear regression analysis between weekly SST and log[Chl] time series (1998-2009, Figure 1.9a).

Weekly Chl climatology were calculated and the coastal values were extracted at the same 172 coastal stations used for SST (Figure 1.3b). However, because of the high variability of Chl close to the coast, a larger box was used than for SST (13x13 pixel box centered at each station) in order to obtain a more robust average. There was a strong zonal variability in the Chl among the coastal stations, which difficult the visualization of the phytoplankton biomass due to the mid-year upwelling. A spatial Chl normalization (i.e. at each station Chl values were normalized by its average Chl, Fig. 9b) was applied in order to enhance the visualization of the mid-year upwelling contribution on phytoplankton biomass. A mean Chl concentration was calculated within a 100 km wide

cross-shelf (Chl_100km) for the eastern and western upwelling areas (Figure 1.10) defined in section 2.1 and from the Caribbean Sea mid-basin (Figure 1.1).

1.3.4 Sea Level

Hourly tide gauge records from Punta de Piedras (1992-1999 and 2001; provided by Fundación La Salle de Ciencias Naturales, Venezuela) were averaged monthly to filter tidal fluctuations and compared with satellite SST extracted close to the sea level station (10.74°N and 63.43°W, Figure 1.1). Three decades of monthly sea level anomalies at the city of Cumaná (Figure 1.1, 1948-1978; data provided by the Instituto Oceanográfico de Venezuela, Universidad de Oriente) were also analyzed (Figure 1.2b).

1.4 Results and Discussion

1.4.1 Persistence and extension of the mid-year upwelling:

From 1996 to the end of 2011, every year of the CARIACO Ocean Time-Series showed the mid-year upwelling in northeastern Venezuela (Figure 1.2a). CARIACO data shows important inter-annual variability in the upwelling cycle, and also a shift in the upwelling temperature. Remarkably, since 2004 the upwelling phenomenon now brings warmer waters to the surface (the 19°C isotherm that was located around 150 m depth before 2004 is now located deeper after 2004, Figure 1.2a). That raised the question of whether the mid-year upwelling pulse is just a modern feature in the area; to answer that we needed to analyze older time series records.

Coastal upwelling causes sea level in the study area to drop as a result of geostrophic adjustment, and also due to cooling of the water (Muller-Karger and Castro

15

1994). Approximately 75% of the variability in monthly sea level at Punta de Piedras was related to variability in SST (r=0.87, n=93, p< 0.01), indicating that older sea level records can be used as a proxy for upwelling off northeastern Venezuela. Three decades of historical monthly sea level anomalies at the city of Cumaná dating back to 1948 clearly showed the occurrence of the mid-year upwelling (Figure 1.1 and Figure 1.2b). Cooling of coastal waters during June-July is evident in oceanographic data from off northeastern Venezuela collected as early as the early 1960's (Fukuoka 1966, Okuda 1975, Febres-Ortega 1975). However, this oceanographic feature was not recognized as part of the seasonal upwelling cycle because of the low temporal and spatial resolution of the data at the time. The 30 years of sea-level records and 16 years of hydrographic time series showing the mid-year upwelling demonstrate that the mid-year upwelling is part of the annual upwelling cycle off northeastern Venezuela.

The mid-year upwelling is not confined to northeastern Venezuela. Fourteen years of satellite-derived SST data along the coast of the southern Caribbean Sea revealed that the mid-year upwelling occurs along the entire margin from 61°W to 75.5°W (Figure 1.3a). These findings agree with the lower SST observed on July for the Colombian Caribbean Sea coast (Bernal *et al.* 2006). The seasonal climatology of coastal SST (Figure 1.3a) shows that mid-year upwelling occurred between June-August at the same geographic locations as the principal seasonal wind-driven upwelling. However, SST is typically about 1-2°C warmer than during the principal upwelling period. Overall, the mean lifetime of the mid-year upwelling was 5.5 weeks (± 2.2 SD, during the period 1994-2009).

(a) Monthly temperature profiles at the CARIACO station

(b) Monthly Sea Level at Cumaná
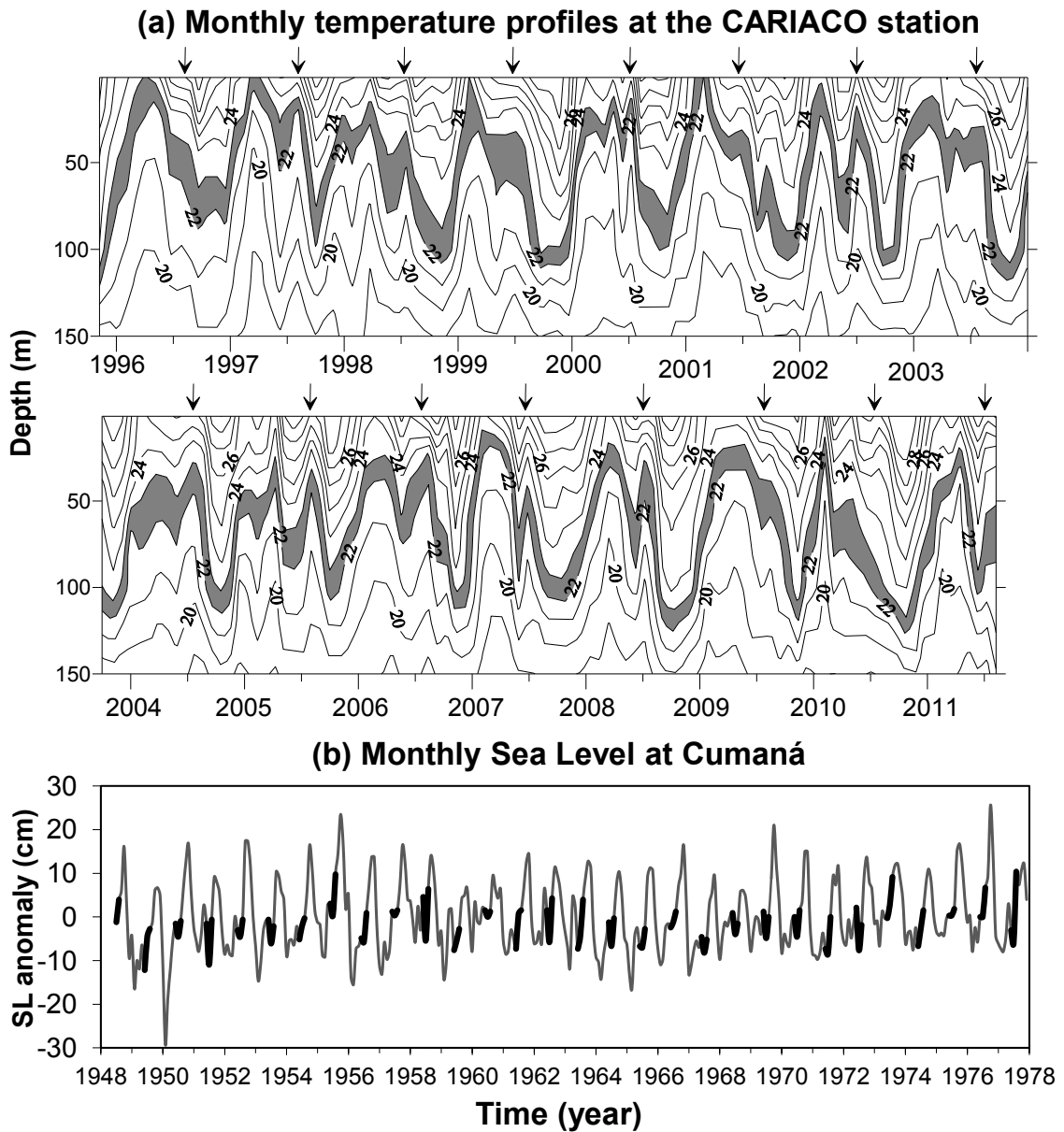
Figure 1.2. (a): Seasonal changes (1996-2011) in the depth of isotherms in the upper 150 m at the CARIACO Ocean Time-Series station (10.5°N, 64.66°W, Figure 1.1). Isotherms are separated by 1°C increments; the shaded area identifies the 22-23°C isotherm interval, to highlight the seasonal upwelling. The mid-year upwelling is marked with arrows. (b): Monthly variations of sea level anomaly at Cumaná (10.46°N, 64.19°W, see Figure 1.1). Sea level in this area follows the seasonal sea surface temperature cycle, including the mid-year upwelling (interval June-July highlighted in bold black).

17
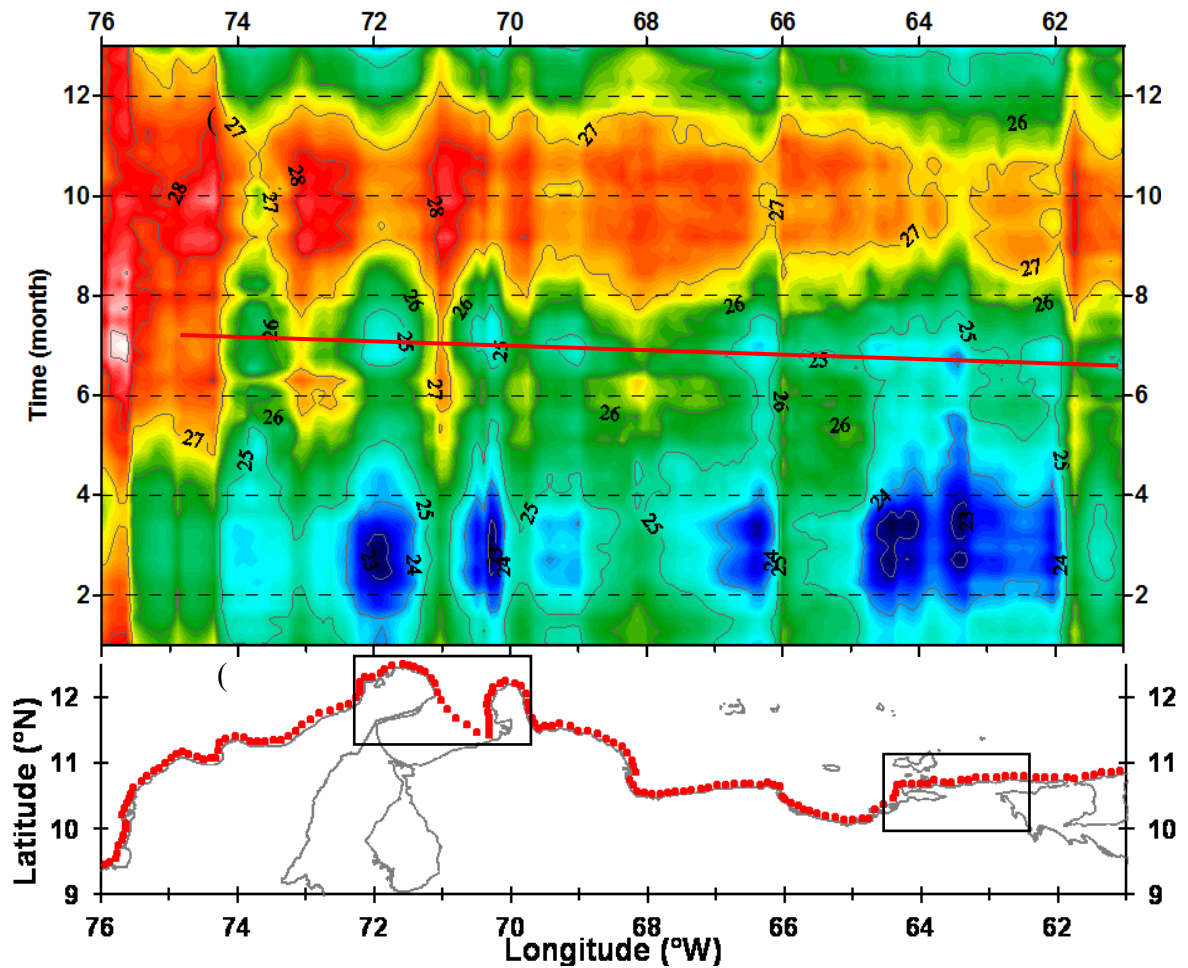
Figure 1.3. (a): Seasonal cycle in sea surface temperature (SST) along the southern Caribbean Sea coast, calculated with long-term weekly SST means (1994-2008) derived from satellites (isotherm contours are every 1°C). SST time series were extracted at 172 coastal stations approximately 13 km offshore, shown in the map (b) as red dots. Two main upwelling regions of the southern Caribbean Sea were compared: the western upwelling area (70-72.5°W) and the eastern upwelling area (63-65°W), identified as squares in panel (b). The principal upwelling season was synchronous in both areas and peaked during February-March; the mid-year upwelling peaked around June-July and it showed a linear lag in time from East to West as shown by slope of red line in panel (a).

Two large areas showed the strongest upwelling signal in the southern Caribbean Sea (Figure 1.3a). One is located off northeastern Venezuela (63-65°W), and the other off northwestern Venezuela and northeastern Colombia (70-72.5°W); they are identified hereafter as the eastern and western upwelling areas, respectively. While the principal

18

upwelling was synchronous for both upwelling areas, the mid-year upwelling occurred with a slight lag in time of up to two weeks to the west (see red line in Figure 1.3a, and Figure 1.4). This lag was then found to be related to a lag in wind conditions, as discussed below in section 3.4.

Muller-Karger and Castro (1994) inferred that the eastern and the western upwelling areas had the same seasonal cycle as the Caribbean Sea mid-basin, although with cooler SST all year round (Figure 1.4). We confirmed this earlier observation with our longer time series; the SST averages for the eastern and the western upwelling areas were 1.9°C and 1.3°C cooler than the central Caribbean Sea, respectively.

There is a midyear SST decrease in the central Caribbean Sea concurrent with the mid-year upwelling, even though northern hemisphere summer should feature warmer SSTs in the Caribbean Sea. We explore the spatial extent of these regional minima and their relationship to regional wind changes in more detail in section 3.2.

1.4.2 Regional Wind speed and wind-curl patterns:

The Caribbean Sea experiences strong seasonal changes in wind regimes, including latitudinal wind gradient (Figure 1.5a). Weaker winds occur along the southern continental margin of the basin compared to stronger winds in the Caribbean Sea mid-basin (~13-15ºN). Land-based meteorological stations in eastern Venezuela show mid-year weakening of wind intensities (Rueda-Roa 2000, Astor *et al.* 2003). However, in the Colombian Caribbean Sea and throughout Central America a slight increment in coastal wind intensity occurs during mid-year. This phenomenon is known as the "Veranillo de San Juan" (Muller-Karger and Fuentes-Yaco 2000, Arevalo-Martinez *et al.* 2008).

Regional patterns of wind and wind curl were analyzed to understand these geographical variations and their impact on upwelling and phytoplankton.
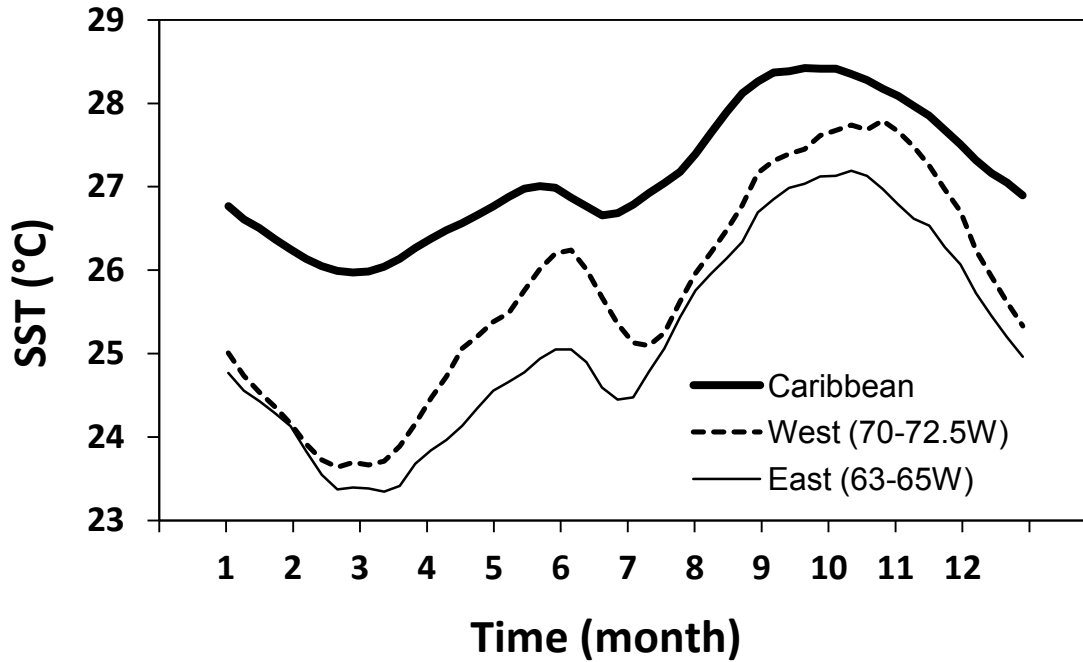
Figure 1.4. Long-term seasonal SST cycle of the central-eastern Caribbean Sea (solid heavy line), and coastal SST averaged for the western and eastern upwelling areas (broken and thin black lines); see locations in Figure 1.1 and Figure 1.3b. Values were filtered with a centered 3-week running mean.

Latitudinal gradients in wind intensity lead to a curl in the wind stress (Gill 1982). The wind-curl was positive in the southern half of the Caribbean Sea, and negative in the northern half all year round (Figure 1.5b). This latitudinal pattern induces open sea upwelling in the southern Caribbean Sea and downwelling in the northern Caribbean Sea throughout the year (Gordon 1967). The strongest seasonal winds over the central Caribbean Sea occurred from November to July off the coast of Colombia (between 74-76°W; Figure 1.5a).
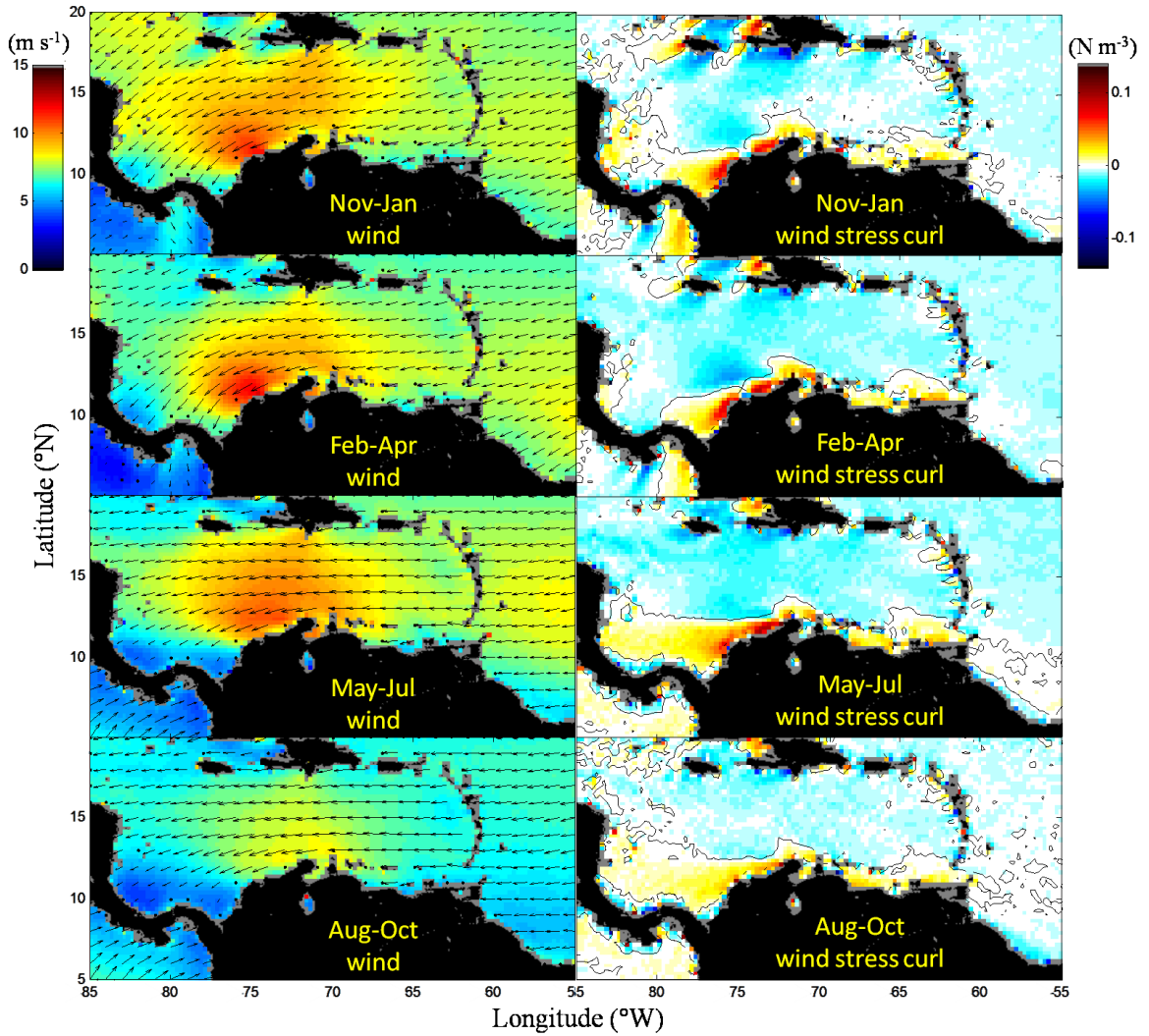
Figure 1.5. Long-term seasonal averages for (a) the wind magnitude (color) and wind direction (vectors) and for (b) the wind stress curl. The southern Caribbean Sea exhibits year-round positive wind stress curl (upwelling favorable in the northern hemisphere). Data derived from the NASA QuikSCAT satellite-based sensor (1999-2008).

During May-July there was a longitudinal intensification of the wind along ~14°N from the Tropical North Atlantic Ocean to the western Caribbean Sea, and wind direction became more aligned with the southern Caribbean Sea coastline (Figure 1.5a). This is identified as the Caribbean Low-Level-Jet (Amador 1998, Whyte *et al.* 2008), which peaks in June-July in the western Caribbean Sea. The Caribbean Low-Level-Jet produced

intensification in the latitudinal wind gradient, which in turn causes a maximum positive EP from June through August along the entire extent of the southern-central Caribbean Sea and along the Atlantic side of the South American continent (see May-July in Figure 1.5b). The area of positive wind curl extended far beyond the southern Caribbean Sea continental slope all year round, ranging from 40 to 190 km offshore, and with a maximum extension during June through August. During this time, the positive wind curl reached farther offshore in the eastern upwelling area (average ~130 km) than in the western one (average ~60 km), probably because the core of stronger winds was closer to the coast in the last area (Figure 1.5a). The annual average of positive (upwelling inducing) wind-curl along the southern Caribbean Sea coast (between 62°W to 74°W) covered an area of 3,345 km^2.

The curl of the wind causes significant upwelling in other upwelling systems, such as off southern California (Oey 1999, Pickett & Paduan 2003) and Cabo Frio, Brasil (Castelao & Barth 2006). The positive wind curl found beyond the continental slope of the southern Caribbean Sea upwelling areas (Figure 1.5b) contributes to open-sea upwelling (Halpern 2002). To explore the possible connections of Tropical Atlantic Ocean processes with the mid-year SST decrease observed in the central Caribbean Sea and the mid-year upwelling seen along the southern Caribbean Sea margin (Figure 1.4) we analyzed SST and wind satellite products in a larger area (30°S to 30°N and 10°E to 85°W). Long term monthly means (2000-2006) were calculated and subtracted the mean of June minus the mean of May for SST, wind stress magnitude and wind stress curl (Figure 1.6). The results show that not only does the Caribbean Sea experience a mid-year SST cooling (Figure 1.4), but that also occurs across the entire tropical North

22

June-May long term means
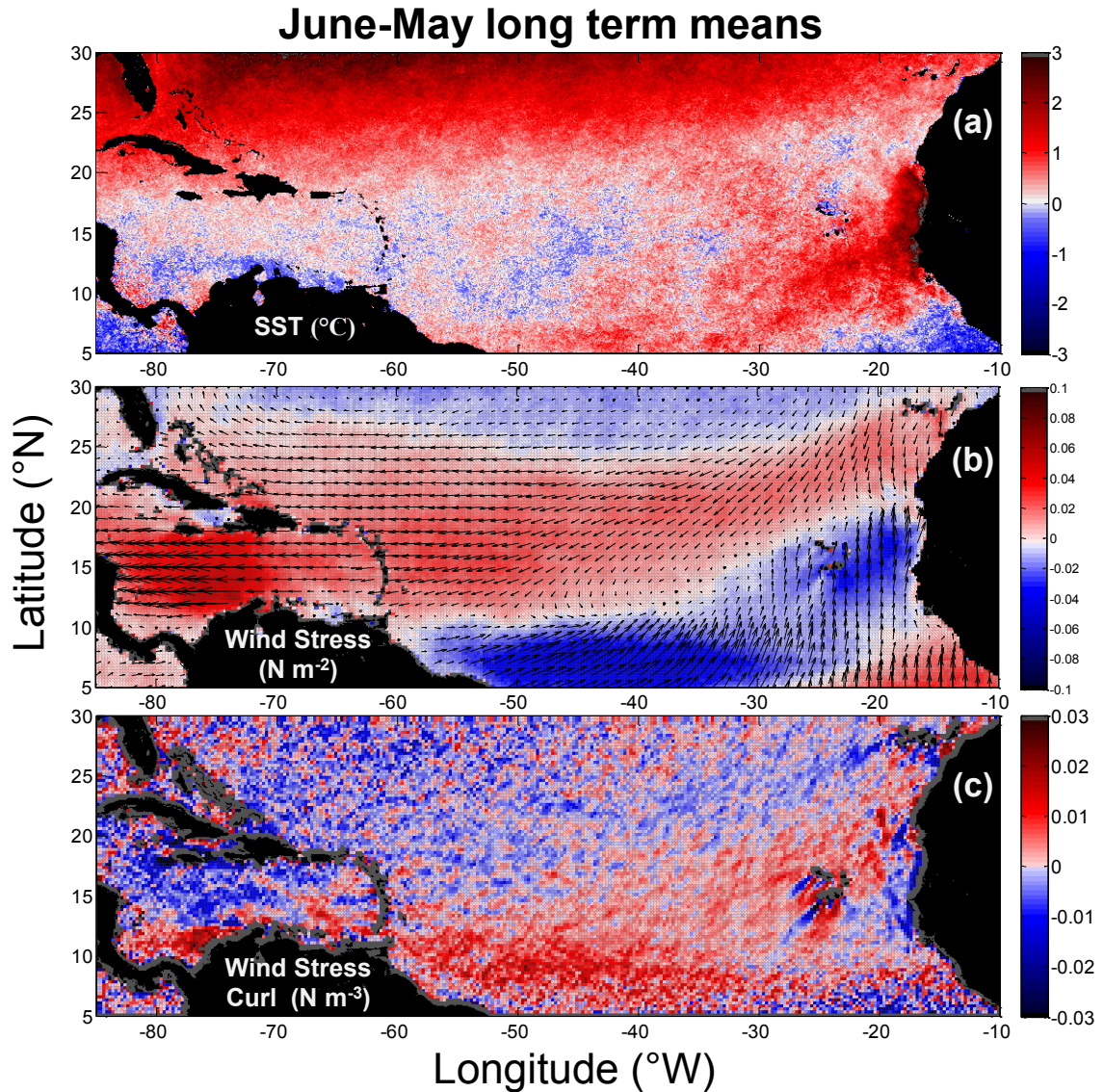
Figure 1.6. Differences between average June minus average May (2000-2006) for: (a) SST (°C), (b) wind stress (N m^{-2}) and (c) wind stress curl (N m^{-3}). The mid-year upwelling along the southern Caribbean Sea showed strong negative SST anomalies; in addition, there was SST cooling along an ocean-wide band across the entire tropical North Atlantic Ocean roughly between 10-20N. Wind stress and wind stress curl patterns were congruent to the spatial pattern of SST cooling.

Atlantic Ocean (Figure 1.6a). The normal summer SST increase, owing to the seasonal warming in the tropical North Atlantic Ocean, was disrupted by a longitudinal band (between roughly 10°N -20°N) of negative SST anomalies that stretched from Africa to

the Caribbean Sea (Figure 1.6a). Indeed, temperatures north of ~20°N continued to increase during this period (Figure 1.6a). The tropical South Atlantic Ocean also showed negative SST anomalies caused by the seasonal cooling in the southern hemisphere (data not presented). The strongest negative SST anomalies were found in the southern Caribbean upwelling system, indicating that the mid-year upwelling is not an imported signal but the result of the upwelling of cooler sub-surface waters.

June minus May wind stress (Figure 1.6b) showed a longitudinal belt of increased magnitude between 10-25°N, and also negative anomalies along its southern edge (5-10°N). This indicates that during June, the easterlies shifted to a more northerly position and became more concentrated, in a narrower band of 10° width. Within this band, the wind direction was intensified to the southwest. The Caribbean Low-Level-Jet in the western Caribbean Sea was very evident, showing the most intense positive anomaly values. The eastern coast of Venezuela showed null to slight negative wind stress anomalies, while the Colombian and Central America Caribbean Sea coasts had positive anomalies. This agrees with reports from land-based meteorological stations of less intense winds over the eastern upwelling area (Rueda-Roa 2000, Astor *et al.* 2003) and intensification of winds over the western upwelling area (Muller-Karger and Fuentes-Yaco 2000, Arevalo-Martinez *et al.* 2008). Wind stress curl anomalies also had increased values (i.e. increased positive curl) along a longitudinal ocean-wide band in the tropical North Atlantic Ocean between about 5-10ºN and in the southern Caribbean Sea (Figure 1.6c), indicating enhanced open sea upwelling in these large areas during June.

The belt of positive anomalies for both the wind stress and wind stress curl was congruent with the negative SST anomalies along the Tropical North Atlantic Ocean and

the Caribbean Sea. Increased wind over the ocean enhances surface mixing and air-sea fluxes. This, and open sea upwelling as a result of the increased positive wind-curl, explains the mid-year cooling in the Caribbean Sea and Tropical North Atlantic Ocean. The mechanistic explanation for this mid-year negative SST ocean-wide band is beyond the scope of this paper; however, it is worth to highlight some aspects that could have an association with the genesis of the mid-year upwelling. The southern portion of the North Atlantic Gyre forms part of the North Equatorial Current that feeds the Caribbean Sea. The location of the increased wind stress band and the enhanced southwest directionality might produce an acceleration of the transport to the Caribbean Sea caused by increased wind-induced surface currents toward the west. This is supported by modeled results of maximum inflow around June in the southern Antilles passages of Saint Vincent and Grenada, and a strongest Caribbean Current in the northern hemisphere summer (Johns *et al.* 2002). This basin- wide phenomenon can contribute to the mid -year upwelling observed in the southern Caribbean Sea in three ways. An acceleration of the mean speed of a current along the continental slope (i.e. the Caribbean Current) would produce rising isotherms, causing dynamical uplift of colder nutrient-rich waters from the deep ocean onto the shelf (Tomczak 1998). Another process that enhances the rising of isotherms during this time frame is the positive wind curl, which reaches its maximum along 10°N in the Caribbean Sea and the Tropical North Atlantic Ocean (Figure 1.6c and Figure 1.5b). This would produce open-sea upwelling (rising of isotherms) in the southern Caribbean Sea margin, and also in the waters that feed the Caribbean Current. Another consideration is the presence of relatively cooler Caribbean Sea surface waters, which reduces stability of the water column, further facilitating upwelling during mid-year.

25

1.4.3 Forcing mechanisms acting along the coast

In this section, the local effects that coastal ET and coastal EP have on the mid-year upwelling are examined by contrasting the western and eastern upwelling areas. Nearshore QuikSCAT satellite wind products were obtained along the coast of the southern Caribbean Sea using the grid cells closest to the shore (~25 km offshore). It was assumed that nearshore QuikSCAT data were accurate and useful to obtain reasonable estimates of upwelling since winds in the region are usually higher than 3m s^{-1}, which is the lower threshold above which satellite-derived winds are expected to be more accurate (Pickett *et al.* 2003).

Along the southern Caribbean Sea there were three areas with very distinctive nearshore wind speed regimes (Figure 1.7, see also Figure 1.5a):

1) From 61°W to 66°W: relatively stable and high wind speed from December to July (> 6 m s^{-1}) and slightly lower wind speed during August-November (4-6 m s^{-1}).

2) From 69°W to 74°W: stronger winds year round (> 6 m s^{-1}), with a maximum in June-July (> 9 m s^{-1}) and a minimum during September-October (6-7 m s^{-1}).

3) From 74°W to 76°W: the area of strongest nearshore winds, with a distinctive maximum during December-April (> 11 m s^{-1}), a secondary maximum in July (~9 m s^{-1}), and a marked minimum during September-October (~5 m s^{-1}).

Wind speed over the eastern upwelling area was ~26% weaker compared with the western area (annual wind speed averages 6.2 and 8.3 m s^{-1}, respectively). However, over the eastern upwelling area, the winds were more aligned with the coastline, with alongshore winds only ~9% weaker than over the western upwelling area (annual alongshore wind averages -5.9 and -6.5 m s^{-1}, respectively). Mid-year QuikSCAT near-

shore winds were high for the eastern upwelling area (Figure 1.7) and indicated sufficient along-the-coast wind forcing to produce the mid-year upwelling (i.e. speeds > 6 m s^{-1} sustained over several days). However, land-based meteorological stations show wind weakening during this time of the year (Rueda-Roa 2000, Astor *et al.* 2003). Fréon and Ans (2003) attributed those differences to terrestrial influence and to a latitudinal gradient in wind speed.
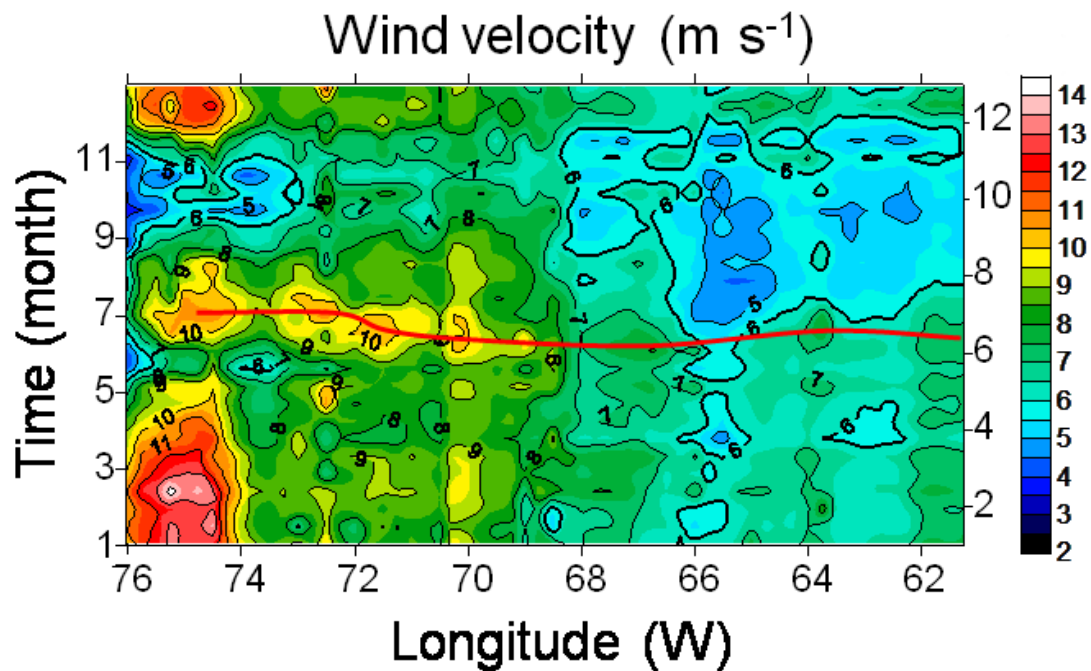
Figure 1.7. Seasonal cycle in satellite-derived nearshore (~25 km) wind speed along the southern Caribbean Sea coast, calculated with long-term weekly means (1999-2008). The red line connects the mid-year wind speed maximum along the coast. Notice the longitudinal variation in the lag in wind intensity toward the west, between 70°W and 73°W.

Between 70° and 73°W there was a lag in the timing of the mid-year peak in wind intensity. This is a partial explanation for the ~2 week SST lag for the mid-year upwelling in the western upwelling area relative to that of the east (Figure 1.3a), since the SST lag increased steadily along the coast toward the west, while the lag in the wind was

more irregular or even abrupt (compare red lines in Figure 1.3a and Figure 1.7). Another possible explanation for the westward lag in timing of the mid-year upwelling could be the propagation of perturbations along the Caribbean Current. The Caribbean Current is fastest along the southern boundary of the Venezuela basin, with a mean speed of 80 cm s^{-1} (Richardson 2005). Models indicate an intensification of the Caribbean Current during June-July (Johns *et al.* 2002). The eastern and western upwelling areas are separated by ~8° of longitude (Figure 1.3), and any perturbation of the Caribbean Current, caused by speed intensification, would reach the west area in around 12 days. Further studies are necessary to understand the mechanisms underlying this lag in timing of the upwelling along the coast toward the west.

Cross-shore Ekman Transport occurred year-round in both the western and eastern upwelling areas (Figure 1.8), with annual ET averages of 2.74 and 2.06 m^3 s^{-1} per meter, respectively. Even the smallest annual values for the western and eastern upwelling areas were relatively large (1.67 and 1.46 m^3 s^{-1} per meter, respectively). These values explain why these areas are always cooler than the mid-Caribbean Sea basin (Figure 1.4). Our values are consistent with Peru offshore ET averages (1.99 m^3 s^{-1} per meter, Bakun 1987; average coastal wind speed of 5.7 m s^{-1}, Chavez and Messié 2009). ET values depend on latitude (Coriolis effect), and the upwelling area off Peru is located at a similar latitudinal range as the southern Caribbean Sea upwelling (6-16°S).

Ekman Pumping integrated through 100 km offshore (EP100km) was also favorable for upwelling year-round for both areas (annual EP100km means 0.31 and 0.41 m^3 s^{-1} per meter for the west and east areas, respectively), aside from slightly negative EP100km during November for the west area (0.02 m^3 s^{-1} per meter).

Total upwelling transport (ET+ EP100km) annual averages were 3.07 and 2.48 m^3 s^{-1} per meter, for the western and eastern upwelling areas respectively (Figure 1.8). For both areas, higher EP100km contribution to the total upwelling was between December and August; however, EP100km contribution was smaller in the west area compared to the east (11% and 20%, respectively). These differences are likely explained by the annual cycles of positive EP offshore (Figure 1.8). Positive EP values were found farther offshore in the eastern upwelling area and had a distinctive peak at the end of June (average 102 km, peak 130 km), while in the west area the peak occurred during December-January (average 82 km, peak 106 km). Both areas showed high wind forcing during the mid-year upwelling; at the end of June total upwelling estimates were high in the east area (2.7 m^3 s^{-1} per meter), and even peaked in the west area (4.2 m^3 s^{-1} per meter).
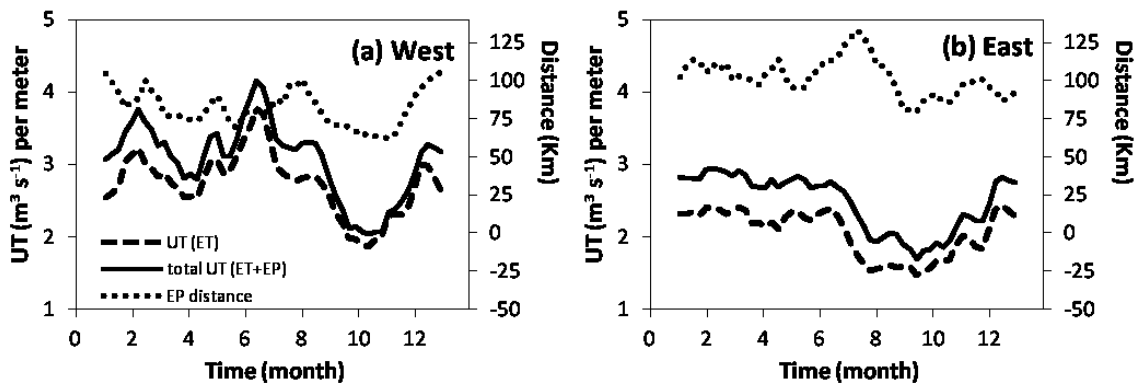
Figure 1.8. Long term means of the upwelling transport (UT) in the western (a) and eastern (b) upwelling areas due to only cross-shore Ekman transport (ET); and total UT due to cross-shore Ekman transport plus Ekman pumping integrated to 100 km offshore (ET+EP). Width of the offshore distance with positive Ekman pumping values (EP distance). Values were filtered with a centered 3-weeks running mean.

These results indicate that in the southern Caribbean Sea, ET was the dominant upwelling mechanism for the eastern and western areas, including for the mid-year

29

upwelling (Figure 1.8). EP100km upwelling transports were one order of magnitude smaller than ET. We believe that EP contribution closer to shore may be more important. There is a ~25 km gap between nearshore QuikSCAT wind and the coastline. Close to shore there is a significant drop-off in coastal wind speed (Capet *et al.* 2004); therefore, nearshore QuikSCAT wind may cause an ET overestimation and EP underestimation (Pickett and Paduan 2003). Nevertheless, nearshore QuikSCAT total transport estimates are very robust even if the relative proportions of ET and EP are biased (Pickett and Paduan 2003). The high mid-year total upwelling transport for both upwelling areas indicates that the mid-year upwelling is mainly wind-driven and that ET contribution is very high nearshore. In the open-sea, EP seemed to play an important role during the mid-year upwelling. The area of positive EP seen expanding between the Southern Caribbean Sea and the Tropical Atlantic Ocean in May-July (Figure 1.5b and Figure 1.6c) suggested that isopycnal shoaling of the Tropical Atlantic Ocean waters that connect with the Caribbean Current could perhaps enhance the southern Caribbean Sea mid-year upwelling. However, no evidence was found of mid-year isotherm shoaling in longitudinal transects extracted along 5°, 8°, 10° and 12°N, from 0-500 m depth, in 1°x1° monthly climatological records (World Ocean Atlas 2005) in the Tropical North Atlantic Ocean. It is possible that both the spatial and historical data density in the World Ocean Atlas is still low. Therefore, more studies are needed to understand the role of the midyear EP expansion into the Tropical Atlantic Ocean on the southern Caribbean Sea mid-year upwelling. Future studies are also needed to help understand the impact of changes in the intensity of the Caribbean Current, in both time and space, on upwelling along the southern Caribbean Sea. For example, the Caribbean Current intensifies

30

seasonally with a peak in flow in June-July (Johns *et al.* 2002, Richardson 2005) which coincides with the mid-year upwelling. How these seasonal changes are affected by long-term changes in the intensification or position of the Caribbean Current are important questions that have relevance to local weather and management of living marine resources

1.4.4 Effects of the mid-year upwelling on phytoplankton biomass:

SST showed strong inverse correlations with Chl (correlation coefficient, r< -0.4) in areas where the upwelling plumes extend offshore of the southern Caribbean Sea coast (dark blue areas in Figure 1.9a). The increased biomass in these plumes is caused by enhanced phytoplankton growth closer to the surface as a result of increased nutrient availability in upwelled cooler waters. There is correspondence between the upwelling plume areas (SST $\leq$ 26°C) and high phytoplankton biomass plumes (Chl $\geq$ 0.4 mg m^{-3}; see Muller-Karger *et al.* 2004, and references therein). Direct and weaker SST *vs*. Chl correlations ($0 \geq r < 0.4$) were found in regions with freshwater influence (e.g. zones 1 to 5 in Figure 1.9a). The most prominent one was the plume of the Orinoco River (zone 1 in Figure 1.9a). *in situ* concentrations of chlorophyll-*a* within the Orinoco River plume are smaller than the ones obtained from satellite Chl (Varela *et al.* 2003). This is caused by the high concentration of CDOM in the Orinoco River plume (Muller-Karger *et al.* 1989, Muller-Karger and Aparicio 1994, Odriozola *et al.* 2007). The surface area of satellite Chl produced by the pigment-rich river plume and by the upwelling plumes changes seasonally, with one or the other dominating the region in different seasons. The seasonal boundary or front between the eastern upwelling plume and the Orinoco River plume was

31

established as the location where no significant SST *vs*. Chl correlation was observed at p
> 0.01 (indicated in grey color in Figure 1.9a). Around the Orinoco discharge area; this
no-correlation-area coincided with the spatial expansion-contraction of the seasonal
boundary between the upwelling plume and the river plume into the Caribbean Sea traced
manually by Muller-Karger and Varela (1990). The lower negative correlations (> -0.3,
light blue) point out transition areas, where the Chl signal from upwelling is influenced
by freshwater in both time and space.

Coastal Chl concentrations showed large regional variability. The annual means
for the 172 coastal stations extracted using SeaWiFS data ranged from 0.2 to 5.8 mg m^{-3}.
This high spatial variability made it somewhat difficult to assess the mid-year upwelling
effect on phytoplankton biomass. To address this problem local variability was removed
applying a spatial normalization of Chl; i.e. developing a time series of Chl anomalies by
subtracting the weekly mean value of each station from their annual average (Figure
1.9b). Within the upwelling areas, with no influence from freshwater discharges, higher
Chl (Figure 1.9b) coincided with the principal and the mid-year upwelling (Figure 1.3a).
There was a prolonged Chl maximum between December and April, and a second shorter
maximum between June-July and June-August, for the eastern and western upwelling
areas, respectively. While there was a clear lag in the mid-year upwelling SST minimum
for the eastern and western upwelling areas (Figure 1.3a), that lag is not obvious for the
mid-year Chl peak. However, the more prolonged mid-year Chl peak in the western
upwelling area could be a result of the mid-year upwelling lag in this area. In portions of
the eastern upwelling area (e.g. around ~64°W) the Chl maxima from both the primary
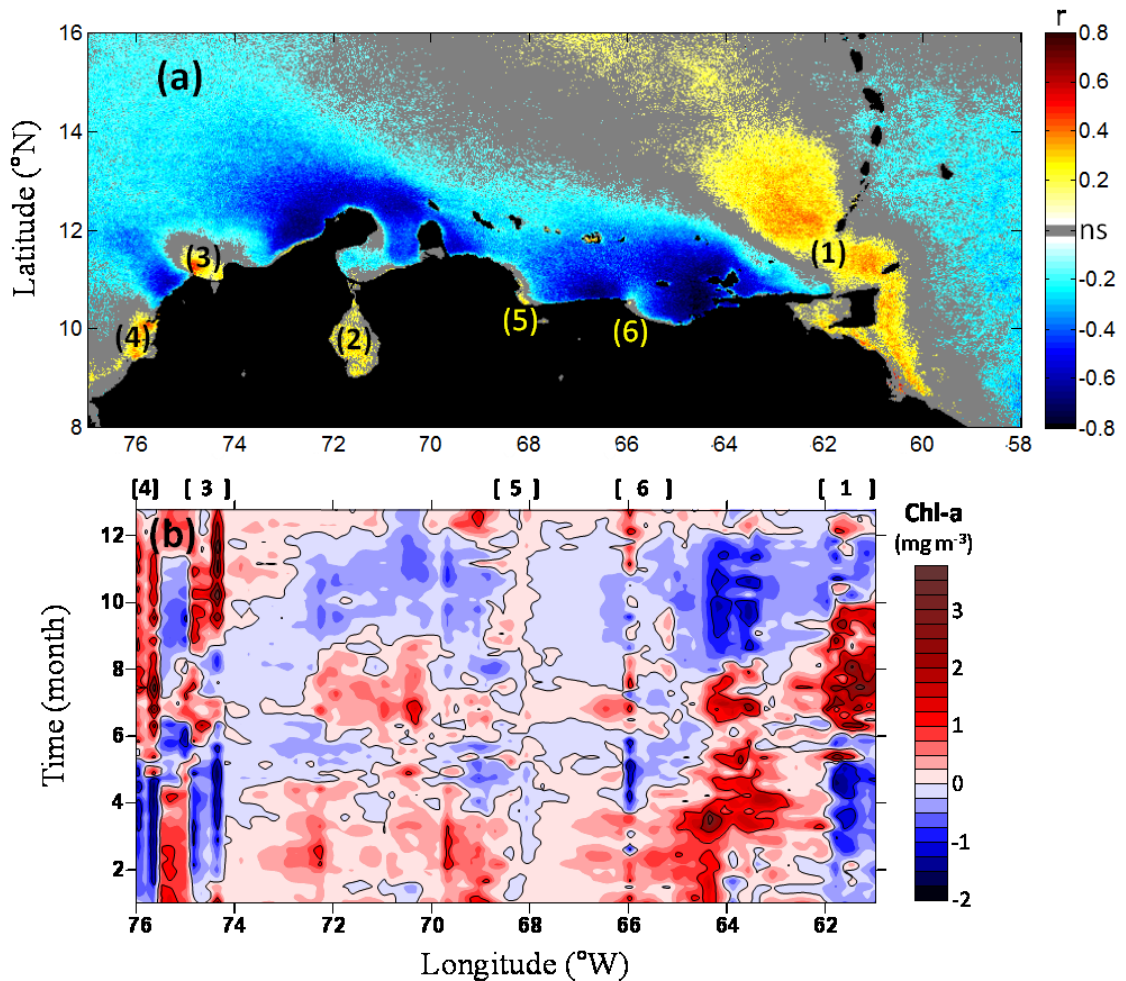
Figure 1.9. (a): Correlation coefficient (r) between weekly time series of satellite SST and log Chl (1998-2009). Non-significant values (p> 0.01) are masked in grey. Upwelling areas showed strong inverse correlations with phytoplankton biomass, while areas with freshwater influence showed a direct correlation as a result of their high content in CDOM. The principal fresh water sources that influenced the satellite Chl were: (1) Orinoco River, (2) Maracaibo Lake, (3) the Magdalena River and Ciénaga Grande, and (4) the Sinú river and Canal del Dique. Additionally, other areas showed contamination of the Chl product very close to the coast because of smaller local freshwater discharges (5: Tocuyo river, and 6: Tuy River). (b) Seasonal cycle of spatial normalized Chl along the southern Caribbean Sea coast, calculated with long-term weekly Chl means (1998-2009). Chl was normalized at each station subtracting its annual Chl average (isolines are every 1 mg Chl m-3 below or above the annual average at each station). Time series were extracted at the same coastal stations as for SST (Figure 1.3b). On top of panel B numbers in brackets show the locations of river discharge occurs, as also shown in panel (a). The approximate extent of the coastal impact of the plume is indicated by the width of the brackets around these numbers.

33

and mid-year almost overlap, which reflects the short transition time between the principal and the mid-year upwelling for that region (Figure 1.3a).

The Chl peak in coastal areas with riverine influence (Figure 1.9b) coincided roughly with the time of maximum discharges. For example, the Margdalena River discharge peaks in October-December (Restrepo and Kjerfve, 2000); the Sinú River peaks in July-November (Lozano-Rivera, 2009); the Orinoco River peaks in July-September (Aparicio 2003). We found that the Chl/CDOM maximum around the Orinoco plume started one month earlier (June) than the maximum discharge, as previously documented by Muller-Karger and Varela (1990) and Hu *et al.* (2004). The reason for this could be the influence of other nearby rivers. For example, the Esequibo River (in Guyana), a large river east of the Orinoco delta, have its peak one month earlier than the Orinoco River (June-Aug, US Army Corps of Engineers, 1998). Also, the flux of the Amazon River into the Caribbean Sea peaks in June (Hu *et al.* 2004).

A weekly time series average of log-Chl was calculated for the longitudinal range of each upwelling area and up to 100 km offshore (Chl_100km, Figure 1.10 a and b). To avoid fresh water contamination in the Chl signal, the pixels with SST *vs*. log-Chl correlation coefficients $\geq$-0.3 were filtered out. The eastern upwelling area had higher Chl_100km than the western area (annual mean 0.55 and 0.37 mg m^{-3}, respectively). These values are modest when compared to the four big upwelling systems (ranging from 1.5 mg m^{-3} in California to 4.3 mg m^{-3} in NW Africa; Chavez and Messié, 2009). However, they are high compared to open sea values in the Caribbean Sea mid-basin (Figure 1.1, annual mean 0.17 mg m^{-3}), where lower concentrations were found during most of the year (October to May, 0.13-0.15 mg m^{-3}) and a peak during June-August

(0.18-0.29 mg m^{-3}). This Chl peak is caused by the dispersal of the Orinoco and Amazon Rivers into the Caribbean Sea (Muller-Karger and Varela 1990, Hu *et al.* 2004). The western and eastern upwelling areas had a Chl_100km maximum during the principal upwelling (0.58 and 1.27 mg m^{-3}, respectively) and another Chl_100km peak during the mid-year upwelling (0.62 and 0.91 mg m^{-3}, respectively); minimum values occurred during October-November (0.23 and 0.28 mg m^{-3}, respectively).
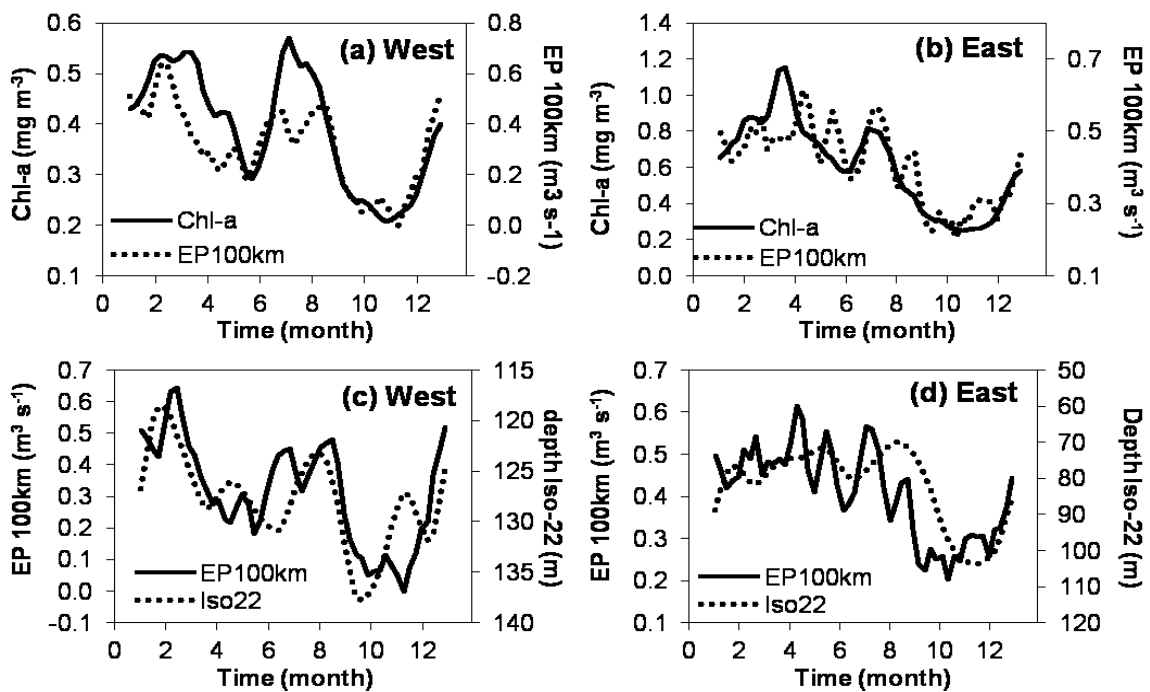
Figure 1.10. Comparison of the long term weekly means of SeaWiFS chlorophyll-*a* averaged to 100 km offshore (Chl), Ekman Pumping integrated up to 100 km offshore (EP100km) and depth of the Subtropical Underwater core (traced with the 22°C isotherm, Iso22) for the western (left) and eastern (right) upwelling areas. Iso22 calculated from climatological temperature profiles next to the continental platform between 70-73°W (west area) and 62-65°W (east area) from the World Ocean Atlas 2005 (1 x 1 degree resolution). Values were filtered with a centered 3-weeks running mean.

The mid-year upwelling process extended the duration during which cool waters are present in surface layers of the southern Caribbean. Together, both upwelling

35

processes provided an average of 8.0 and 8.5 months of SSTs ≤ 26°C, in the western and

eastern upwelling areas respectively, with a range between 6.2-10 months (e. g. Figure

1.3). The prolonged availability of upwelled waters into the euphotic zone had a direct

effect in phytoplankton biomass throughout the year. High concentrations of Chl_100km

(≥ 0.35 mg m^{-3}) were present during 8 and 9.5 months on average, for the western and

eastern upwelling areas, respectively. The threshold of Chl_100km ≥ 0.35 mg m^{-3} to

denote high chlorophyll concentrations in the southern Caribbean upwelling system was

selected because it is above the mean seasonal maximum found in the Caribbean Sea

mid-basin (0.29 mg m^{-3}). The west area showed similar Chl_100km (and coastal Chl)

values for both the principal and the mid-year upwelling events (Figure 1.10a and Figure

1.9b, respectively). Visual analysis of Chl time series maps confirmed that the mid-year

high Chl was not produced by nearby freshwater discharges but were originated at the

upwelling cores, principally at 70.1 and 72.3°W.

Chl_100km had high inverse correlations with SST (Table 1.1), as it is expected

in areas with enhanced primary production due to upwelling. In general, Chl_100km

(Figure 1.10 a and b) also followed the inverse of the SST annual cycle (Figure 1.4).

Better correlations for Chl_100km and SST were usually found with a lag of 1-2 weeks

after the wind products. Higher correlations for both Chl_100km and SST were found

with the total upwelling calculated with ET plus EP100km (Table 1.1). This could be

attributable to offshore EP causing a rise in isopycnals to the depths of the waters feeding

the coastal upwelling. To further examine this idea the depth of the 22°C isotherm

(Iso22) was calculated as an index of the Subtropical Underwater high salinity core in the

southern Caribbean Sea (Morrison and Nowlin 1982). We used climatological temperature profiles extracted from the grid points of the World Ocean Atlas (2005) closest to the coast at 70-73°W (west area) and 62-65°W (east area). The seasonal variation of Iso22 depth follows EP100km (Figure 1.10 c and d), especially in the western upwelling area; this is an indication that offshore EP has an effect on open sea isopycnal shoaling, enhancing the coastal upwelling.

Table 1.1 Pearson correlation coefficients between weekly time series (2000-2009) of Chl, SST and wind derived parameters for the western and eastern upwelling areas. QuikSCAT wind derived parameters: (ET: cross-shore Ekman Transport calculated with nearshore winds; EPcoast: coastal Ekamn Pumping; EP100km: Ekman Pumping integrated until 100 km offshore. Chl_100km (SeaWiFS chlorophyll-*a* averaged until 100 km offshore). SST (AVHRR sea surface temperature close to the coastline). Weekly averages of each parameter were calculated for the longitudinal range of the western and the eastern upwelling areas. All correlations were significant (p< 0.01). The best lagged correlation is presented and the lag of the first variable, in weeks, is indicated between parentheses.

Variables	Western area (70-72.5°W)		Eastern area (63-65°W)	
Chl_100km *vs.* SST	-0.69	(0)	-0.80	(0)
Chl_100km *vs.* ET	0.44	(+2)	0.40	(+2)
Chl_100km *vs.* EPcoast	0.21	(+1)	0.27	(0)
Chl_100km *vs.* ET+EPcoast	0.45	(+2)	0.44	(+2)
Chl_100km *vs.* EP100km	0.41	(+1)	0.38	(+1)
Chl_100km *vs.* ET+EP100km	0.50	(+1)	0.54	(+1)
SST *vs.* ET	-0.33	(+2)	-0.47	(+1)
SST *vs.* Epcoast	-0.20	(+1)	-0.24	(+1)
SST *vs.* ET+EPcoast	-0.34	(+2)	-0.51	(+1)
SST *vs.* EP100km	-0.38	(+1)	-0.38	(0)
SST *vs.* ET+EP100km	-0.41	(+2)	-0.59	(+1)

Our results show increased Chl concentrations during the mid-year upwelling in the southern Caribbean Sea (Figure 1.9b, Figure 1.10 a and b). In general, seasonal variations of Chl_100km were tightly coupled with upwelling (SST), except for the midyear Chl_100km peak at the western upwelling area, with concentrations as high as

the principal upwelling and coincident with the local annual wind speed maximum (~10 m s^{-1}, Figure 1.7). The disproportionally high magnitude of this midyear Chl_100km peak could be related to the enhanced turbulence at the western upwelling area. The averaged annual turbulence (calculated as a function of the cube of the wind speed, Chavez and Messié 2009) was 656 m^3 s^{-3}, which is at the top of the range found in the four principal upwelling ecosystems of the world's ocean (from 225 to 610 m^3 s^{-3}, Chavez and Messié 2009). At the end of June, mean turbulence peaked at 1000 m^3 s^{-3} in this area. Near-surface turbulence in nutrient-rich areas has a bottom-up effect on phytoplankton, increasing the relative importance of autotrophic components and favoring big-size phytoplankton (Arin *et al.* 2002, Peters *et al.* 2006). That seems to be caused by the suspension of phytoplankton cells in the euphotic zone (especially for the larger species) and by the turbulent transport of nutrients from the thermocline to the euphotic zone (Ghosal *et al.* 2000). This mechanism helps to increase Chl during the mid-year upwelling at the western upwelling area, when the seasonal Ekman depth reached its maximum (70 m depth during the second half of June, calculated as Messié *et al.* 2009).

The mid-year upwelling pulse in the southern Caribbean Sea causes a longer upwelling season (i.e. from December to August) and, therefore, a more prolonged period of active nutrient supply into the upwelling system than has been considered previously (December-May). This knowledge permits a better understanding of the impacts on the ecology of the organisms living within the upwelling system. For instance, off northeastern Venezuela the Spanish sardine *Sardinella aurita* accumulate energy during the upwelling season and reaches a maximum in the condition factor during August (Freón *et al.* 1997). The condition factor (the length-weight relationship) characterizes

the relative robustness of a fish; its variations reflect the degree of nourishment and the state of sexual maturity of the fish. The maximum in *S. aurita* condition factor is explained by the high phytoplankton biomass present until August due the mid-year upwelling; however, it could not be explained with the traditional view of the upwelling season ending in May.

1.5 Conclusions

A mid-year upwelling pulse was observed to be part of the annual upwelling cycle of the southeastern Caribbean Sea, as confirmed using 16 years of *in situ* data from the CARIACO Ocean Time-Series and historical sea-level records that date back to 1948. Fourteen years of satellite-derived Sea Surface Temperature (SST) reveal that the mid-year upwelling occurs along the entire southern margin of the Caribbean Sea from 61°W to 75.5°W. This short-lived event (~5 weeks) is not as cold as the principal upwelling event (~1.5°C warmer); yet the effect is that, in combination with the principal upwelling, cool waters (< 26°C) are present in the euphotic zone of the region for an extended period (~8 months).

Two large areas with the strongest upwelling signal in the southern Caribbean Sea were compared: the western (between 70-72.5°W) and the eastern upwelling areas (between 63-65°W); the latter located off northeastern Venezuela. The principal upwelling is synchronous in both upwelling areas, but the mid-year upwelling occurs later in time in the western area by up to approximately two weeks. Two reasons may be the cause of this lag: (a) One may be related to the wind cycle, which shows a lagged intensification between 70°W and 73°W. (b) Another possible cause is the propagation of perturbations along the Caribbean Current that could reach the western upwelling area in

about 12 days. It is possible that perturbations of the Caribbean Current during mid-year take place as the Caribbean Current intensifies. Further studies are necessary to clarify the mechanisms underlying the longitudinal lag in the mid-year upwelling.

The mid-year upwelling in the southern Caribbean Sea is concurrent with the development of a cooler band across the entire tropical North Atlantic Ocean during June, spanning from the Caribbean Sea to the northwestern African coast. This cooling disrupts the seasonal warming of the tropical North Atlantic Ocean, at a time when the Atlantic Ocean continues to warm up north of about 20ºN. The strong and concurrent negative SST anomalies observed along the southern Caribbean Sea coast indicate that the mid-year upwelling is not a signal imported from the Tropical Atlantic Ocean, but that it is a process that leads to localized upwelling. This basin-wide, mid-year cooling seems to be related to wind stress magnitude and wind stress curl patterns.

Although during the middle of the year winds measured on land along the coast are starting to decline at northeastern Venezuela coastal stations, there is a wind intensification along ~14°N offshore in the Caribbean Sea (the Caribbean Low Level Jet). This causes winds ~25km offshore to remain high (eastern area), and even peak (western area) during the northern summer, which produces high offshore Ekman Transport (ET) during the mid-year upwelling (2.4 and 3.8 m^3 s^{-1} per meter, respectively).

The Caribbean Sea has a year-round wind-curl latitudinal pattern that produces positive Ekman Pumping (EP) in the southern Caribbean Sea (open-sea upwelling) and negative EP in the northern Caribbean Sea (downwelling). This pattern is intensified during mid-year. Also during this period, positive EP increases along a band from the southern Caribbean Sea coast throughout the tropical North Atlantic Ocean. This process

enhances the mid-year upwelling by the lifting of isotherms in the open sea, and these waters feed the mid-year upwelling process. The acceleration of the Caribbean Current during summer could also be related to isotherm uplift during this period, which needs further investigation.

The mid-year upwelling increases coastal Chlorophyll-a (Chl) along the entire southern Caribbean upwelling system. Chl, averaged up to 100 km offshore (Chl_100km) of the western and eastern upwelling areas, shows peaks during the principal upwelling (0.58 and 1.27 mg m^{-3}, respectively) and also during the mid-year upwelling (0.62 and 0.91 mg m^{-3}, respectively). High concentrations of Chl_100km ($\geq$ 0.35 mg m^{-3}) were present during 8 and 9.5 months on average, for the western and eastern upwelling areas, respectively. In general, Chl_100km annual cycles at both areas were tightly coupled with upwelling (SST), except for the strong mid-year Chl_100km peak at the western upwelling area, with concentrations disproportionally higher compared to the SST cooling. This Chl_100km peak coincides with the local annual wind speed maximum ($\sim$10 m s^{-1}) and is likely enhanced by mixing of nutrients between the thermocline and the surface within the euphotic zone by enhanced turbulence in the deeper Ekman spiral (70 m) occurring during this time-frame.

Nearshore QuikSCAT winds indicate that the mid-year coastal upwelling is driven mostly ($\sim$90%) by offshore Ekman Transport due to alongshore winds. However, as a result of the inherent coastal gap ($\sim$25km) of QuikSCAT products, a higher contribution of Ekman Pumping closer to the coast is still possible. Open-sea EP upwelling might enhance the coastal upwelling by the shoaling of isopycnals on the waters feeding the coastal upwelling. This is supported by the alignment between the

41

annual cycles of EP100km and of the depth of the 22°C isotherm. Further studies are needed to understand the relationship between those two processes. Higher correlations of Chl_100km and SST with ET+EP100km, indicate the importance of offshore EP on the southern Caribbean Sea upwelling process.

1.6 Acknowledgements

1.7 References

Amador JA (1998) A climate feature of the tropical Americas: The trade wind easterly jet. *Tópicos Met. Oceanogr.*, 5(2): 91-102.

Aparicio R (2003) Review of the oceanographic characteristics on the continental shelf of northeastern Venezuela [*Revisión de las características oceanográficas de la plataforma nororiental de Venezuela*]. Pp. 171-200 *In*: Frèon P and Mendoza J

(eds.) The sardine (*Sardinella aurita*), its environment and exploitation in Eastern Venezuela. IRD (Colloques et Séminaires), Paris.

Arevalo-Martinez DL, Franco-Herrera A (2008) Características oceanográficas de la surgencia frente a la ensenada de Gaira, departamento de Magdalena, época seca menor de 2006. *Bol. Invest. Mar. Cost.*, 37 (2): 131-162.

Arin L, Marrasé C, Maar M, Peters F, Sala MM, Alcaraz M (2002) Combined effects of nutrients and small-scale turbulence in a microcosm experiment. I. Dynamics and size distribution of osmotrophic plankton. *Aquatic Microbial Ecology*, 29: 51-61.

Astor Y, Muller-Karger F, Scranton MI (2003) Seasonal and interannual variation in the hydrography of the Cariaco Basin: implications for basin ventilation. *Cont. Shelf Res.*, 23, 125-144.

Bakun A (1973) Coastal upwelling indices, west coast of North America, 1946-71. U.S. Dept. of Commerce, *NOAA Tech. Rep.*, NMFS SSRF-671, 103p.

Bakun A (1987) Monthly variability in the ocean habitat off Peru as deduced from maritime observations, 1953 to 1984. Pp. 46-74 *In*: Pauly D. and I. Tsukayama (Eds). The Peruvian Anchoveta and its Upwelling Ecosystem: Three Decades of Change, ICLARM Conference Proceedings, Instituto del Mar del Perú (IMARPE), Deutsche Gesellschaft für Technische Zusammenarbeit (GTZ) and International Center for Living Aquatic Resources Management (ICLARM). 351 pp.

Bernal G, Poveda G, Roldán P, Andrade C (2006) Patrones de variabilidad de las temperaturas superficiales del mar en la Costa Caribe Colombiana. *Rev. Acad. Colomb. Cienc.*, 30 (115): 195-208. 2006.

Brown OB, Brown JW, Evans RH (1985) Calibration of advanced very high resolution radiometer infrared observations. *J. Geophys. Res.,* 90:11667-11678.

Capet XJ, Marchesiello P, McWilliams JC (2004) Upwelling response to coastal wind profiles. *Geophys. Res. Lett.*, 31: L13311.

Castelao RM, Barth JA (2006) Upwelling around Cabo Frio, Brazil: The importance of wind stress curl. *Geophys. Res. Lett.*, 33: L03602.

Chavez FP, Messié MA (2009) comparison of eastern boundary upwelling ecosystems. *Progr. Oceanogr*. 83: 80–96.

Chereskin TK (1995) Direct evidence for an Ekman balance in the California Current. *J. Geophys. Res.,* 100: 18261–18269.

Fréon P, Ans L (2003) Comparison between coastal wind data,merchant ship data and sea surface temperaturein northeastern Venezuela [*Comparación de datos de viento costeros con vientos marítimos y temperatura superficial del mar en el nororiente de Venezuela*] Pp. 233-262 *In*: Fréon P and Mendoza J (eds.) The sardine (*Sardinella aurita*), its environment and exploitation in Eastern Venezuela IRD (Colloques et Séminaires), Paris.

Fréon P, El Khattabi M, Mendoza J, Guzman R (1997) Unexpected reproductive strategy of *Sardinella aurita* off the coast of Venezuela. *Mar. Biol.*, 128, 363–372.

Fukuoka J (1966) Coastal upwelling near Venezuela. 2. Certain periodicities of hidrographic conditions. *Bol. Inst. Oceanogr Univ. Oriente,* 5: 84-95.

Freilich MH, Dunbar RS (1999) The accuracy of the NSCAT 1 vector winds: Comparisons with National Data Buoy Center buoys. *J.Geophys. Res.*, 104, 11231–11246.

Ghosal S, Rogers M, Wray A (2000) The Turbulent Life of Phytoplankton. In: Studying Turbulence Using Numerical Simulation Databases VIII Proceedings of the 2000 Summer Program. Center forTurbulence Research (Stanford Univ.&NASAAmes Research Ctr.) VIII, 31–4.

Gill AE (1982) Atmosphere-Ocean Dynamics, Academic Press, San Diego, CA, 662 pp.

Gordon, A. L. 1967: Circulation of the Caribbean Sea. *J. Geophys. Res*., 72(24): 6207-6223.

Herrera L, Febres-Ortega G (1975) Kinematics of Me wind-generated velocity field in the surface waters off eastern Venezuela, Caribbean Sea. *Bol. Inst. Oceanogr. Univ. Oriente*, 14(2):165-186.

Hoffman RN, Leidner SM (2005) An introduction to the near-real-time QuikSCAT data. *Weather and Forecasting*, 20: 476-493

Hu C, Montgomery ET, Schmitt RW, Muller-Karger FE (2004) The dispersal of the Amazon and Orinoco River water in the tropical Atlantic and Caribbean Sea: observation from space and S-PALACE floats. *Deep-Sea Res. part II*, 51: 1151–1171.

Hu C, Muller-Karger F, Murch B, Myhre D, Taylor J, Luerssen R, Moses C, Zhang C, Gramer L, and Hendee J (2009) Building an Automated Integrated Observing System to Detect Sea Surface Temperature Anomaly Events in the Florida Keys. *IEEE Tran. Geosc. Remote Sens.,* 47(6):1607–1620.

Johns WE, Townsend TL, Fratantoni DM, Wilson WD (2002) On the Atlantic inflow to the Caribbean Sea. *Deep-Sea Res. part I*, 49: 211-243.

Locarnini RA, Mishonov AV, Antonov JI, Boyer TP, Garcia HE, (2006) World Ocean Atlas 2005, Volume 1: Temperature. S. Levitus, Ed. NOAA Atlas NESDIS 61, U.S. Government Printing Office, Washington, D.C., 182 pp. http://www.nodc.noaa.gov/OC5/WOA05/pr_woa05.html

Lozano-Rivera P (2009) Mapping suspended sediment concentration using the diffuse attenuation coefficient Kd and multi spectral and spatiotemporal images in Caribbean coastal waters of Colombia. Master of Sciences thesis, Enschede, ITC.

McClain EP, Pichel WG, Walton CC, Ahmad Z, Sutton J (1983) Multi-channel improvements to satellite-derived global sea-surface temperatures. *Adv. Space Res*., 2(6):43-47.

Mendo J, Pizarro L, Castillo S (1987) Monthly turbulence and Ekman transport indexes 1953 to 1985, based on local wind records from Trujillo and Callao, Peru. *In*: Pauly D, Tsukayama I (eds.) <u>The Peruvian anchoveta and its upwelling ecosystem: three decades of change</u>. *ICLARM Studies and Reviews*, 15:75–88.

Minnett PJ (991) Consequences of sea surface temperature variability on the validation and applications of satellite measurements. *J. Geophys. Res.,* 96(C10): 18475-18489.

Morrison J M, Nowlin Jr WD (1982) General Distribution of Water Masses Within the Eastern Caribbean Sea During the Winter of 1972 and Fall of 1973. *J. Geophys. Res.,* 87(C6): 4207–4229.

Muller-Karger FE, McClain CR, Fisher TR, Esaias WE, Varela R. (1989) Pigment distribution in the Caribbean Sea: observations from space. *Progr. Oceanogr.*, 23: 23-69.

Muller-Karger FE, Aparicio R (1994) Mesoscale Processes Affecting Phytoplankton Abundance in the Southern Caribbean Sea. *Cont. Shelf Res.,* 14(2-3): 199-221.

Muller-Karger FE., Varela R (1990). Influjo del Río Orinoco en el Mar Caribe: observaciones con el CZCS desde el espacio. *Mem. Soc. Cien. Nat. La Salle*, 50(133–134): 361-390.

Muller-Karger FE, Varela R, Thunell R, Scranton M, Bohrer R, Taylor G, Capelo J, Astor Y, Tappa E, Ho TY, Walsh JJ (2001) Annual cycle of primary production in the Cariaco Basin Response to upwelling and implications for vertical export. *J. Geophys. Res*., 106: 4527–4542.

Muller-Karger FE, Varela R, Thunell R, Astor Y, Zhang H, Luerssen R, Hu C (2004) Processes of coastal upwelling and carbon flux in the Cariaco Basin. *Deep-Sea Res. part II*, 51: 927–943

Muller-Karger FE, Fuentes-Yaco C (2000) Characteristics of Wind-Generated Rings in the eastern tropical Pacific Ocean. *J. Geophys. Res.*, 105: 1271-1284.

Odriozola AL, Varela R, Hu C, Astor Y, Lorenzoni L, Muller-Karger FE (2007) On the absorption of light in the Orinoco River plume. *Cont. Shelf Res.,* 27(10-11): 1447-1464

Oey LY (1999) A forcing mechanism for the poleward flow off the southern California coast. *J. Geophys. Res*., 104, 13529 -13539.

Oey LY, Ezer T, Wang DP, Fan SJ, Yin XQ (2006) Loop Current warming by Hurricane Wilma. *Geophys. Res. Let.,* 33: L08613

Oey LY, Ezer T, Wang DP, Yin XQ, Fan SJ (2007) Hurricane-induced motions and interaction with ocean currents. *Cont. Shelf Res.,* 27: 1249-1263.

Okuda T (1975) Características hidroquímicas del Golfo de Santa Fe y áreas adyacentes. *Bol. Inst. Oceanog. Univ. Oriente,* 14: 251-268.

O'Reilly JE, Maritorena S, Siegel D, O'Brien MC, Toole D, Mitchell BG, Kahru M, Chavez FP, Strutton P, Cota G, Hooker SB, McClain CR, Carder KL, Muller-Karger F, Harding L, Magnuson A, Phinney D, Moore GF, Aiken J, Arrigo KR, Letelier R, and Culver M (2000) Ocean color chlorophyll a algorithms for SeaWiFS, OC2, and OC4: Version 4. Pp: 9-23 *In*: Hooker SB and Firestone ER (eds.) <u>SeaWiFS Postlaunch Technical Report Series</u>, Volume 11, SeaWiFS Postlaunch Calibration and Validation Analyses, Part 3. NASA, Goddard Space Flight Center, Greenbelt, Maryland.

Peters F, Arin L, Marrasé C, Berdale Et, Sala MM (2006) Effects of small-scale turbulence on the growth of two diatoms of different size in a phosphorus-limited medium. *J. Mar. Syst.,* 61: 134–148.

Peterson LC, Haug GH (2006) Variability in the mean latitude of the Atlantic Intertropical Convergence Zone as recorded by riverine input of sediments to the Cariaco Basin (Venezuela). *Palaeogeogr. Palaeoclimatol. Palaeoecol.,* 234(1): 97-113.

Pickett MH, Paduan JD (2003) Ekman transport and pumping in the California Current based on the U.S. Navy's high-resolution atmospheric model (COAMPS). *J. Geophys. Res*., 108(C10): 3327.

Pickett M H, Tang W, Rosenfeld LK, and Wash CH (2003) QuikSCAT satellite comparisons with nearshore buoy wind data off the U.S. west coast. *J. Atmos. Oceanic Technol*., 20: 1869–1879.

Restrepo, J. D., & Kjerfve B. (2000). Magdalena River: Interannual variability (1975-1995) and revised water discharge and sediment load estimates. *J. Hydrology*. 235: 137-149.

Richards F (1960) Some chemical and hydrographic observations along the north coast of South America. *Deep-Sea Res*., 7: 163-182.

Richardson PL (2005) Caribbean Current and eddies as observed by surface drifters. *Deep-Sea Res.,* 52: 429-463.

Rueda-Roa D (2001) Variabilidad temporal de la distribución vertical de la biomasa fitoplanctónica en la Cuenca de Cariaco y sus relaciones con los aspectos hidrográficos del estrato superficial (1996-1998). Master Thesis to obtain the title of M.Sc. in Marine Sciences, Univ. de Oriente, 190 pp.

Scranton MI, McIntyre M, Taylor GT, Muller-Karger F, Fanning K, Astor Y (2006) Temporal variability in the nutrient chemistry of the Cariaco Basin, Pp 139–160 *In*: Neretin LN (ed.) Past and Present Marine Water Column Anoxia, NATO Sci. Ser. IV (64): 139–160, Springer, New York.

Smith RL (1968) Upwelling. *Oceanogr Mar. Biol. Ann. Rev*., 6: 11–46.

Smith R L (1981) A comparison of the structure and variability of the flow field in three coastal upwelling regions: Oregon, Northwest Africa, and Peru. Pp. 107–118 *In*: Richards FA (ed.) Coastal Upwelling, Amer. Geophys. Union.

Strong AE, McClain E (1984) Improved Ocean Surface Temperatures From Space-Comparisons With Drifting Buoys. *Bull. Am. Meteorol. Soc*., 85: 138.

Tomczak M (1998): Upwelling dynamics in deep and shallow water; *In*: Shelf and Coastal Oceanography, chapter 6, accessed on September 10 2011 at: http://www.es.flinders.edu.au/~mattom/ShelfCoast/chapter06.html

Thunell R, Benitez-Nelson C, Varela R, Astor Y, Muller-Karger F (2007) Particulate organic carbon fluxes along upwelling-dominated continental margins: Rates and mechanisms. *Global Biogeochem. Cycles*, 21: GB1022,

US Army Corps of Engineers. (1998). Water Resources Assessment of Guyana. Mobile District & Topographic Engineering Center, US.

Walton CC (1988) Nonlinear Multichannel Algorithms for Estimating Sea Surface Temperature with AVHRR Satellite Data. *J. Appl. Met.*, 27(2): 115-124.

Whyte FS, Taylor MA, Stephenson TS, Campbell JD (2008) Features of the Caribbean low level jet. *International J. Climatol.*, 28(1) 119-128.

Varela R., Carvajal F., Muller-Karger F (2003). The phytoplankton of the continental shelf of northeastern Venezuela [*El fitoplancton en la plataforma nororiental de Venezuela*]. Pp. 263-294 *In*: Frèon P and Mendoza J (eds.) <u>The sardine (*Sardinella aurita*), its environment and exploitation in Eastern Venezuela</u>. IRD (Colloques et Séminaires), Paris.

CHAPTER TWO

Southern Caribbean Upwelling System: characterization of sea surface temperature, Ekman forcing and chlorophyll concentration.

2.1 Abstract

The southern Caribbean Sea experiences wind driven coastal upwelling from about 61° to 75.5°W along approximately 11-12°N. Two particular regions show stronger upwelling: the 'eastern area' between 63-65°W in the eastern Caribbean Sea, and the 'western area' between 70-73°W in the central Caribbean. These two areas contain more than 95% of the small pelagic biomass of the whole southern Caribbean upwelling system, but with important differences between them (78% and 18% for the eastern and western area, respectively). To understand those biological differences, we looked into the upwelling dynamics variations along southern Caribbean upwelling system. The seasonal cycles of sea surface temperature (SST), chlorophyll-*a* (Chl) and wind were examined using synoptic satellite observations along the coastline of the southern Caribbean Sea, beside of climatological hydrographic data from the NOAA World Ocean Atlas 2005. Both the western and eastern upwelling areas showed temperature minima (SST< 26°C) for over six months every year (6.9 and 8.5 months, respectively). The eastern area featured the lowest average SST (25.24°C) and the highest average Chl (1.65 mg m $^{-3}$) in the southern Caribbean upwelling system. The average wind intensity in the

eastern area was 6.12 m s $^{-1}$, and the 22ºC isotherm depth was on average 85 m. The western area had stronger average winds (8.23 m s $^{-1}$) but the 22ºC isotherm was deeper (115 m). This led to an average SST of 25.53°C and more moderate average Chl (1.15 mg m $^{-3}$). Chlorophyll cycles in the entire region generally followed an inverse and coherent relationship with SST. However, the western area had a disproportionately high mid-year Chl maximum concurrent with the wind annual maximum (~10 m s $^{-1}$). This is likely related to localized vertical nutrient flux as a result of the thermocline erosion caused by wind-driven turbulence during this period. The differences in the upwelling dynamics between the eastern upwelling area (medium wind speeds, shallower offshore isotherms, slightly cooler SSTs and higher phytoplankton biomass) compared to the western upwelling area (higher wind speeds, deeper isotherms, slightly warmer SSTs and lower phytoplankton biomass) helped explain the higher fish productivity of the eastern area. We hypothesize that the factors that most inhibits fish production in the western upwelling area are the high level of turbulence, by inducing strong dispersion of plankton and larvae, and the stronger offshore transport, by causing offshore loss of eggs and larvae and the export of nutrients before they are fully used within the coastal upwelling system.

2.2 Introduction

The Southern Caribbean Sea (Figure 2.1) experiences strong wind-driven coastal upwelling between approximately January and May (Richards 1960, Herrera and Febres-Ortega 1975, Muller-Karger and Aparicio 1994, Muller-Karger *et al.* 2004). The southern Caribbean upwelling system extends along the continental margin between about 61°W

and 74°W from Trinidad and Tobago to Colombia. At least 13 major upwelling foci have been documented in this region using satellite-derived sea surface temperature (SST) (Castellanos *et al.* 2002).
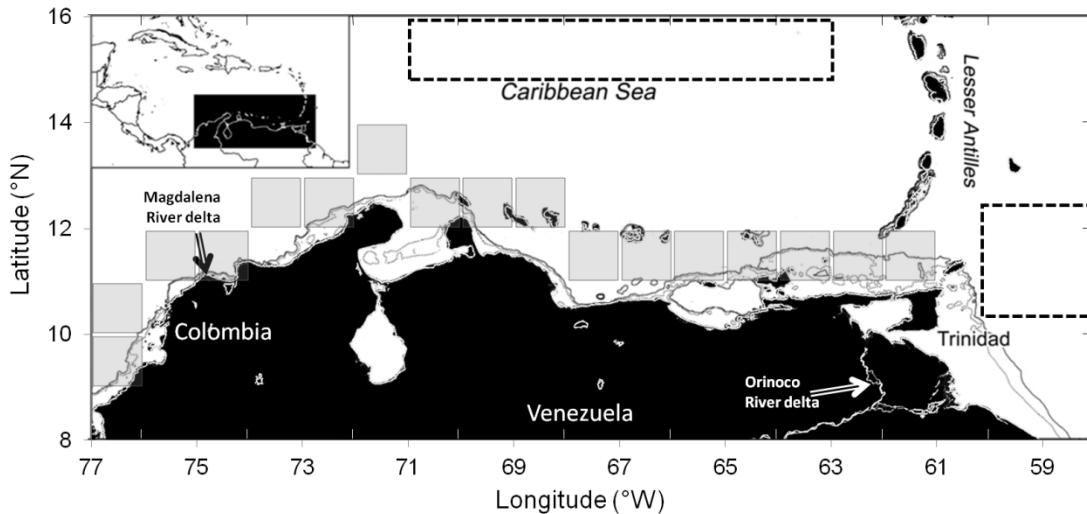
Figure 2.1. Map of the study region (8-16ºN and 58-77º W). The 100 and 200 m isobaths are shown in increasing shades of gray. SST data was extracted from the central-eastern Caribbean Sea (top dashed rectangle, 15-16 ºN and 63-71 ºW) and the northwestern equatorial Atlantic Ocean (right dashed rectangle, 10.5-12.5ºN and 58-60ºW). Grey squares mark areas where climatological temperature profiles were extracted from the 1x1 degree World Ocean Atlas 2005.

Two particular regions show the cooler upwelling (Rueda-Roa *et al.* first chapter in this dissertation): the 'eastern upwelling area' located off northeastern Venezuela between 63°W to 65°W in the eastern Caribbean Sea, and the 'western upwelling area' which is located off northeastern Colombia and northwestern Venezuela between 70°W to 73°W in the central Caribbean. Acoustic fisheries surveys conducted in the southern Caribbean between 61°W and 74.5°W estimated a total biomass of small pelagics of 1,580,000 tonnes (Stromme and Saetersdal 1989) which includes clupeids, anchovies,

carangid, scombrids and barracudas. Nearly all this biomass (95%) is concentrated in the eastern and western upwelling areas; however, the eastern area had a disproportionally higher biomass of small pelagics (78%).

Synoptic satellite-derived products allow construction of time series of along-shore wind stress and wind-curl, which force the upwelling process. The response of the system was examined using sea surface temperature (SST) and phytoplankton biomass (satellite Chlorophyll-a concentration or Chl). The seasonal cycles of SST, Chl and wind products were studied along the entire southern Caribbean upwelling system showing high regional variability. In this study we focused on the impacts of the wind on upwelling, fully recognizing that geostrophic processes associated with the Caribbean Current could also play an important role in the setup of the thermocline along the southern margin of the Caribbean Sea. We found important differences in the wind forcing and response of the upwelling between the eastern and western upwelling areas, which help to explain their differences in fish biomass.

2.3 Methods

2.3.1 Sea Surface Temperature

High resolution (pixel size 1km, resolution ~1 km^2) Sea Surface Temperature (SST) satellite images collected by the Advanced Very High Resolution Radiometer (AVHRR, National Oceanic and Atmospheric Administration/NOAA) were used to construct weekly SST means over the period 1994-2008 for the southern Caribbean Sea (8º-16ºN, 77º-58ºW). Images were collected using a ground-based L-band antenna located at the University of South Florida (St. Petersburg, Florida, U.S.A.). SST was

derived using the Multi-Channel Sea Surface Temperature split-window techniques (Walton 1988; Strong and McClain 1984; McClain *et al.* 1983). The nominal accuracy of AVHRR SST retrievals is in the range of ±0.3 to ±1.0 °C (Brown *et al.* 1985, Minnett 1991). AVHRR imagery contains false cold pixels due to cloud contamination; therefore, a cloud filter similar to that of Hu *et al.* (2009) was used to improve data quality. The filter was based on a weekly climatology derived for each pixel. All daily values in the time series larger than two standard deviations above the climatology or one standard deviation below were discarded. These values were selected by trial and error and work well for the tropical SSTs in the Caribbean Sea where the upwelled waters produce the coolest seasonal SST signal in the area. The filtered daily images were then used to calculate new weekly composites and a new long-term weekly climatology.

To analyze the variability of SST along the continental margin of the southern Caribbean Sea, SST time series were extracted from 172 points distributed along the coast, approximately 10 km from the coast from Trinidad to the central coast of Colombian Caribbean Sea (Figure 2.2b). Each point represented an average of the SST in a 5x5 pixel box (~25 km^2) centered at each station.

2.3.2 Chlorophyll-a

We used high resolution (pixel resolution ~1 km^2) satellite chlorophyll-*a* (Chl), produced with the default NASA chlorophyll algorithm (O'Reilly *et al.*, 2000) from images collected by the ocean color scanner Sea-viewing Wide Field-of-view Sensor (SeaWiFS). Data were downloaded for the study area from NASA and mapped to a uniform spatial grid using Matlab routines provided by NASA. Weekly averages of Chl

were calculated from January 1998 to December 2009. Because chlorophyll is approximately log-normally distributed, all calculations were made using log[Chl].

Riverine discharge can produce a very strong signal in the satellite derived Chl product because of high concentrations of CDOM (Colored Dissolved Organic Matter). The SeaWiFS default Chl algorithm fails in turbid coastal waters with high concentrations of CDOM, producing erroneous high estimates of pigment concentration (Carder *et al.* 1999). The southern Caribbean Sea is influenced by two large rivers (Orinoco and Magdalena, Figure 2.1) and several other small rivers. In order to separate the influence of upwelling from the freshwater discharge on Chl levels, it was used a linear regression analysis between weekly SST and log[Chl] time series (1998-2009, Figure 2.6a). A weekly Chl climatology was calculated and the coastal values were extracted at the same 172 coastal stations used for SST (Figure 2.2b); but, to obtain sufficient valid pixels, it was used a larger box than that used for SST (a 13x13 pixel box centered at each station).

2.3.3 Wind

Synoptic surface ocean wind observations from the NASA QuikSCAT satellite for the period 1999-2008, gridded to a spatial resolution of 0.25 degrees, were obtained from the Physical Oceanography Distributed Active Archive Center (PO.DAAC) at the NASA Jet Propulsion Laboratory. Away from coastal zones, scatterometer wind retrievals are estimated to be accurate to better than 2 m s^{-1} in speed and 20° in direction, similar to the accuracy of *in situ* buoy measurements (Freilich and Dunbar 1999). Due to contamination by radar backscatter from land in the antenna side lobes, there is at least a

~25-30 km gap between the QuikSCAT measurements and the coast (Hoffman and Leidner 2005).

QuikSCAT data were used to calculate long-term average wind patterns, Ekman Transport (ET) due to alongshore winds and Ekman Pumping (EP) due to the wind curl over the Caribbean Sea and the Tropical Atlantic Ocean (5-30°N and 10-85°W). Daily zonal and meridional QuikSCAT wind speed components (u,v) were used to estimate the wind stress components (τx , τy and τxy, Bakun 1973) using a drag coefficient which includes curve fits for low and high wind speeds (Oey *et al.* 2006 and 2007). Alongshore wind speed, in a direction parallel to the direction of the nearest coast, was computed to examine coastal ET (Castelao and Barth 2006, see details in appendix A). This allowed computation of the alongshore wind stress (Mendo *et al.* 1987) and the cross-shore ET (Chereskin 1995) at each QuikSCAT grid point closest to the coast. Positive/negative values indicate offshore/onshore ET (upwelling/downwelling). EP was calculated based on wind curl estimates (curl_τxy, Smith 1968) computed from weekly means of wind stress, using one pixel to the east/west and to the north/south from each QuikSCAT grid point. Positive wind curl means counterclockwise vorticity that induces upward EP. Time series of the suite of nearshore wind products were extracted from the pixels closest to the coast between longitudes 61°-77°W. More details on the equations used for the wind products are presented in Appendix A.

2.4 Results and Discussion

2.4.1 Upwelling foci of the southern Caribbean Sea:

SST imagery shows that the southern Caribbean upwelling system extends from the northeastern tip of Trinidad (61°W) to Cartagena, Colombia (75.5°W, Figure 2.2 and Figure 2.3). A total of 21 recurrent coastal upwelling foci were found (f1 to f21, Figure 2.3). The foci locations are consistent with the 13 major upwelling foci documented by Castellanos *et al.* (2002) using SST imagery for 1996. Our longer time series helped better resolve the location of adjacent foci and identify two additional foci (f1 and f2) in the western area. Location names for each upwelling focus are presented in Appendix B.

The zone of active coastal upwelling has a characteristic offshore distance determined by the internal Rossby radius, R = square root $(g \, \Delta\rho/\rho \, h) \, / f$, which depends of the mean depth ($h = 35$ m), the gravity ($g = 9.81$ m s^{-2}) adjusted by the ratio between local vertical density differences and the density ($\Delta\rho/\rho$: 0.9 kg m^{-3} / 1025 kg m^{-3}, at the CARIACO time series -between 0 and 35m-), and the coriolis value ($f = 2.9\text{x}10^{-5}$ s^{-1}). The southern Caribbean upwelling system showed active coastal upwelling, observed in the satellite SST images as a band of cold water adjacent to the coast (Figure 2.3), within the internal Rossby radius for this region (~ 19 km).

To examine the similarity in timing and upwelling intensity between the foci, it was applied a hierarchical cluster analysis (Pang-Ning *et al.* 2005) to SST time series extracted from each upwelling focus (boxes depicted in Figure 2.3). SST time series were also included from the central-eastern Caribbean Sea and from the northwestern equatorial Atlantic Ocean (see Figure 2.1). Figure 2.4 shows that upwelling foci located adjacent to each other have coherent upwelling cycle. A similarity index threshold of 0.1

Figure 2.2. (a): Seasonal cycle in satellite sea surface temperature (SST) along the coast of the southern Caribbean Sea upwelling system (isotherms contours every 1°C), calculated with long-term weekly SST means (1994-2008, isotherms contours every 1°C). SST time series were extracted at 172 coastal stations approximately 13 km offshore, shown in the map (b) as red dots. Two regions of interest were compared: the west upwelling area (70-73°W) and the east area (63-65°W) highlighted by black dotted line under Figure 2.(a).
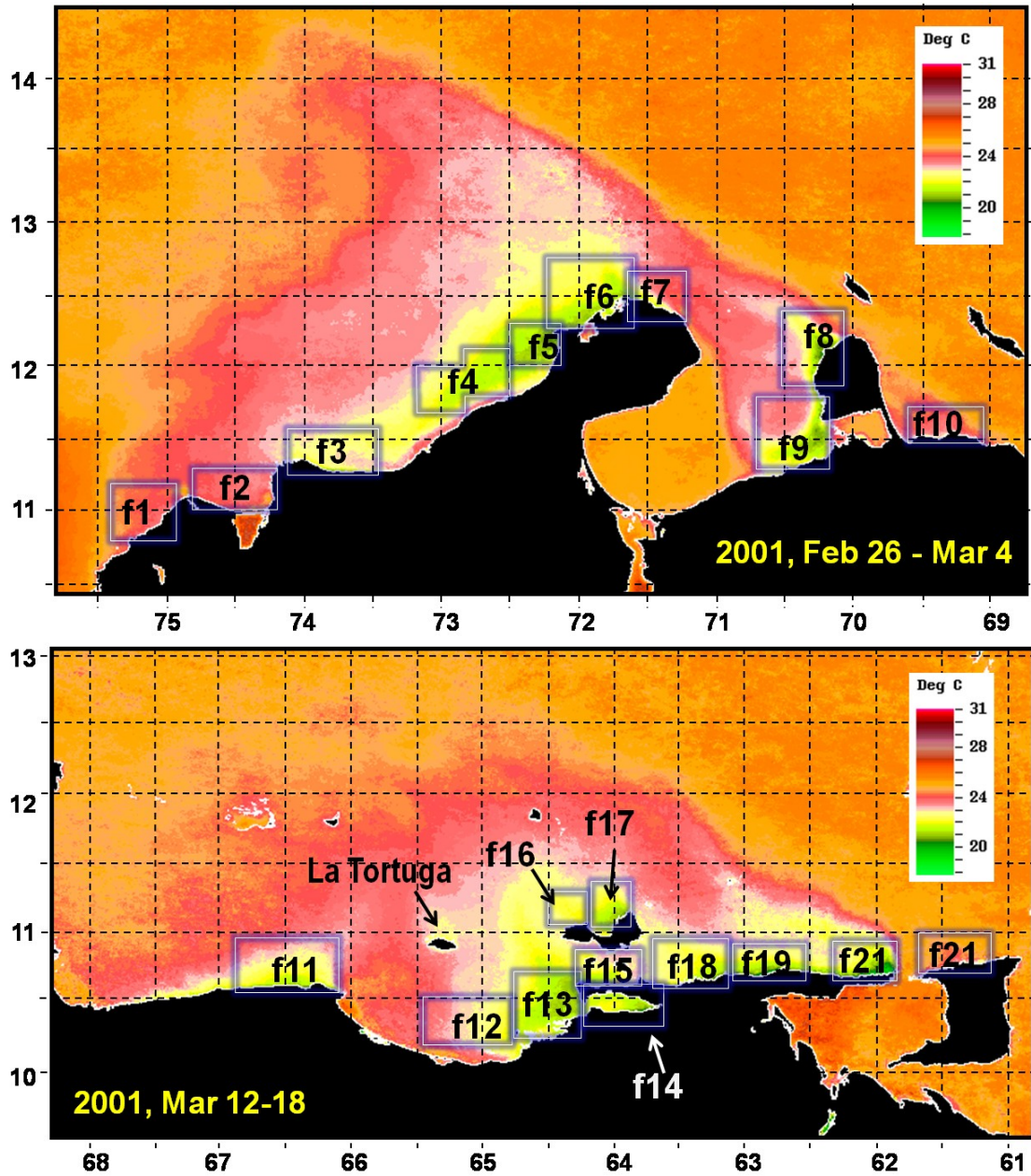
Figure 2.3. Location of the upwelling foci along the southern Caribbean upwelling system (top: western region, bottom: eastern region). The squares show the area used to extract SST time series and statistics for each upwelling focus (e.g. see Figure 2.5 and Appendix C).

58

shows seven groups within three larger subdivisions (Spearman rank correlation r=0.85): (a) two groups in the westernmost region from Barranquilla to Sta. Marta (f1-2 and f3), located close to the Colombia-Panama gyre, showed the highest dissimilarity with the other foci; (b) one upwelling focus in the easternmost region off Trinidad (f21) showed high similarity with the western equatorial Atlantic Ocean annual cycle; and (c), four groups in the central area showed SST cycles similar to those of the central-eastern Caribbean Sea. Within them, two groups include numerous upwelling foci with the lowest SST, and hereafter we refer to these as the western upwelling area (f4-9) located between 70-73°W, and the eastern upwelling area (f12-18), located between 63-65°W.

The zone of active coastal upwelling has a characteristic offshore distance determined by the internal Rossby radius, R = square root ($g\ \Delta\rho/\rho\ h$) / f, which depends of the mean depth (h = 35 m), the gravity (g = 9.81 m s^{-2}) adjusted by the ratio between local vertical density differences and the density ($\Delta\rho/\rho$: 0.9 kg m^{-3} / 1025 kg m^{-3}, at the CARIACO time series -between 0 and 35m-), and the coriolis value (f = 2.9x10^{-5} s^{-1}). The southern Caribbean upwelling system showed active coastal upwelling, observed in the satellite SST images as a band of cold water adjacent to the coast (Figure 2.3), within the internal Rossby radius for this region (~ 19 km).

To examine the similarity in timing and upwelling intensity between the foci, it was applied a hierarchical cluster analysis (Pang-Ning *et al.* 2005) to SST time series extracted from each upwelling focus (boxes depicted in Figure 2.3). SST time series were also included from the central-eastern Caribbean Sea and from the northwestern equatorial Atlantic Ocean (see Figure 2.1). Figure 2.4 shows that upwelling foci located adjacent to each other have coherent upwelling cycle. A similarity index threshold of 0.1

shows seven groups within three larger subdivisions (Spearman rank correlation r=0.85): (a) two groups in the westernmost region from Barranquilla to Sta. Marta (f1-2 and f3), located close to the Colombia-Panama gyre, showed the highest dissimilarity with the other foci; (b) one upwelling focus in the easternmost region off Trinidad (f21) showed high similarity with the western equatorial Atlantic Ocean annual cycle; and (c), four groups in the central area showed SST cycles similar to those of the central-eastern Caribbean Sea. Within them, two groups include numerous upwelling foci with the lowest SST, and hereafter we refer to these as the western upwelling area (f4-9) located between 70-73°W, and the eastern upwelling area (f12-18), located between 63-65°W. The upwelling foci SST cycle showed a semiannual cycle (Figure 2.5). The primary cooling period (principal upwelling) occurred between December and April, typically showing 2-4 upwelling pulses and peaking during February-March. Around May, there typically was a slight increase in SST, followed by a secondary cooling in June-August (midyear upwelling). The highest SST values were observed in September-October (upwelling relaxation). With exception of f1-f2, the upwelling foci showed cooler SSTs than the central Caribbean Sea by 1-2°C year-round (Figure 2.5, Appendix C). The western limit of the upwelling system was 75.5°W. Further west (i.e. to 77°W) the annual cycle of coastal SST had a brief SST minimum during mid-March (~26°C) and a broad maximum between mid-April to January (> 27°C), with the highest values around June-August (> 28°C) and an annual average of 27.4°C.

Of the upwelling foci studied, Barranquilla and Ciénaga, on either side of the Magdalena River delta (f1 and f2, respectively) had the shortest upwelling season (Jan-March), the weakest SST decrease, and the highest annual SST means (Figure 2.5a,
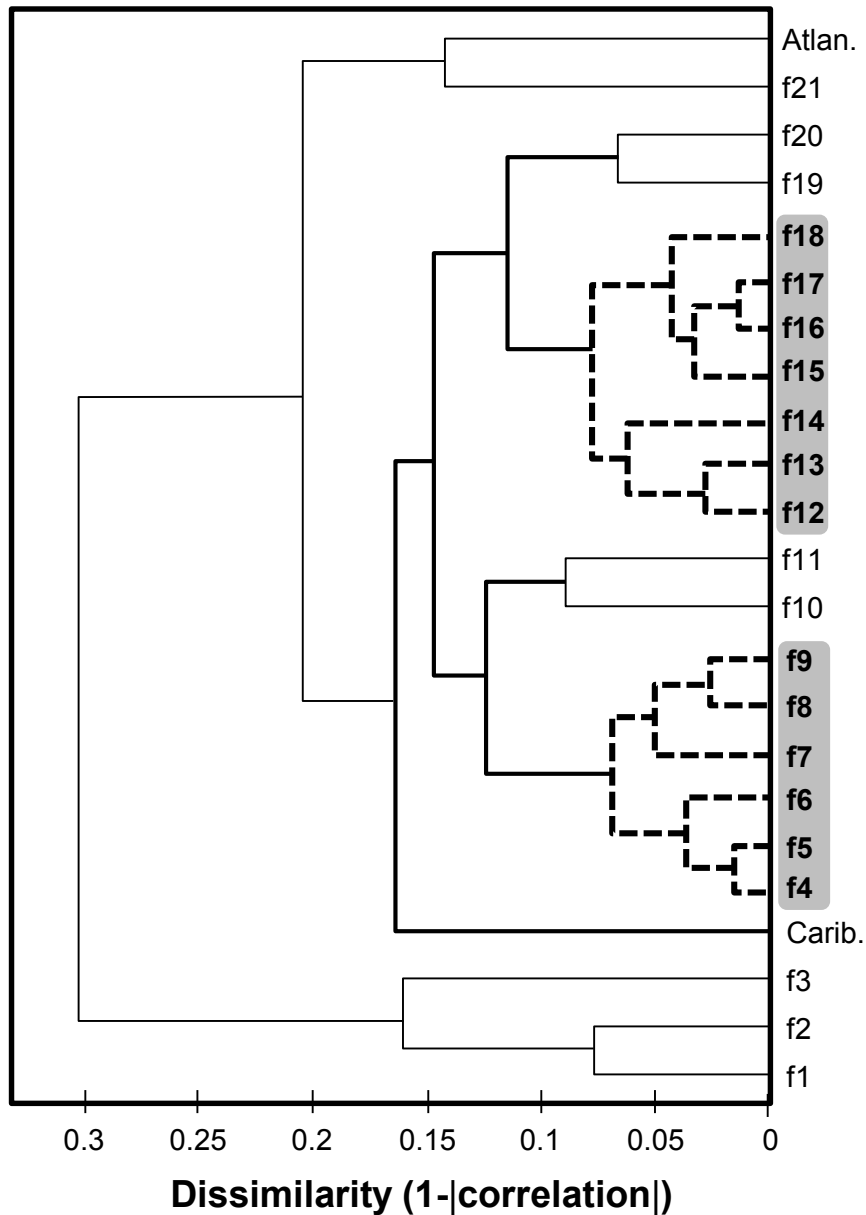
Figure 2.4. Dendrogram (Spearman rank correlation r=0.85) showing similarities in the SST seasonal cycles among the different upwelling foci (Figure 2.3 and Figure 2.5) and two open sea areas in the central-eastern Caribbean Sea and the western Tropical Atlantic Ocean (Figure 2.1). Upwelling foci are in longitudinal order from the west (bottom) to the east (top). Foci with SST cycle similar to that of the Caribbean Sea (bold lines) showed cooler SST. Two homogeneous areas (dashed lines and shaded names) were contrasted: the western (f4 to f9) and the eastern upwelling areas (f12 to f18)

Appendix C). Santa Marta (f3) had relatively small annual SST amplitude (2.8°C) and showed the most prolonged mid-year upwelling of the region (Figure 2.5a). The most likely cause of the weaker upwelling in this area is the added water column stability caused by the Magdalena River discharge and the proximity of the warm and deep Panama-Colombia Gyre (Bernal *et al.* 2006). The upwelling off the northern coast of Trinidad Island (f21) exhibited the second warmest principal upwelling (~25°C, Figure 2.5c, Appendix C). This focus had waters 0.3-0.9°C cooler than the western equatorial Atlantic Ocean, but during the mid-year upwelling the difference was minimal (~0.15°C). Although not studied here, some of the islands located in the southern Caribbean Sea within about 150 km of the coast of Venezuela also showed upwelling activity. An example is La Tortuga Island (i.e. 10.9°N-65.3°W; Figure 2.3).

The central continental margin area experienced the coolest SST of the whole southern Caribbean upwelling system. Upwelling foci from the western area (f4-9) had warmer mean SSTs than those in the east (f12-f18, Figure 2.5b). Their SST cycles differed by up to 1°C between mid-March to mid-July and between October to November (significant differences with t-test, p< 0.05). The strongest cooling due to the upwelling started at both places simultaneously during February with similar SSTs, but it remained cooler in the eastern upwelling area until July. The mid-year upwelling cooling also started simultaneously in both the western and eastern areas; however, the western mid-year SST minimum lagged the one in the east by 1-2 weeks (Figure 2.5b, see also Figure 2.2). During upwelling relaxation (September-October) the western upwelling area presented the highest SSTs compared to the other upwelling foci (with exception of f1-2). The highest SST annual amplitude in the western area occurred at foci f5 and f9 (~4°C,
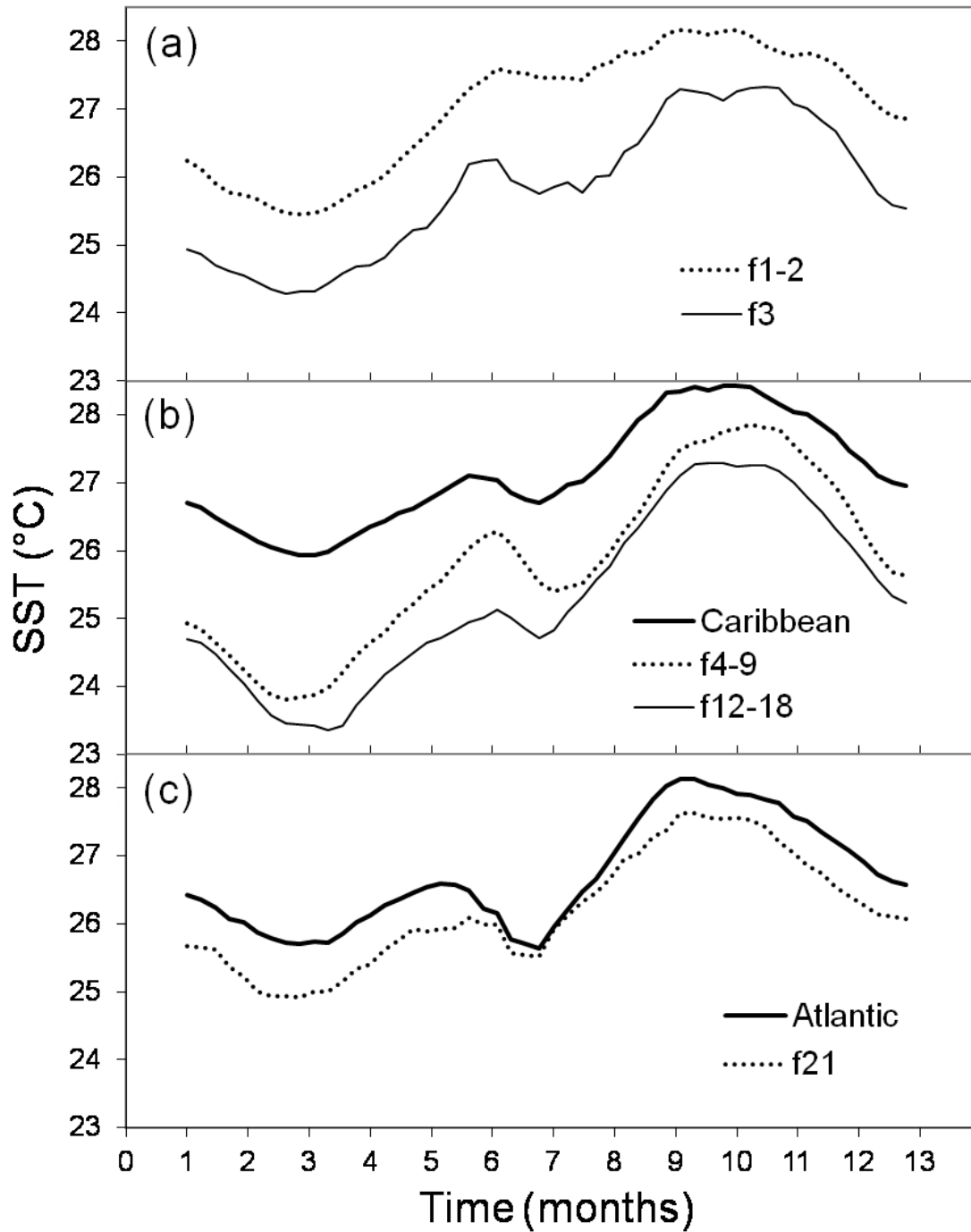
Figure 2.5. Comparison of the long-term seasonal SST cycles for upwelling foci clusters (Figure 2.4) from three large subdivisions of the Southern Caribbean Upwelling System: (a) west of 73.5°W; (b) western (70-73°W) and eastern (63-65°W) upwelling areas; and (c) east of 61.7°W. SST cycles from the central-eastern Caribbean Sea and the west Tropical Atlantic Ocean are presented for comparison (refer to Figure 2.1 and Figure 2.3 for locations).

Appendix C). Puerto Cumarebo (f10) and Cabo Codera (f11) are transition zones that experienced upwelling cycles with characteristics shared between the western and eastern areas.

The eastern upwelling area experienced the lowest SST values of the region all year round and a longer principal upwelling (Figure 2.5b). In this region, the Gulf of Cariaco (f14) experienced the coolest SSTs (Appendix C). This is caused by the connection of the Gulf of Cariaco to deeper Caribbean Sea waters and the Cariaco Basin through a submarine canyon (Caraballo 1982). The f19-20 cycle was similar to that of the eastern group, but with cooler temperatures during the secondary upwelling and the relaxation period (Appendix C).

In most of the upwelling foci examined along the southern Caribbean, the coldest waters occur within 1-3 km of the coast and the direction of the surface upwelling plume was roughly 45° to the right of the prevailing Trade Wind. This is typical for coastal ET on "deep water conditions" (Tomczak 1998a). At Punta Cardón (f9, Figure 2.3) where depths were > 30 m upwelling plumes turned 45° to the right of the wind; however, close to the coast where depths were < 15 m, upwelling plumes extended in the direction of the wind (to the west). This later is consistent with Tomczak's (1998b) "inner zone conditions" where ET is more aligned with the direction of the wind in shallower waters. At Rio Hacha (f4, Figure 2.3), the surface upwelling plume was 45° to the right of the wind 7-13 km offshore. However, closer to shore a band of warm water was persistently seen year round. This area is very shallow, and cooler temperatures were observed only farther offshore beyond the 10 m isobath. A similar situation, although less prominent,

was observed in the area immediately to the south of the central and western Cariaco Basin (focus f12, Figure 2.3).

2.4.2 Chlorophyll cycle:

There were strong inverse correlations between Chl vs. SST (Pearson correlation coefficient, $r < -0.4$, $p < 0.01$) in the upwelling plumes (dark blue areas in Figure 2.6a). The higher phytoplankton biomass in the plumes is stimulated by nutrient availability in upwelled waters (Muller-Karger *et al.* 2004). Direct and weaker SST-Chl correlations ($r < 0.4$) were found in regions with freshwater influence (e.g. zones 1 to 5 in Figure 2.6a). In the Orinoco River plume (zone 1 in Figure 2.6a) satellite Chl is overestimated because of high CDOM concentrations (Muller-Karger *et al.*, 1989; Muller-Karger and Aparicio 1994; Varela *et al.* 2003; Odriozola *et al.*, 2007).

The surface area of the upwelling plumes with high Chl and of the high CDOM river discharge changes seasonally, with one or the other dominating the region in different seasons. We established the seasonal boundary or front between the eastern upwelling plume and the Orinoco River plume using the location where no significant SST-Chl correlation was observed at $p > 0.01$ (indicated in grey color in Figure 2.6a). Around the Orinoco discharge region, this no-correlation-area coincided with the spatial expansion-contraction of the seasonal boundary between the upwelling plume and the river plume into the Caribbean Sea traced manually by Muller-Karger and Varela (1990). Low negative correlations (> -0.3, light blue) point to transition areas, where the Chl signal from upwelling is still influenced by freshwater in both time and space. For
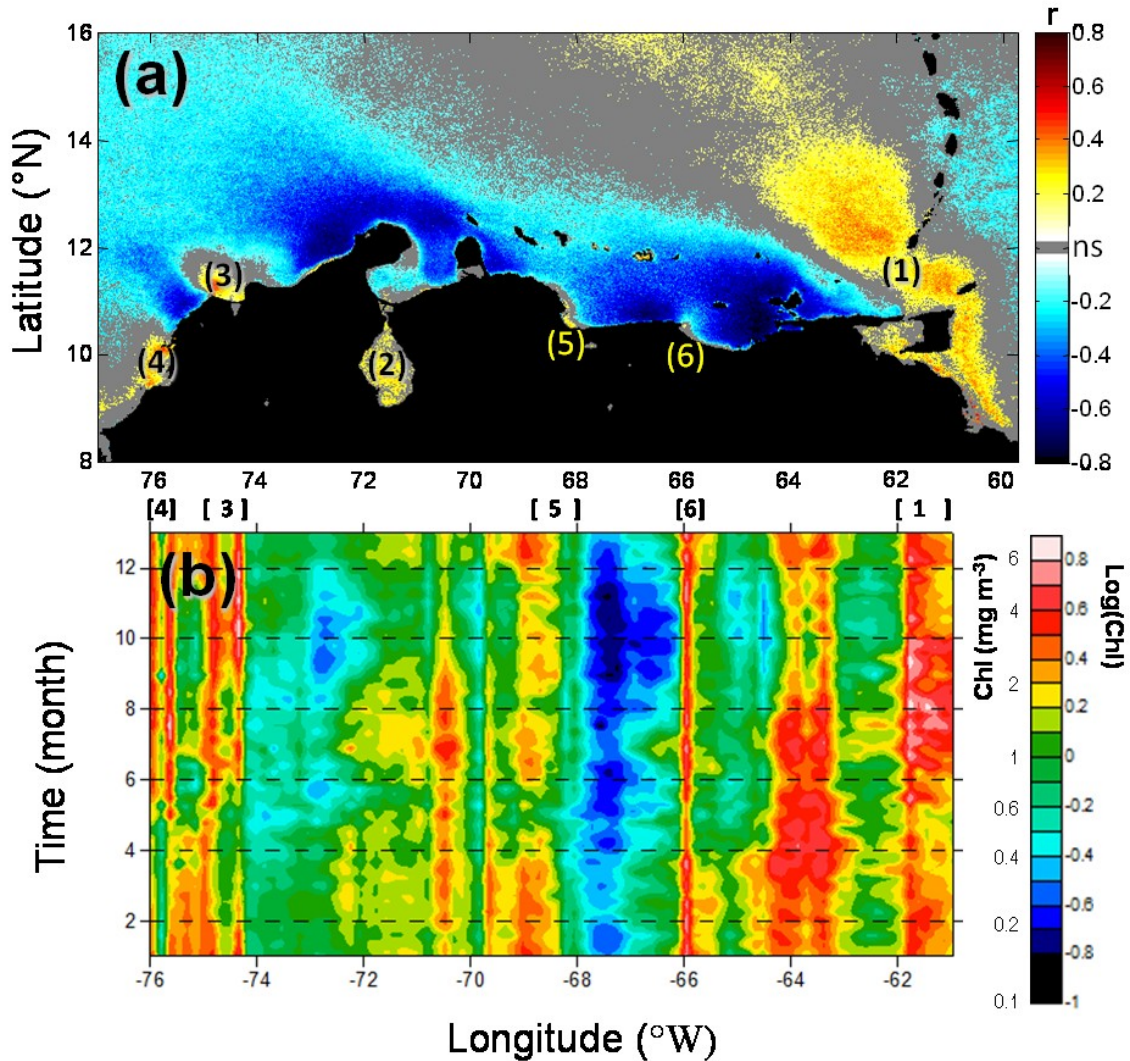
Figure 2.6. Correlation coefficient (r) between weekly time series of satellite SST and log Chl (top, a) and seasonal cycle of long-term weekly Chl means (bottom, b) for the period 1998-2009. (a): Non-significant values (p> 0.01) are masked in grey. Upwelling areas showed strong inverse correlations with phytoplankton biomass, while areas with freshwater influence showed a direct correlation with Chl caused by their high content in CDOM. The principal fresh water sources that influenced the satellite Chl were: (1) Orinoco River, (2) Maracaibo Lake, (3) the Magdalena River and Ciénaga Grande, and (4) the Sinú river and Canal del Dique. Other areas showed contamination of the Chl product very close to the coast due to smaller local freshwater discharges (5: Tocuyo River, and 6: Tuy River). (b): Time series were extracted at the same coastal stations as for SST (Figure 2.2b). On top of panel 'b' numbers in brackets show the locations where river discharge occurs, as shown in panel 'a'. The approximate extent of the coastal impact of the plume is indicated by the width of the brackets around these numbers.

example, the correlation map (Figure 2.6a) showed high interference of the outflow from Maracaibo Lake between 70° and 71.2°W (Figure 2.2b).

In areas without riverine influence, coastal Chl maxima were coherent with the upwelling cycle (Figure 2.2a and Figure 2.6b). There was a prolonged Chl maximum between December-April, and a second shorter maximum between June-July. Annual means (first peak/second peak) for the west and east upwelling areas were 1.15 (1.33/1.35) mg m^{-3} and 1.65 (3.19/2.05) mg m^{-3}, respectively. The western and eastern upwelling areas had phytoplankton biomass $\geq$ 1 mg Chl m^{-3} during 7.5 and 10 months, respectively.

Although in the west upwelling area the mid-year upwelling SST minimum was ~1.5°C warmer than the principal upwelling (Figure 2.5b), this area had similar Chl maxima during both periods. Visual analysis of the Chl time series maps confirmed that in this area the mid-year Chl peak was not caused by advection of freshwater discharges but originated at the upwelling cores.

Time series of log[Chl] and SST along the coast (1998-2009) showed the highest inverse correlations in the upwelling cores situated far away from freshwater inputs (Figure 2.6a). for example at 'a': 72-73°W (Eq. 1, r= -0.69, p< 0.01) and 'b': 64-65°W (Eq. 2, r= -0.80, p< 0.01). The correlation equations for those areas were:

$$\log(\text{Chl}) = -0.135 \text{ SST(a)} + 3.341 \qquad\qquad \text{(Eq. 1)}$$

$$\log(\text{Chl}) = -0.164 \text{ SST(b)} + 4.211 \qquad\qquad \text{(Eq. 2)}$$

Using equation 1 and 2, Chl is similar for both areas at SST=30°C (0.20 mg m^{-3}); but at lower SSTs, Chl is higher at 64-65°W (for example, at SST=22°C, Chl is about 2.4 and 4.0 mg m^{-3}, for areas 'a' and 'b, respectively). Something similar was found by

Muller-Karger and Aparicio (1994) with higher variations of Chl with sea level (which tracks the upwelling) at 63-65°W, compared to 66-68°W. The Subtropical Underwater feeds the southern Caribbean upwelling system. Therefore it is assumed that, for the different upwelling foci, waters upwelled with similar SSTs should also have similar nutrients content. Further analysis, beyond the scope of this study, are necessary to establish if the waters upwelled in the eastern and western upwelling areas have indeed the same concentration of nutrients. Another explanation for the phytoplankton biomass/SST discrepancy between those areas could be related to differences in their continental shelf width (see Figure 2.1). The eastern upwelling area has a very wide continental shelf (60-90km, Herrera and Febres 1975), while the continental shelf at the western upwelling area is narrower (10-40km, Cuello *et al.* 2007). Upwelling occurring in wide and relatively shallow continental shelves can generate resuspension and transport of essential microelements from the benthic boundary layer to the surface, enhancing phytoplankton productivity (Dale *et al.* 2002, Huhn *et al.* 2007).

2.4.3 Forcing mechanisms along the coast

Nearshore QuikSCAT satellite wind products were extracted from the pixels closest to the shore (~25 km offshore). Along the southern Caribbean Sea three areas showed distinctive wind speed regimes (Figure 2.7). The area east of 68°W (foci f11-f21) had relatively stable high wind speed (> 6 m s^{-1}) from December to July and slightly lower during August-November (4-6 m s^{-1}). Between 69° and 74°W (foci f3-f10), stronger winds (> 6 m s^{-1}) occurred year round, with a maximum in June-July (> 9 m s^{-1}) and a minimum in September-October (6-7 m s^{-1}). The strongest wind speed occurs from

74° to 76°W (foci f1-f2), with maximum during December-April (> 11 m s^{-1}), a secondary maximum in July (~9 m s^{-1}), and a minimum during September-October (~5 m s^{-1}). West from 76°W the winds decreased sharply to averages maxima of ~6 m s^{-1} between January to April and a minimum < 4 m s^{-1} between May-November.

On average, winds in the western upwelling area were 1.3 times stronger and offshore ET was 1.5 higher than in the eastern area (Table 2.1). This means that induced water column turbulence (a function of the cube of the wind speed) was ~2.5 higher in the western area than in the eastern one (557 and 229 m^3 s^{-3}, respectively). The direction of the wind with respect to the coast was roughly alongshore along the entire southern Caribbean Sea margin. The wind direction showed some seasonality. The eastern area had on average half a year with alongshore winds (~1.7° variation from the alongshore direction, May-October); during the principal upwelling (November to April) the direction was more onshore (~12°). The western area had slightly offshore winds (~ -14°) during the entire year, excepting October-November (~ 0.2°).

Offshore ET due to alongshore winds (Figure 2.7b) was upwelling favorable (positive) year-round. It closely followed changes in nearshore winds except where the coast is nearly perpendicular to the predominant wind direction (for example at 65.7°W, 68.3°W, 69.75°W and 71°W). Nearshore EP due to the wind-curl (Figure 2.7c) also caused positive vertical velocities (upwelling favorable) in both the eastern and western upwelling areas (at 62-64°W and 72-74.5°W) with minimum values around October. EP was noisy even after averaging in time, consistent with the findings of Wunsch (2011). This is in part the result of aliasing caused by the satellite sampling pattern (Milliff and Morzel 2000). The area west of 72.5°W experiences the strongest positive nearshore EP,

Figure 2.7. Long term averages of QuikSCAT-derived wind speed (a), offshore Ekman Transport (b) and Ekman Pumping (c). Positive velocities of Ekman transport and Ekman pumping indicate upwelling.

with a maximum around July. Intermittent negative EP (downwelling) was found only at three foci, around 75°W (foci f1 and f2) and between 68-70°W (focus f10). Strong

positive EP also occurs around 76°W; however, in that area surface SST does not suggest upwelling of deeper cooler waters (Figure 2.2).

On average, winds in the western upwelling area were 1.3 times stronger and offshore ET was 1.5 higher than in the eastern area (Table 2.1). This means that induced water column turbulence (a function of the cube of the wind speed) was ~2.5 higher in the western area than in the eastern one (557 and 229 m^3 s^{-3}, respectively). The direction of the wind with respect to the coast was roughly alongshore along the entire southern Caribbean Sea margin. The wind direction showed some seasonality. The eastern area had on average half a year with alongshore winds (~1.7° variation from the alongshore direction, May-October); during the principal upwelling (November to April) the direction was more onshore (~12°). The western area had slightly offshore winds (~ -14°) during the entire year, excepting October-November (~ 0.2°).

Offshore ET due to alongshore winds (Figure 2.7b) was upwelling favorable (positive) year-round. It closely followed changes in nearshore winds except where the coast is nearly perpendicular to the predominant wind direction (for example at 65.7°W, 68.3°W, 69.75°W and 71°W). Nearshore EP due to the wind-curl (Figure 2.7c) also caused positive vertical velocities (upwelling favorable) in both the eastern and western upwelling areas (at 62-64°W and 72-74.5°W) with minimum values around October. EP was noisy even after averaging in time, consistent with the findings of Wunsch (2011). This is in part the result of aliasing caused by the satellite sampling pattern (Milliff and Morzel 2000). The area west of 72.5°W experiences the strongest positive nearshore EP, with a maximum around July. Intermittent negative EP (downwelling) was found only at three foci, around 75°W (foci f1 and f2) and between 68-70°W (focus f10). Strong

positive EP also occurs around 76°W; however, in that area surface SST does not suggest

upwelling of deeper cooler waters (Figure 2.2).

Table 2.1. Comparison between the west (70°-73°W) and east (63°-65°W) upwelling areas regarding their long term coastal averages (and minimum/maximum values) of satellite products of: wind speed (W), turbulence (Turb) calculated with W^3, alongshore wind speed (alongW), offshore Ekman Transport due to alongshore wind (offshET), vertical transport due to Ekman Pumping integrated to 100km offshore (EP100), sea surface temperature (SST), chlorophyll-*a* (Chl). Depth of the 22°C isotherm (Iso22) was calculated from climatological temperature profiles (1 degree resolution) from the World Ocean Atlas (2005) extracted at 12.5°N, 72.5°W and 11.5°N-64.5°W for the west and east upwelling areas, respectively. Values of latitude (Lat) and coriolis are also compared.

	West			East		
	Average	(Minimum :	Maximum)	Average	(Minimum :	Maximum)
W (m s^{-1})	8.23	(0.13 :	14.39)	6.12	(0.00 :	12.90)
Turb (m^3 s^{-3})	638	(285 :	1096)	255	(121 :	366)
alongW (m s^{-1})	-7.00	(-14.38 :	7.48)	-5.77	(-12.68 :	6.49)
offshET (m^2 s^{-1})	3.04	(-3.50 :	11.68)	2.02	(-1.08 :	9.19)
EP100 (m^2 s^{-1})	0.48	(-10.17 :	7.56)	0.38	(-7.76 :	5.39)
SST(°C)	25.53	(19.93 :	30.53)	25.24	(20.31 :	30.08)
Chl (mg m^{-3})	1.15	(0.01 :	23.00)	1.65	(0.02 :	24.56)
Iso22 (m)	115	(87 :	140)	85	(65 :	105)
Lat (°N)	12.23	(11.50 :	12.75)	10.88	(10.25 :	11.25)
Coriolis f (s^{-1})	3.09E-5	(2.91E-5 :	3.22E-5)	2.75E-5	(2.60E-5 :	2.85E-5)

The western upwelling area showed a more energetic aeolic system than the

eastern area. ET was ~1.5 times higher in the west upwelling area compared to the

eastern area (Table 2.1, Figure 2.7b). Since wind stress (and ET) is a quadratic function

of the wind, with the mean wind speed for those areas (Table 2.1) we would expect a

higher offshore ET difference (around ~1.8 times higher in the western area instead of

~1.5 times). The upwelling mechanism in the west responds to the transfer of wind

energy less efficiently (Table 2.2). Two factors are responsible for this: (a) Due to the

small difference in latitude (Table 2.1 and Table 2.2) the Coriolis effect is ~10% smaller

in the western area compared to the eastern. (b) The western upwelling area experienced

a lower proportion of alongshore winds compared to the eastern area during the year (85 and 94%, respectively, Table 2.1). Therefore, less of the total wind speed energy is converted to upwelling in the western area compared to the eastern (72 and 89%, respectively, Table 2.2). Between these two factors, there was a ~28% less effective transfer from wind to offshore ET in the western area.

Table 2.2. Comparison of the effect of latitude and of the proportions of along shore wind (alongW) on the calculation of offshore Ekman Transport (ET) in the west and east upwelling areas. Case 1: the same hypothetical wind speed (W) with 100% alongW was used for both areas, differing only in their coriolis parameter (from Table 2.1). Case 2, in top of the differences caused by coriolis, it is added the effect of the typical proportion of alongW for each upwelling area (from Table 2.1). For each upwelling area it was calculated the efficiency of the transference of wind to upwelling (wind efficiency) dividing ET(case 2) by ET(case 1). The differences between the areas on the ET calculations was obtained dividing ET(west) by ET(east) for each case.

Case	Area	coriolis	W	% alongW	alongW	ET	Wind efficiency	ET differences
1	West	3.1E-5	7.00	100	7.00	2.21		case 1: -11%
1	East	2.8E-5	7.00	100	7.00	2.49		
2	West	3.1E-5	7.00	85	5.95	1.59	West: 72%	case 2: -28%
2	East	2.8E-5	7.00	94	6.58	2.21	East: 89%	

Regardless to the higher ET, the western area showed similar or warmer SSTs than the eastern area (Figure 2.2 and Figure 2.5). To examine the hypothesis that this is caused by differences in the depth of the upwelling source waters, we studied the climatological vertical temperature structure of waters in the region (World Ocean Atlas 2005, Locarnini *et al.* 2006, Figure 2.1). The seasonal variability of the depth of the 22°C isotherm (Figure 2.8) was extracted, as this temperature traces the Subtropical Underwater core (Morrison and Nowlin 1982).

The depth of the Subtropical Underwater core (22°C isotherm) showed three distinctive areas where it behaved consistently; these coincided with the subregions that

showed consistent wind speed behavior (Figure 2.7a). The shallowest depths were found

east of 68°W (annual mean 85 m, Figure 2.8); the deepest between 68-74°W (annual

mean 115 m); between 74-76°W the isotherm was slightly shallower (annual mean 109

m). During January to about August-September the 22°C isotherm in the southern

Caribbean Sea was shallower than the rest of the year. EP, integrated up to 100 km

offshore, showed remarkable coincidence with the seasonal cycle of the 22°C isotherm

depth (Figure 1.10 in Rueda-Roa *et al.* first chapter in this dissertation); which is

explained by the isopycnals rise caused by EP open-sea upwelling.

22°C isotherm depth (m)
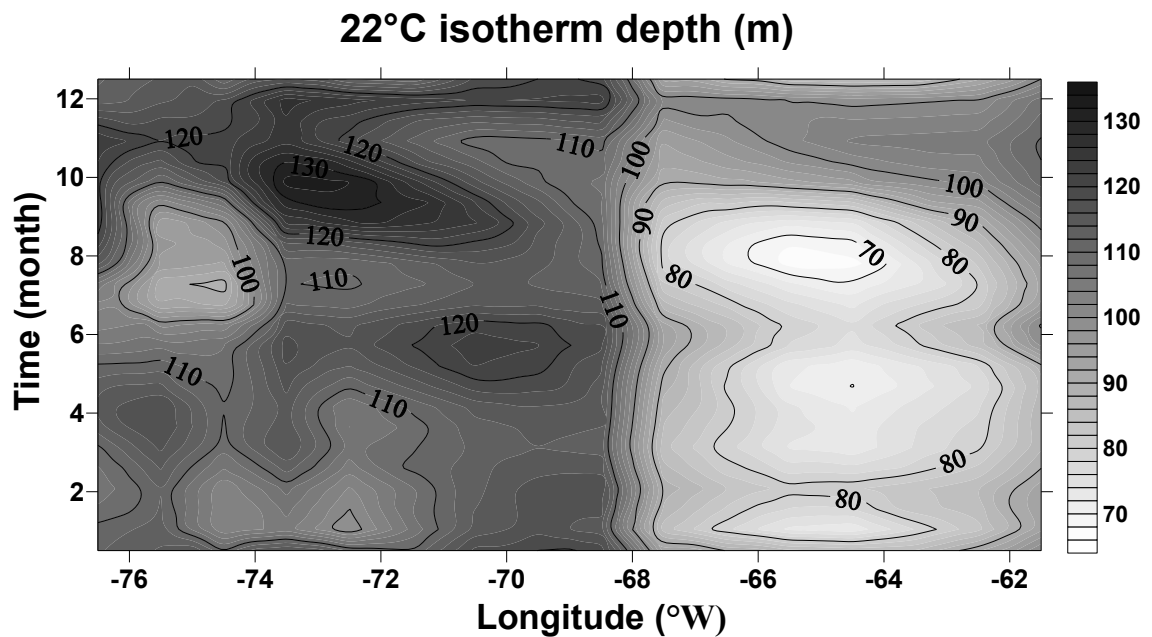
Figure 2.8. Climatological variation of the depth of the Subtropical Underwater core (traced with the 22ºC isotherm) along the southern Caribbean upwelling system area, (calculated from the World Ocean Atlas 2005, see location in Figure 2.1).

We examined the degree of correlation between the climatology of a number of

parameters, including SST, Chl, nearshore wind speed (W), wind direction, offshore ET,

coastal EP, EP integrated up to 100 km offshore (EP100), offshore extension of positive
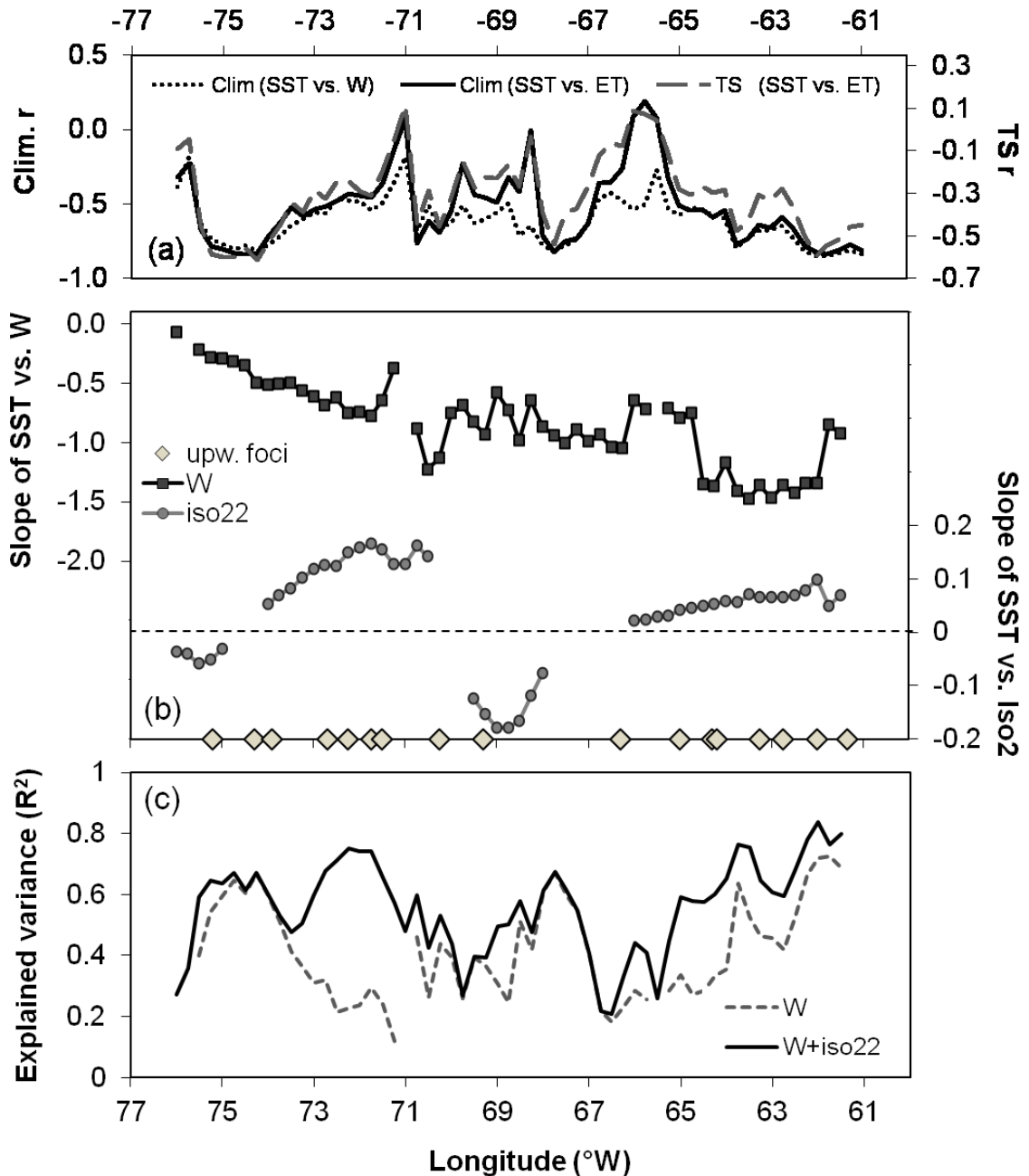
Figure 2.9. (a) Comparison of correlation coefficients (r) obtained with weekly climatologies (solid line) and with weekly time series (dashed line) for sea surface temperature (SST) *vs*. offshore Ekman Transport (ET) along the coast, and for the climatologies of SST vs. nearshore wind speed (W) (dotted line). (b) Rate of change (slope) for the simple regressions of SST *vs*. W and of SST *vs*. the 22°C isotherm depth (iso22) for each grid point along the coast. The positions of upwelling foci are shown for reference (diamonds). (c) Explained variance (R^2) for the single regression between SST *vs*. W (dashed line), and for the multiple regression of SST *vs*. W and iso22 (solid line). Calculations for (b) and (c) were done with weekly climatologies, and only significant values ($p < 0.05$) are shown.

EP and the 22°C isotherm depth (iso22). All parameters were interpolated to the same temporal and spatial resolution (1 week and 0.25° of longitude). A comparison of the correlations using climatological data with those performed with time series data set (for all the variables but iso22) showed nearly identical shape in their variations along the coast (see for example Figure 2.9a). However, the values of the correlation coefficients (r) and the rate of changes (slope) were lower when using time series. Therefore, we describe proportionality when comparing the correlations of climatology data between the eastern and western upwelling areas instead of the actual values.

Correlation coefficients for SST vs. ET were very similar as for SST *vs.* W (Figure 2.9a). This is due to the high proportion of alongshore wind this area experiences. However, correlations with W were higher in two regions, at 68-70°W (foci f10) and 65.75-66.5°W (f11). This indicates that these areas experience upwelling under a different range of wind directions, probably because of local characteristics, e.g. mean depth or other alongshelf bathymetric variations (Smith 1981, Tomczak 1998b).

The slope of the SST vs. W regression computed for each grid point (Figure 2.9b) showed that the wind speed had a higher effect on SST in the eastern coastal areas. These longitudinal differences seem to be related to the increasing depth of upwelling source waters toward the west, as shown by the slope of the iso22 depth vs. SST (Figure 2.9b).

A multiple regression between the QuikSCAT nearshore wind speed and the depth of the 22°C isotherm explained coastal SST variability better than a single regression of SST vs. W (Figure 2.9c). The improvement was especially marked in the western upwelling area (71-73°W). The deeper position of the Subtropical Underwater core in that area (~30 m deeper, Figure 2.8) produced higher sensitivity of the SST to the

22°C isotherm depth (Figure 2.9b and Figure 2.9c). This also explains the warmer SST during upwelling (Figure 2.2 and Figure 2.5) in spite of the higher offshore ET (Figure 2.7a and Table 2.1) seen here compared to the eastern area.

The upwelling in the southern Caribbean Sea could be also influenced by mesoscale geostrophic features which requires further analysis. For example, the Caribbean Current moves westward and faster (~70 cm s^{-1}) near the southern boundary of the southern Caribbean Sea, off the continental shelf-break between 62-72°W (Fratantoni 2001, Centurioni and Niiler 2003); it has a mixed annual/semiannual character with maxima in spring (Secondary maximum) and summer (highest maximum) and minimum in fall (Johns *et al.* 2002). Seasonal variations in the strength and position of the Caribbean Current could influence the depth of the Subtropical Underwater core. For instance, the shallowest depth of the 22°C isotherm (August, Figure 2.8) coincides with the seasonal maximum in the strength of the Caribbean Current.

2.4.4 Phytoplankton response to the differences in upwelling regimes along the southern Caribbean Sea

Both the eastern and western upwelling areas showed upwelling during more than half a year (SSTs below 26°C during 6.9 and 8.5 months for the west and east upwelling areas, respectively, Figure 2.2b). Chl concentrations were about 1.4 times higher in the eastern area compared to the western (Figure 2.6b, Table 2.1), regardless of their similarity in SST. In both areas, the Chl cycle was coherent with the SST cycle (Figure 2.10a and 2.10b), with exception of the mid-year Chl peak in the west upwelling area. The disproportionally high magnitude of the Chl peak in the western area compared to the corresponding SST is related to the enhanced turbulence in the west upwelling area

during that time frame, reaching over 1000 m^3 s^{-3} (Table 2.1, Figure 2.10a). Wind-stress

drives entrainment of colder waters into the mixed layer and leads to further turbulent
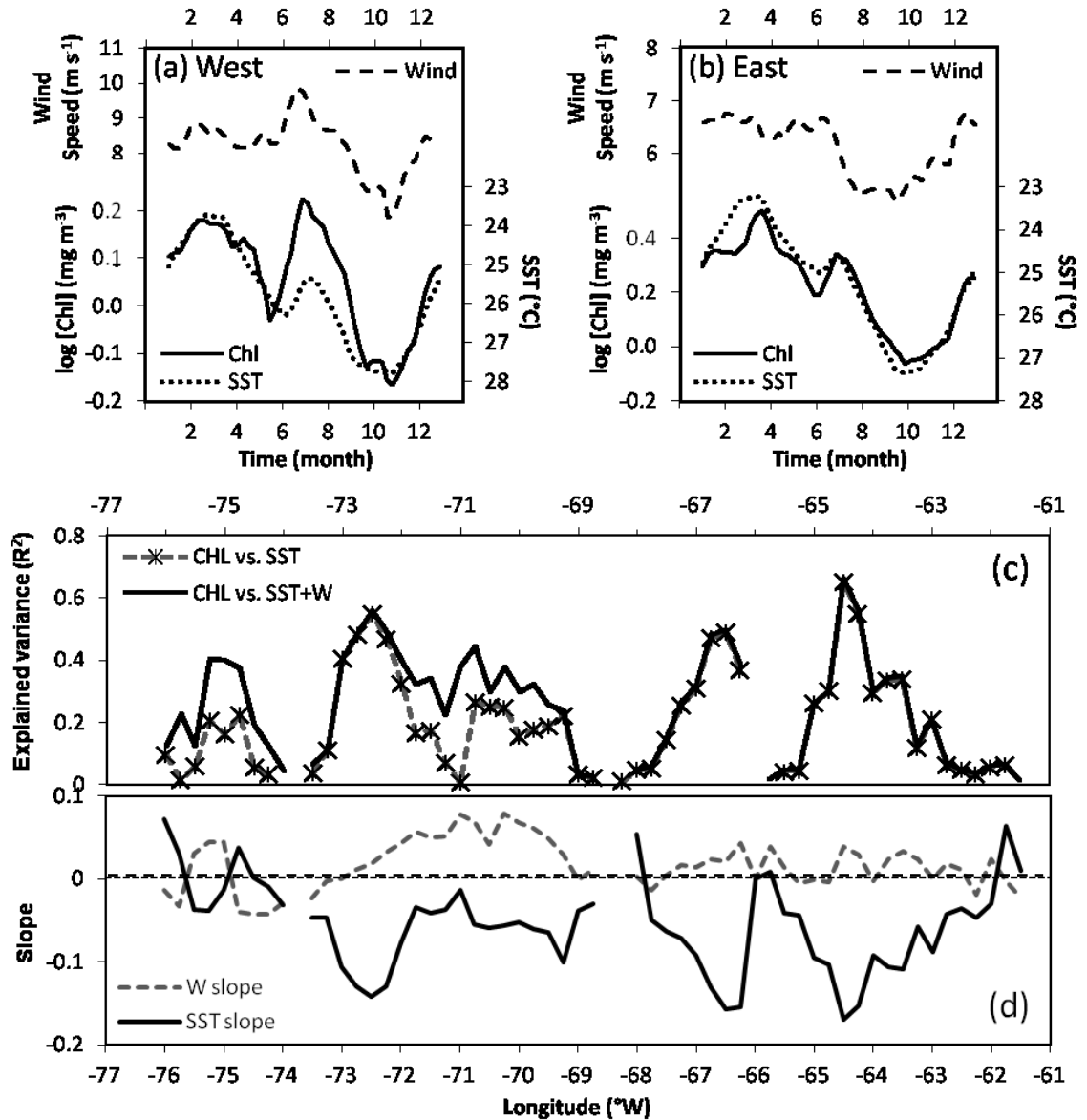
Figure 2.10. (a) and (b) Long term coastal values means of SST, Chl and wind speed (W) averaged for (a) the west upwelling area (70-73) and (b) the east upwelling area (63-65°W). SST values are presented in reverse order for a better comparison with Chl. (c) Explained variance for the single regression between Chl vs. SST weekly time series (dashed line), and for the multiple regression between Chl vs. SST and W (solid line). (d) Rate of changes (slope) of the parameters SST and W for the multiple regressions of Chl vs. SST and W. Only significant values (p < 0.05) are shown for the correlations.

vertical nutrient flux as a result of the erosion of the thermocline (Klein and Coste 1984). A multiple regression of Chl vs. SST and wind speed (W) time series (Figure 2.10c) increased considerably the explained variance along the west upwelling area (between 69.5-72°W, and also along 74-76°W) but for the rest of the coastline the values were similar than for the single regression of Chl vs. SST. Values obtained with W were similar or slightly higher than the obtained using turbulence (W3) or offshore ET. The relationship of the wind was directly related with Chl (positive slopes, Figure 2.10d), confirming that in the western upwelling area, the mid-year Chl was enhanced by turbulence. During mid-year mixed layers are relatively shallow in that area (between 10-30m depth for the period of June-July 1997, Andrade 2000), which would make easier the turbulent entrainment of nutrients from the thermocline erosion.

The eastern upwelling area has four times higher small pelagic biomass than the western area (Stromme and Saetersdal 1989). The enhanced upwelling in the eastern area results in a longer season of high Chl (1.6 months longer) and a phytoplankton biomass that is 1.4 times higher than those in the western area (Figure 2.6b, Table 2.1). Furthermore, the eastern area shows higher Chl increases at an equivalent lower SST (upwelling) than the western area (i.e. Eq. 1 and Eq. 2). This seems related to its wider continental shelf (Figure 2.1). Comparing the upwelling dynamics, the western area had a more energetic wind field (1.5 higher offshore ET and 2.5 higher turbulence, Table 2.1), but similar or warmer SSTs than the eastern upwelling area (Table 2.1, Figure 2.5) due to the deeper position of the Subtropical Underwater core in the western area (Figure 2.8 and Figure 2.9).

79

The 'optimal environmental window' theory stresses the importance of a balance between the upwelling of nutrient-rich water and calm conditions for encouraging successful clupeoid recruitment (Cury and Roy, 1989). This theory has been successfully tested and, in the major upwelling ecosystems, clupeoid recruitment is dome-shaped with the upwelling, turbulence and SST (Cole and McGlade 1998, MacKenzie 2000 and references therein). The 'optimal environmental window' establishes an optimum wind speed of ~6 m s^{-1} for recruitment of small pelagics in wind driven upwelling systems (Cury and Roy, 1989). This is the case for the eastern upwelling area with an annual wind speed average of 6.2 m s^{-1}. Above this value turbulence increases, as in the western area with winds > 8 m s^{-1}. The effect of turbulence in the biology of the western area was demonstrated by its effect on Chl (i.e. Figure 2.10) which is not seen for the eastern area. Since the western area has relatively similar SSTs as the eastern area, the level of enrichment due to upwelling is also comparable, but the higher offshore ET, and especially the much higher turbulence, place this upwelling ecosystem in the right (negative) side of the dome-shaped relationship between the intensity of upwelling/turbulence and the small pelagics recruitment. Higher turbulence mixes surface waters dispersing plankton and larvae, which often inhibits successful first feeding (Lasker 1975, 1978) and reduces the ability of larvae to catch prey (MacKenzie *et al.* 1994). Higher turbulence also reduces phytoplankton production by mixing cells below the critical depth (Steele 1974 as cited in Bakun 2010). In addition, stronger offshore transport may cause the loss of eggs and larvae from their coastal habitat (Parrish *et al.* 1981) and leads to nutrients being exported before they are fully used within the coastal upwelling system.

Bakun's triad hypothesis (Bakun, 1993, 1996) generalizes three oceanographic processes in diverse marine systems that can influence recruitment success: (a) enrichment of the food chain, (b) retention of the eggs and larvae within suitable nursery areas, and (c) concentration of food particles for the first-feeding larvae and subsequent development stages. In coastal upwelling systems, enrichment (a) is produced by the upwelled waters, retention (b) is related to moderate offshore ET, and concentration of food (c) is related to moderate turbulence. Retention (b) is also influenced by recirculation due to topography; topographical features minimize offshore transport and allow retention of eggs and larvae in the favorable coastal habitat (Lett *et al.* 2006). Comparing the upwelling plumes extension (Figure 2.3) with the continental shelf extent (Figure 2.1) it is clear that in the western upwelling area the upwelling plume extends broadly offshore beyond the continental shelf. However, in the eastern region the upwelling plumes bathe a wide continental shelf with high topographic complexity (i.e. the Cariaco Gulf, the Margarita Island and other small islands) that increase and diversify retention mechanisms for eggs and larvae.

2.5 Conclusions

The southern Caribbean upwelling system (61°W to 75.5°W, 10 to 12.5ºN) features a strong semiannual SST cycle, with a principal upwelling season between December and April, a mid-year upwelling during June-August. The weakest upwelling is seen in during September-October. Satellite Chl shows maxima near specific coastal upwelling foci. In areas without riverine influence, the coastal Chl maxima are coherent with the upwelling cycle, showing the same (but inverse) seasonality as SST. Nearshore

winds are mainly aligned with the coastline and they are upwelling favorable all year-round. There are three areas with distinctive wind regimes. (1) The coast east of 68°W showed relatively stable high wind speed (> 6 m s^{-1}) from December to July and lower winds between August-November (4-6 m s^{-1}). (2) The region between 69-74°W experienced stronger winds (> 8 m s^{-1}) year round, with a maximum in June-July (> 9 m s^{-1}). (3) The strongest nearshore winds occurred around 74-76°W, with a distinctive maximum during December-April (> 11 m s^{-1}) and a marked minimum during September-October (~5 m s^{-1}).

The southern Caribbean Sea has 21 upwelling foci. Adjacent upwelling foci tend to have coherent upwelling cycles. Seven groups of foci can be identified with different characteristics in their seasonal SST cycle. There are two large sections of coast which experience the strongest SST decrease and which also are the most important fisheries grounds: The east upwelling area, between 63-65°W, which showed the lowest SST (annual mean 25.24°C) and the highest Chl (annual mean 1.65 mg m^{-3}), moderate winds (annual mean 6.12 m s^{-1}), and shallower offshore isotherms (22°C isotherm annual mean at 85m depth). The west upwelling area, between 74-69.5°W, with stronger winds (annual mean 8.23 m s^{-1}) but deeper offshore isotherms (22°C isotherm annual mean at 115 m depth) that limit the upwelled waters to SST similar or higher than in the east area (annual mean 25.53°C), and with lower Chlorophyll concentrations (annual mean 1.15 mg m^{-3}). . The western upwelling area has very energetic eolic conditions. However, the transference of energy from the wind stress to the water column is not as efficient as in the east area in generating upwelling owing to a lower proportion of alongshore winds (85 and 94%, for the west and east areas, respectively) and because the western coast is

located at a higher latitude. These two factors cause a ~28% less effective transfer of energy from wind to offshore ET. Regardless, offshore ET in the western upwelling area is ~1.5 higher than in the eastern area. Chlorophyll cycles are inverse and coherent with SST cycles, indicating that the increase in phytoplankton biomass is driven by upwelling. An exception of this is the mid-year Chl peak in the western upwelling area, which is disproportionately high compared to the SST mid-year upwelling and it is concurrent with the wind maxima. This midyear Chl maximum is enhanced by wind stress turbulence which leads to additional entrainment of nutrients from the thermocline.

The differences in the upwelling dynamics between the eastern upwelling area (medium wind speeds, shallower offshore isotherms, slightly cooler SSTs and higher phytoplankton biomass) and the western upwelling area (high wind speeds, deeper isotherms, slightly warmer SSTs and lower phytoplankton biomass) helped explain the higher fish productivity of the eastern upwelling area (~90% of the southern Caribbean Sea captures, FAO). The wind speed at the eastern upwelling area (annual mean 6.12 m s^{-1}) is very close to the optimum wind speed for recruitment of small pelagics (~6 m s^{-1}, 'optimal environmental window' theory), which generates moderate offshore Ekman Transport and moderate turbulence, that in turn produce the highest recruitment. Furthermore, the wider continental shelf and higher topographic complexity in the eastern area increase and diversify retention mechanisms for eggs and larvae. Possibly, the most important factors that quench secondary production to fish in the western area are the high degree of turbulence and strong offshore transport. This produces strong dispersion of plankton and larvae, which in turn would affect larvae feeding and mortality and export of nutrients, plankton and larvae from the coastal upwelling system.

2.6 Acknowledgements

2.7. References

Bakun A (1973) Coastal upwelling indices, west coast of North America, 1946-71. U.S. Dept. of Commerce, NOAA Tech. Rep., NMFS SSRF-671, 103p.

Bakun A (2010) Linking climate to population variability in marine ecosystems characterized by non-simple dynamics: conceptual templates and schematic constructs. *J. Mar. Syst*. 79: 361–373.

Bernal G, Poveda G, Roldán P, Andrade C (2006) Patrones de variabilidad de las temperaturas superficiales del mar en la Costa Caribe Colombiana. *Rev. Acad. Colomb. Cienc.*, 30 (115): 195-208.

Brown OB, Brown JW, Evans RH (1985) Calibration of advanced very high resolution radiometer infrared observations. *J. Geophys. Res.* 90:11667-11678.

Caraballo LF (1982) Golfo de Cariaco. Parte I: Morfología y batimetetría submarina. Estructura y tectonísmo reciente. *Bol. Inst. Oceanogr. Univ. Oriente*, 21 (1-2):13-35.

Castelao RM, Barth JA (2006) Upwelling around Cabo Frio, Brazil: The importance of wind stress curl. *Geophys. Res. Lett.*, 33, L03602.

Castellanos P, Varela R, Muller-Karger F (2002) Descripción de las areas de surgencia al sur del Mar Caribe examinadas con el sensor infrarrojo AVHRR. *Mem. Soc. Cien. Nat. La Salle,* 154: 55-76.

Centurioni LR,Niiler PP (2003) On the surface currents of the Caribbean Sea. *Geophys. Res. Lett*., 30(6): 1279.

Chereskin TK (1995) Direct evidence for an Ekman balance in the California Current. *J. Geophys. Res*., 100: 18261-18269.

Cury P, Roy C (1989) Optimal environmental window and pelagic fish recruitment success in upwelling areas. *Canad. J. Fish. Aquatic Sci.*, 46(4): 670-680.

Dale AW, Prego R (2002) Physico-biogeochemical controls on benthic-pelagic coupling of nutrient fluxes and recycling in a coastal upwelling system. *Mar. Ecol. Prog. Ser*., 235: 15–28.

Fratantoni DM (2001) North Atlantic surface circulation during the 1990's observed with satellite-tracked drifters. *J. Geophys. Res.*, 106: 22067-22093.

Freilich MH, Dunbar RS (1999) The accuracy of the NSCAT 1 vector winds: Comparisons with National Data Buoy Center buoys. *J. Geophys. Res*., 104: 11231- 11246.

Herrera L, Febres-Ortega G (1975) Kinematics of Me wind-generated velocity field in the surface waters off eastern Venezuela, Caribbean Sea. *Bol. Inst. Oceanogr. Univ. Orient*e, 14(2):165-186.

Hoffman RN, Leidner SM (2005) An introduction to the near-real-time QuikSCAT data. *Weather Forecast.*, 20: 476-493.

Hu C, Muller-Karger F, Murch B, Myhre D, Taylor J, Luerssen R, Moses C, Zhang C, Gramer L, and Hendee J (2009) Building an Automated Integrated Observing System to Detect Sea Surface Temperature Anomaly Events in the Florida Keys. *IEEE Trans. Geosc. Remote Sens.*, 47(6):1607-1620.

Huhn K, Paul A, Seyferth M (2007) Modeling sediment transport patterns during an upwelling event. J. *Geophys. Res., 112: C10003.*

Klein P and Coste B (1984) Effects of wind-stress variability on nutrient transport into the mixed layer. *Deep Sea Res.*, 31(1):21-37.

Lasker R (1975) Field criteria for survival of anchovy larvae: the relation between inshore chlorophyllmaximum layers and successful first feeding. *Fish. Bull.U.S.,* 73: 453-462.

Lasker R (1978) The relation between oceanographic conditions and larval anchovy food in the California Current: identification of the factors leading to recruitment failure. *Rapp. P.-v. Réun. - Cons. Int. Explor. Mer*, 173, 212-230.

Locarnini RA, Mishonov AV, Antonov JI, Boyer TP, Garcia HE, (2006) World Ocean Atlas 2005, Volume 1: Temperature. S. Levitus, Ed. NOAA Atlas NESDIS 61, U.S. Government Printing Office, Washington, D.C., 182 pp. http://www.nodc.noaa.gov/OC5/WOA05/pr_woa05.html

McClain EP, Pichel WG, Walton CC, Ahmad Z, Sutton J (1983) Multi-channel improvements to satellite-derived global sea-surface temperatures. *Adv. Space Res.,* 2(6):43-47.

MacKenzie BR (2000) Turbulence, larval fish ecology and fisheries recruitment: a review of field studies. *Oceanol. Acta*, 23(4): 357-375.

MacKenzie BR, Miller TJ, Cyr S, Leggett WC (1994) Evidence for a dome-shaped relationship between turbulence and larval fish ingestion rates. *Limnol. Oceanogr.*, 39(8): 1790-1799

Mendo J, Pizarro L, Castillo S (1987) Monthly turbulence and ET indexes 1953 to 1985, based on local wind records from Trujillo and Callao, Peru. In: Pauly D, Tsukayama I (ed) <u>The Peruvian anchoveta and its upwelling ecosystem: three decades of change</u>. ICLARM Studies and Reviews 15:75-88

Milliff RF, Morzel J (2000) The global distribution of the time-average wind-stress curl from NSCAT. *J. Atmosph. Sci.*, 58(2):109-131.

Minnett PJ (1991) Consequences of sea surface temperature variability on the validation and applications of satellite measurements. *J. Geophys. Res.,* 96(C10):18475-18489.

Morrison J M, Nowlin Jr WD (1982) General Distribution of Water Masses Within the Eastern Caribbean Sea During the Winter of 1972 and Fall of 1973. *J. Geophys. Res.*, 87(C6), 4207-4229

Muller-Karger FE, Aparicio R (1994) Mesoscale Processes Affecting Phytoplankton Abundance in the Southern Caribbean Sea. *Cont. Shelf Res..,* 14(2/3): 199-221.

Muller-Karger FE, McClain CR, Fisher TR, Esaias WE, Varela R. (1989) Pigment distribution in the Caribbean Sea: observations from space. *Progr. Oceanogr.*, 23: 23-69.

Muller-Karger FE, Varela R (1990). Influjo del Río Orinoco en el Mar Caribe: observaciones con el CZCS desde el espacio. *Mem. Soc. Cien. Nat. La Salle*, 50(133–134): 361-390.

Muller-Karger FE, Varela R, Thunell R, Astor Y, Zhang H, Luerssen R, Hu C (2004) Processes of coastal upwelling and carbon flux in the Cariaco Basin. *Deep-Sea Res. part II*, 51: 927-943

Oey LY, Ezer T, Wang DP, Fan SJ, Yin XQ (2006) Loop Current warming by Hurricane Wilma. *Geophys. Res. Let*., 33: L08613.

Oey LY, Ezer T, Wang DP, Yin XQ, Fan SJ (2007) Hurricane-induced motions and interaction with ocean currents. *Cont. Shelf Res*., 27: 1249-1263.

Pang-Ning T, Steinbach M, Kumar V (2005) Introduction to Data Mining. Addison-Wesley, 1st edition, May 2005.

Parrish RH, Nelson CS, Bakun A (1981) Transport mechanisms and reproductive success of fishes in the California Current. *Biol. Oceanogr*., 1: 175-203.

Richards F (1960) Some chemical and hydrographic observations along the north coast of South America. *Deep-Sea Res*., 7: 163-182.

Rueda-Roa D, Ezer T, Muller-Karger F (in preparation) Contribution of Ekman transport and pumping on the mid-year Southern Caribbean upwelling and on phytoplankton biomass. (First chapter on this dissertation).

Smith RL (1968) Upwelling. *Oceanogr. Mar. Biol. Ann. Rev*., 6: 11-46.

Smith R L (1981) A comparison of the structure and variability of the flow field in three coastal upwelling regions: Oregon, Northwest Africa, and Peru. Pp. 107–118. *In*: Richards FA (ed.) Coastal Upwelling, *Amer. Geophys. Union*, 107–118.

Stewart RH (2007) *Introduction to Physical Oceanography*; R. H. Stewart, Ed; Dept. of Oceanography, Texas A & M University: College Station: TX, 2002; available online: http://oceanworld.tamu.edu/resources/ocng_textbook/contents.html.

Strong AE, McClain E (1984) Improved ocean surface temperatures from space-comparisons with drifting buoys. *Bull. Am. Meteorol. Soc*., 85: 138.

Steele JH (1974) <u>The Stucture of Marine Ecosystems</u>. Harvard Univ. Press, Cambridge, Mass. 128 pp.

Tomczak M (1998a) Ekman layer dynamics for shallow seas with stratification; in: <u>Shelf and Coastal Oceanography</u>, chapter 3, accessed on September 10 2011 at: http://www.es.flinders.edu.au/~mattom/ShelfCoast/chapter03.html

Tomczak M (1998b): Upwelling dynamics in deep and shallow water; in: <u>Shelf and Coastal Oceanography</u>, chapter 6, accessed on September 10 2011 at: http://www.es.flinders.edu.au/~mattom/ShelfCoast/chapter06.html

Walton CC (1988) Nonlinear Multichannel Algorithms for Estimating Sea Surface Temperature with AVHRR Satellite Data. *J. Appl. Meteor.*, 27(2) 115-124.

Wunsch, (2011) The decadal mean ocean circulation and Sverdrup balance. *J. Mar. Res.*, 69: 1-18.

2.8 Appendices

Appendix A

Daily zonal and meridional QuikSCAT wind speed components (u, v respectively, in m s^{-1}) were used to estimate the wind stress components ($\tau_x = c_a\,\rho_a\,|u|\,u$; $\tau_y = c_a\,\rho_a\,|v|\,v$; and $\tau_{xy} = c_a\,\rho_a\,|W|^2$, Kg m^{-1} s^{-2} or N m^{-2}, Bakun 1973); where ρ_a is the air density (1.2 kg m^{-3}), W is the scalar wind magnitude ($W = \text{sqrt}(u^2 + v^2)$, m s^{-1}), and C_D is a drag coefficient (dimensionless) used by Oey *et al.* (2006 and 2007) and which includes curve fits for low and high wind speeds: C_D x 10^3 = 1.2 ($W \leq 11$ m s^{-1}; = 0.49 + 0.065 W ($11 < W \leq 19$ m s^{-1}), = 1.364 + 0.0234 W - 0.0002 $f2$ ($19 < W \leq 100$ m s^{-1}).

The geographic direction of the wind (*Windθ*) is defined as the angle of the wind vector (where the wind goes) calculated clockwise from a unitary vector pointing north: *Windθ* = *atan2 (u, v)* (*180/π*); 360° is added for negative u values. The coastline angle (*Coastθ*) is defined by the Pacific Fisheries Environmental Laboratory (http://www.pfeg.noaa.gov/) as the clockwise angle that the landward side of the coastline makes with a vector pointing north. The coastline angle, *Coastθ* = F + acos($slope$/sqrt($1+slope^2$)) (180/π), was obtained for each coast segment of 0.25° of longitude, calculating the *slope* of a linear fit for each coast segment with data points at 1 km resolution (Castelao and Barth 2006) and using a factor of F=180° when the land mass is mainly in the southern/southeastern quadrants and, F=0° when the land mass is mainly in the northern/ northwestern quadrants.

The alongshore wind stress, $\tau_{along\text{-}shore} = \tau_{xy}\cos(Coast\theta - Wind\theta)\,(\pi/180)$ (in Kg m^{-1}s^{-2}, Mendo *et al.* 1987) and the cross-shore Ekman volume transport, *ETcross-shore* = - $\tau_{along\text{-}shore}$ / $\rho_w f$ (in m^2 s^{-1}, Chereskin 1995) were calculated at each QuikSCAT grid point closest to the coast. We used a seawater density ρ_w = 1025 kg m^{-3} and the coriolis parameter (f= 2Ω sin(9), in s^{-1}) calculated for each wind pixel latitude (9) with the angular speed of earth rotation Ω = 7.29211538 x 10^{-5} (radians/second). Positive cross-shore ET means offshore transport that induces coastal upwelling.

The relative vorticity of wind stress curl was calculated using the wind stress components one pixel to the east/west and to the north/south from each grid point: *curl_τ_{xy}* = ((τ_y *east* - τ_y *west*)/ ∂x) - (τ_x *north* - τ_x *south*)/∂y)), where ∂x and ∂y are the distance in meters between pixel centers (Kg m^{-2} s^{-2} or N m^{-3}, Stewart 2007). The wind stress curl was used to calculate the EP vertical velocity, EP = *curl_τ_{xy}* / $\rho_w f$, (m s^{-1}, Smith 1968). Positive wind curl means counterclockwise vorticity that induces upward EP.

Geographical location of the upwelling foci along the Southern Caribbean Upwelling System shown in Figure 2.3.

Focus	Localization
f1:	**Barranquilla**: from Galerazamba to Río Magdalena, Bolívar and Atlántico departments, Colombia
f2:	**Ciénaga**: Ciénaga Grande, Magdalena department, Colombia
f3:	**Sta. Marta**: from Tyrona to Río Don Diego (East of Santa Marta), Magdalena department, Colombia
f4:	**Río Hacha**: from Río Hacha to Manaure, middle sector of the Guajira peninsula, La Guajira department, Colombia
f5:	**El Cabo**: West from El Cabo, La Guajira department, Colombia
f6:	**Cabo de la Vela**: from Cabo de la Vela to Punta Gallinas, La Guajira department, Colombia
f7:	**Punta Gallinas**: from Punta Gallinas to Puerto Estrella, La Guajira department, Colombia
f8:	**Cabo San Román**: from Cabo San Román to Punta Macama, northwest of Paraguaná Peninsula, state of Falcón, Venezuela
f9:	**Punta Cardón**: Punto Fijo: from Punta Cardón to the entrance of the Golfete de Coro, west of Paraguaná Peninsula, state of Falcón, Venezuela
f10:	**Puerto Cumarebo**: from Puerto Cumarebo to Campechano, state of Falcón, Venezuela
f11:	**Cabo Codera**: from Marina Grande (Vargas state) to Cabo Codera (state of Miranda), Venezuela
f12:	**Unare**: north from Laguna de Unare (South of the Cariaco basin), state of Anzoátegui, Venezuela
f13:	**Mochima**: Between Puerto La Cruz, Cumaná and the west of the Araya Peninsula, (states of Anzoátegui and Sucre) Venezuela
f14:	**Golfo de Cariaco**: Golfo de Cariaco, state of Sucre, Venezuela
f15:	**El Guamache**: northeast of the Araya peninsula, state of Sucre, Venezuela
f16:	**Macanao**: North of Macanao (from Punta El Faro to Punta de Tigre), northwest of Margarita island, Venezuela
f17:	**Manzanillo**: from La Salineta to Manzanillo, north of Margarita island, Venezuela
f18:	**Carúpano**: from Guaca to El Morro de Puerto Santo, state of Sucre, Venezuela
f19:	**Las Galdonas**: from Playa Medina to San Juan de Unare, Paria Peninsula, state of Sucre, Venezuela
f20:	**Don Pedro**: from Ensenada de Mejillones to the easternmost tip of the Paria peninsula, state of Sucre, Venezuela
f21:	**Trinidad**: North of Trinidad island, Trinidad and Tobago

Long term SST averages and standard deviation (in parenthesis) for the different upwelling foci (Figure 2.3 and Appendix B) for the principal upwelling (February-March), mid-year upwelling (from June 17 to July 21), SST maximum (September-October) and annual mean. Averages calculated from weekly SST time series for the period 1994-2008. *The warm season for the Caribbean Sea and the Atlantic Ocean is shorter and was calculated for September only. The areas used to extract the averages are shown in Figures 1 and 3.

Areas	Principal upwelling		Mid-year upwelling		Low-upwelling (maximum SST)		Annual Mean	
f1	25.62	(0.60)	27.53	(0.63)	27.95	(0.74)	26.98	(1.10)
f2	25.58	(0.69)	27.46	(0.67)	28.22	(0.76)	27.06	(1.16)
f3	24.45	(0.79)	25.89	(0.78)	27.25	(0.91)	25.84	(1.30)
f4	24.36	(0.89)	26.21	(0.74)	27.95	(0.69)	26.18	(1.44)
f5	23.68	(0.98)	25.61	(0.87)	27.63	(0.77)	25.70	(1.58)
f6	23.97	(0.88)	25.47	(0.76)	27.55	(0.65)	25.74	(1.42)
f7	24.39	(0.69)	25.79	(0.72)	27.58	(0.63)	25.96	(1.26)
f8	23.95	(0.78)	25.35	(0.76)	27.62	(0.70)	25.77	(1.44)
f9	23.83	(0.89)	25.36	(0.86)	27.78	(0.94)	25.79	(1.59)
f10	24.53	(0.75)	25.31	(0.70)	27.35	(0.68)	25.87	(1.20)
f11	24.09	(0.85)	24.94	(0.85)	27.34	(0.92)	25.60	(1.40)
f12	24.12	(0.91)	25.37	(0.83)	27.61	(0.72)	25.84	(1.41)
f13	23.33	(0.90)	24.94	(0.86)	27.34	(0.80)	25.35	(1.59)
f14	23.11	(0.80)	24.44	(0.87)	26.80	(0.92)	24.93	(1.51)
f15	23.54	(0.74)	24.92	(0.78)	27.13	(0.88)	25.26	(1.46)
f16	23.85	(0.75)	25.36	(0.72)	27.54	(0.75)	25.62	(1.47)
f17	23.45	(0.73)	25.00	(0.74)	27.23	(0.78)	25.26	(1.50)
f18	23.46	(0.70)	24.73	(0.74)	26.86	(0.77)	25.06	(1.38)
f19	23.74	(0.90)	25.04	(0.82)	27.09	(0.75)	25.33	(1.40)
f20	23.42	(0.93)	24.59	(0.90)	26.85	(0.84)	25.04	(1.46)
f21	25.02	(0.64)	25.82	(0.78)	27.52	(0.80)	26.18	(1.08)
Caribbean	26.07	(0.34)	26.87	(0.52)	28.38	(0.40)*	27.14	(0.89)
Atlantic	25.81	(0.50)	25.95	(0.78)	28.10	(0.67)*	26.72	(0.99)

CHAPTER THREE

Spatial variability of Spanish sardine (*Sardinella aurita*) abundance as related to the upwelling cycle of the southeastern Caribbean Sea

3.1 Abstract

The southeastern Caribbean Sea (10-12°N and 61.5-65°W) is an area of pronounced seasonal wind-driven upwelling that supports an important Spanish sardine (*Sardinella aurita*) fishery that accounts for 90% of the small pelagic fish within the Caribbean Sea. This artisanal fishery largely takes place in the first ~10 km from shore. To understand the effects of the upwelling on the spatial patterns of Spanish sardine distribution, a comparison was made between the number of small pelagics schools (Schools) and *S. aurita* biomass (sAsardine) obtained from 8 acoustic surveys (1995-1998) to satellite-derived products including sea surface temperature (SST, as a proxy for upwelling), SST gradients (SSTgrad) and chlorophyll-*a* (Chl, only available for the last two surveys) and also with distance to upwelling foci and latitude-longitude. Spatially averaged SSTs for the surveys were similar to long term SST averages for the study area. The surveys were gruped according to three seasons: strong, weak, and transition upwelling periods and compared each group's sAsardine with the environmental variables using Generalized Additive Models. During the strongest upwelling (February-March) sAsardine was widely distributed in the cooler, Chl rich upwelling plumes over

the ~70 km continental shelf. During the weakest upwelling (September-October) sAsardine was larger near upwelling foci where Chl concentrations of 1-3 mg m^{-3} were observed within the first 10 km of the coast, and avoided distances farther than 30 km from the upwelling foci. During this season with high riverine discharge, sAsardine evaded the southeast-northwest haline front formed between clear Caribbean Sea waters and the turbid Orinoco River plume. Higher coastal concentrations of sAsardine increase the availability (and possibly the catchability) for the artisanal fishery during the period of weakest upwelling. Higher numbers of small pelagics schools were found closer to the shore all year round, which increases catchability regardless of the total stock. We hypothesize that the 2005 collapse of the *S. aurita* fishery off northeastern Venezuela was caused by a combination of sustained stressful environmental conditions (weak upwelling and warmer water temperatures from 2004 to 2010) and overfishing as a result of the increased catchability of the stock caused by aggregation of the fish in the cooler coastal upwelling cells.

3.2 Introduction

The southern Caribbean Sea (Figure 3.1a) is an area of pronounced seasonal coastal upwelling during the first half of the year (Richards 1960, Herrera and Febres-Ortega 1975, Muller-Karger and Aparicio-Castro 1994). The nutrient-rich upwelled waters produce important phytoplankton growth that leads to bountiful fisheries; especially in the northeastern Venezuelan shelf (Figure 3.1b), which is one of the most important fishing grounds in the Caribbean Sea. The Spanish sardine, *Sardinella aurita* (also called round sardinella), is one of the most important fisheries in this area. Spanish

sardine catches in northeastern Venezuela represent nearly 90% of the small pelagic fish catch for the Caribbean Sea (FAO-FIGIS, 1980-2011). This relatively small shelf area of 23,200 km^2 (Figure 3.1b) has a Spanish sardine biomass between 0.6 to 1.3 million tons, estimated by means of acoustic surveys (Stromme and Saetersdal 1989; Cárdenas and Achury 2002; Cárdenas 2003). Spanish sardine is an opportunistic filter feeder and its stomach content has the same composition of plankton as the surrounding surface waters of the study area (Cervigón 1991; Cellamare and Gómez 2007). In addition to the plankton richness in this area due to upwelling, the complex topographic features and wide continental shelf (Figure 3.1b, Fréon and Mendoza 2003), and its characteristic upwelling dynamics (Rueda-Roa and Muller-Karger, see second chapter in this dissertation) favor the development of Spanish sardine biomass. Despite the wide distribution of the Spanish sardine population on the shelf (Figure 3.1b, Cárdenas 2003; Guzmán *et al.* 2003), fishing activities only take place in areas close to shore (up to ~10 km from shore) owing to the artisanal nature of the fishery which is protected by Venezuelan laws (Freón and Mendoza 2003; González *et al.* 2005, INAPESCA 2001). Fishermen catch Spanish sardine schools using relatively small boats with traditional fishing gear like artisanal beach seines without bags or using artisanal purse seines and operated manually from small boats and from shore.

Fishery management of clupeoid fishes has proven difficult because the high variability in ocean conditions, such as upwelling, can threaten or enhance the survival of early life-history stages (Lasker 1975, Cury and Roy 1989, Bakun 1996). Short life cycles make any fluctuations in recruitment translate rapidly into fluctuations in population size. A reasonable level of exploitation during years with good recruitment, if unchanged, may
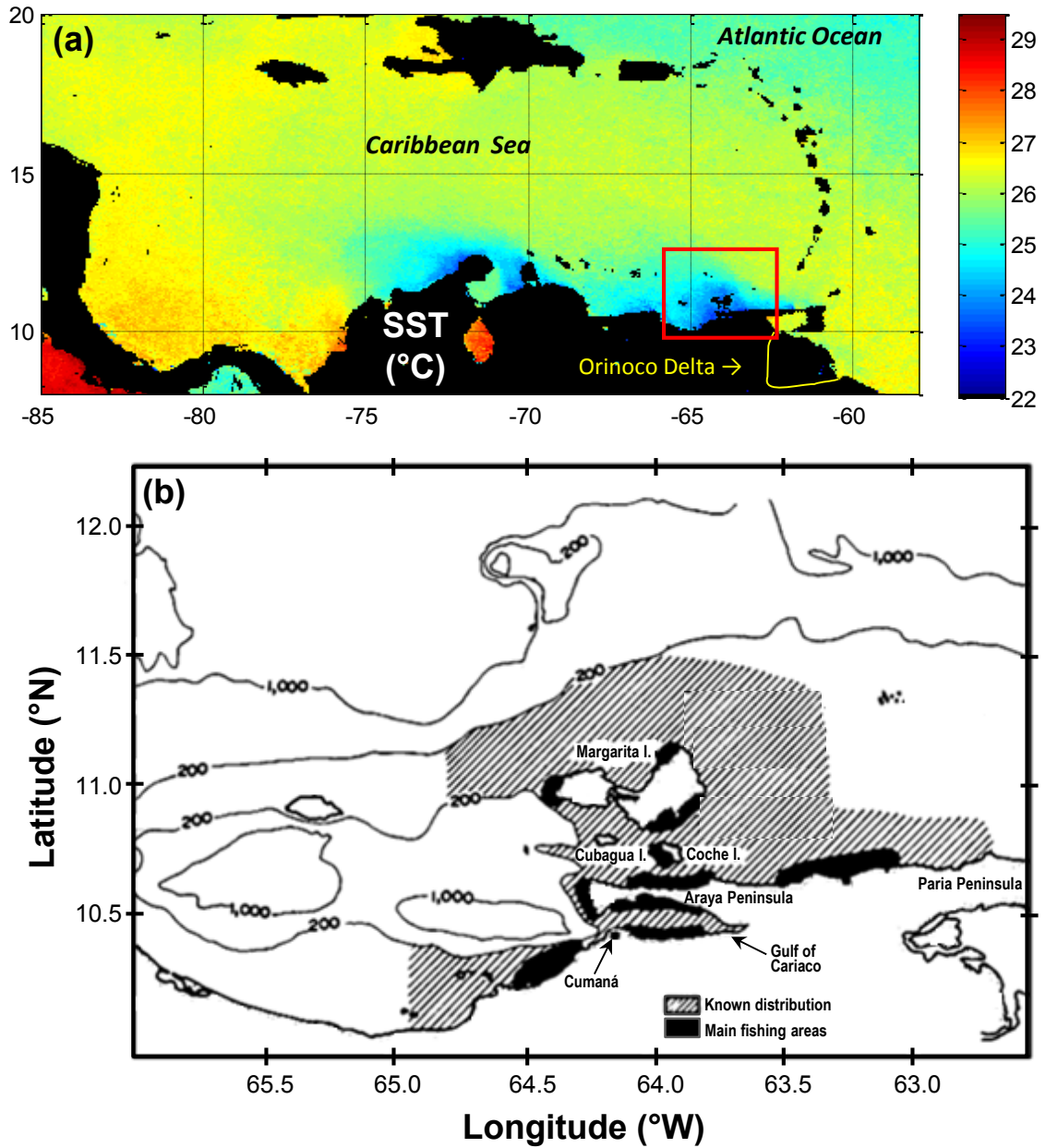
Figure 3.1. The Caribbean Sea (a) and northeastern Venezuela (b). (a): Sea surface temperature (SST) climatology (20-24 February, 1994-2009) of the Caribbean Sea showing the upwelling in the southern region. The study area (red rectangle) off northeastern Venezuela shows seasonal upwelling and it is also influenced by the Orinoco River discharge. (b): Eastern coast of Venezuela bathymetry with known *Sardinella aurita* distribution (hatched) and main fishing areas (solid black).
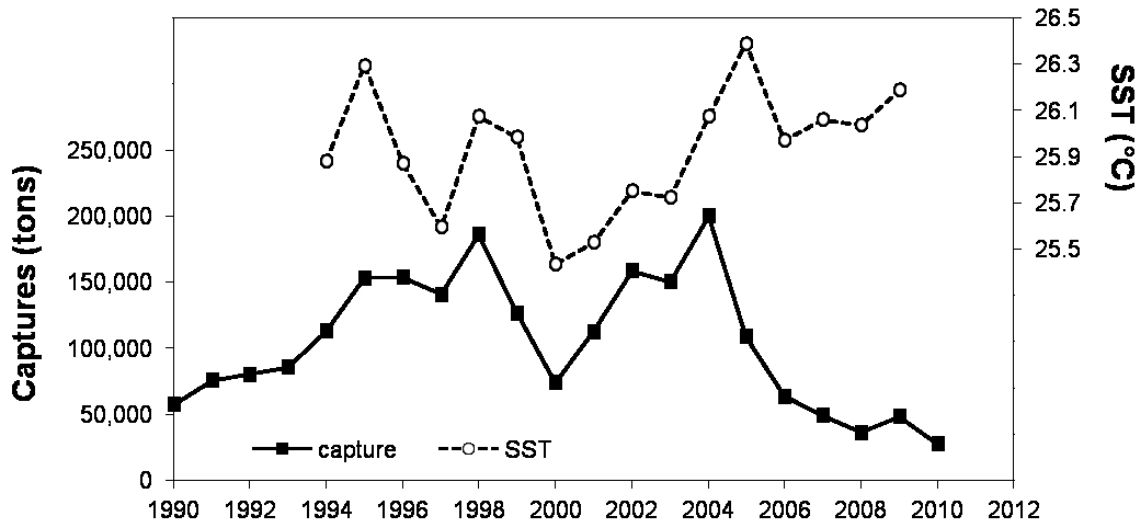
Figure 3.2. Annual capture of *Sardinella aurita* in northeastern Venezuela compared to annual SST averages for the study area. Spanish sardine capture data from INSOPESCA (2012). SST spatial averages for the study area were calculated excluding the Orinoco mask (see Figure 3.3). Long term SST average (1994-2009) was 25.9°C.

lead to overfishing during unfavorable environmental conditions and could have disastrous consequences. Sardine fishery landings off the northeastern Venezuela (provided by the Venezuelan Government Fisheries and Aquaculture Administration, INSOPESCA) showed that *S. aurita* annual landings from 1980 to 1993 were 61,760 tons in average. After 1994 catches were higher (Figure 3.2) as a result of a higher market demand (Barrios *et al.* 2010). However, consecutive years of weak upwelling starting in 2004-2005 (Figure 3.2) have contributed to a crash in the Venezuelan Spanish sardine fishery. This created great economic havoc which included the closing of several sardine canneries. As of 2011, the fishery had not recovered to previous yields (34,754 tons in 2011 and maintains the descending trend), which caused the closing of several factories related to sardine processing (El Nacional newspaper 03/21/2009). The economic and

social problems arising from the collapse of the Spanish sardine fishery in this area highlights the need for better fishery management strategies.

The main objective of this research was to understand the response of *S. aurita* to changes in upwelling in the southeastern Caribbean Sea. This information is needed for competent fishery management. Our first approach was to study the fluctuations in *S. aurita* landings in the main fishing areas (Figure 3.1b) and relate them to inter-annual variation of the strength of the upwelling. Fishery data for *S. aurita* were compiled by INSOPESCA, the institute responsible for compiling fishing information and for the sustainable management of the fishery resources. The main source of the Spanish sardine fishery data come from the canning factories, which are required to provide INSOPESCA with a monthly summary of the amount landed in their facilities and the capture area of the Spanish sardine they purchase. In 2002, the information form to be filled required much more details and requested data for each transaction, e.g. the total weight (kilos) of fish bought, name of the provider, place and date of the capture, etc. The forms are sent to INSOPESCA on paper, from which they extract the monthly summary and add it to the fishery statistics. We worked with INSOPESCA personnel to transcribe the detailed information contained on paper into electronic files. These contained the spatial and temporal resolution needed for the analysis. Unfortunately, it was found that an important number of forms returned from various canneries or fishing entities over time were missing and this prevented a systematic study of the fishery patterns using these data.

We needed a way to determine if the spatial patterns of Spanish sardine distribution are related to the upwelling annual cycle. An analysis of such patterns would clarify if availability to the fishery is influenced by the upwelling cycle. For this purpose

we used data from acoustic surveys that provide historical estimates of fish abundance and their spatial and temporal distributions in the region (Simmonds *et al.* 1992). There have been several hydroacoustics surveys to estimate stock abundance and distribution of *S. aurita* off northeastern Venezuela. The series of VECEP program acoustic surveys performed from 1995 through 1998 was used; which coincided with the availability of satellite-derived Sea Surface Temperature (SST) imagery. These surveys had been analyzed using *in situ* oceanographic data (Cárdenas and Achury 2000), but these data lacked the synoptic coverage offered by satellite SST. The satellite SST products were used to define a proxy for upwelling in this study area.

The main finding is that during the upwelling season, Spanish sardine is widely distributed in the cooler waters of the continental shelf, while during the lowest-upwelling season the sardine is concentrated closer to the coast in nearshore upwelling foci that still have cells of cooler waters near the coast. This coastal concentration increases Spanish sardine availability to the artisanal fishery operating within 10 km of the coast. The possibility arises that after an anomalous period of weak upwelling, reproductive output is negatively impacted, and larval survival and recruitment of the Spanish sardine are negatively affected at the same time that the availability and catchability is increased. This poses a "perfect-storm" scenario in which overfishing can occur on an already environmentally strained population.

3.3 Methods

3.3.1 Study Area:

The study area (10-12°N and 61.5-65°W; Figure 3.1 and Figure 3.3) is located along the southeastern boundary of the Caribbean Sea, off northeastern Venezuela, with a continental shelf roughly oriented east-west. It has a variable continental platform extension that ranges from 5 to 100 km, with depths between 7-115 m (Freón and Mendoza 2003). The shelf topography is complex (Figure 3.1b) presenting several islands, capes, offshore banks, a long and narrow gulf (Gulf of Cariaco) and a deep depression (Cariaco Basin). The prevailing trade winds along with the coastline orientation and shelf topography favor year-round wind-induced coastal upwelling in this region, with seasonal intensification during the time of stronger Trade Winds between December and April (Richards 1960, Herrera and Febres-Ortega 1975, Muller-Karger and Aparicio-Castro 1994). A recent analysis of a long record of oceanographic observations in the area (the CARIACO Ocean Time-Series program) revealed that a secondary upwelling event occurs every year around July (Rueda-Roa 2001, Astor *et al.* 2003, Rueda-Roa *et al.* first chapter in this dissertation). The warmest sea temperatures in the region occur during September-November; these are ~1°C cooler than SST in the central Caribbean Sea (Muller-Karger and Aparicio-Castro 1994); this is caused by the weaker upwelling that occurs during this period (Rueda-Roa and Muller-Karger second chapter in this dissertation). This continental margin area experiences moderate winds during July (mean 6.12 m s^{-1}) and shallow offshore isotherm depths (22°C isotherm mean depth, 85 m) due to the geostrophic Caribbean Current. This leads to moderate coastal SST (25.24°C) and moderately high Chl (1.65 mg m^{-3}). The coastal upwelling area

presents relatively high levels of primary production with a high temporal and spatial variability, ranging from 3 $gCm^2 d^{-1}$ in coastal upwelling areas to 0.2 $gCm^2 d^{-1}$ in other areas (Varela *et al.* 1997).
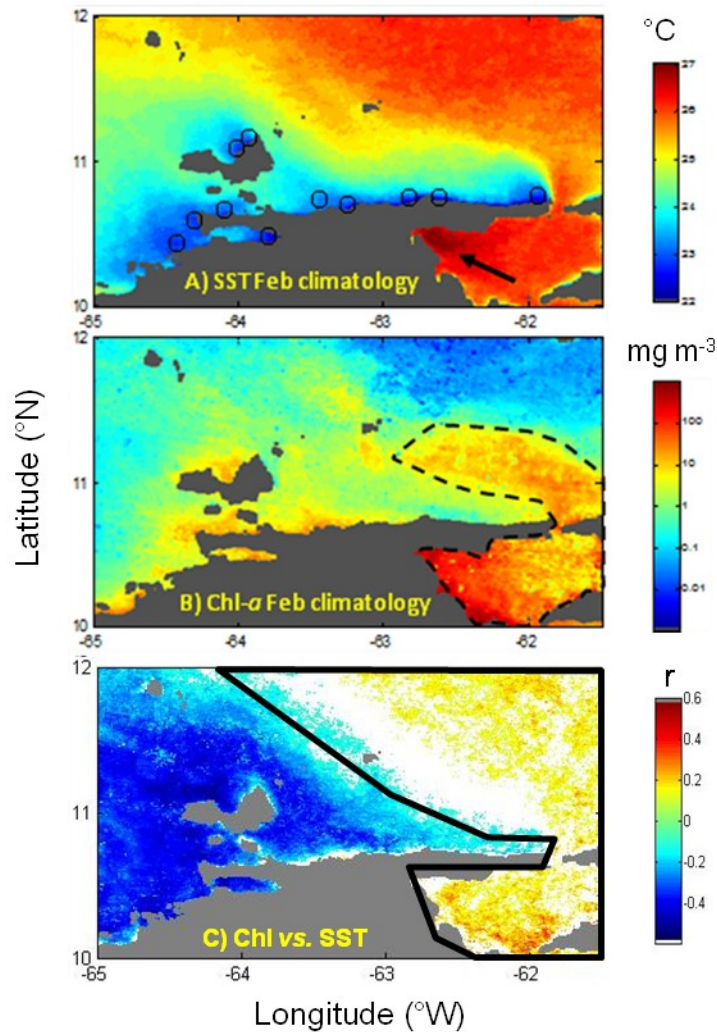
Figure 3.3. Study area used to calculate the spatial averages for satellite SST (10°N to 12°N and 61.5°W to 65°W). (a) SST climatology for February is presented as an example of upwelling conditions, showing the upwelling foci (blue circles) and the upwelling plumes, and also the extreme high SSTs in the Gulf of Paria (arrow). (b) Chl climatology for February shows high levels related to upwelled waters and also high apparent pigment concentrations in the Orinoco river plume (dotted black line) caused by high levels of CDOM. (c) Correlation coefficient between weekly SST and Chl time series (1998-2009). A mask (black polygon) was applied to avoid the inclusion of data from the Gulf of Paria and the Orinoco plume. The mask was established as the area with no significant ($p > 0.05$) or with positive correlations.

100

The Orinoco is the third largest river in the world based on discharge and its plume extends towards the northwest as it enters the Caribbean Sea (Figure 3.3b). The strong freshwater discharge from the Orinoco River (Figure 3.3c) adds complexity to the hydrological and optical environment of the region. Maximum discharge occurs between July-October (Aparicio-Castro 2003) and the plume extends to its maximum at that time, reaching as far north into the Caribbean Sea as Puerto Rico (see references in Muller-Karger *et al.* 1989).

3.3.2 Acoustic survey data:

Spanish sardine density and spatial distribution were obtained from eight VECEP program acoustic surveys performed during 1995-1998 with the R/V Hermano Ginés (Fundación La Salle de Ciencias Naturales), under the Technical Cooperation Programme for Fishing UE-VECEP ALA 92/43 between the European Union and Venezuela, Colombia, Ecuador and Peru. Pelagic fish acoustic backscattering strength was measured with a split-beam echo sounder SIMRAD EK500 at 38 and 120 kHz, and processed using a digital echo integrator from Agenor (Protechno). A frequency of 120 kHz is the optimum for the relatively shallow depths around the study area (from 10 to 150 m). The navigation velocity for the echo-surveys was 10 knots (18.5 km h^{-1}) and the basic sampling unit was one nautical mile (1.85 km). Calibrations of the echosounder were performed before every survey with two copper spheres. More details of the echo survey methodology can be found in Cárdenas and Achury (2002).

Acoustic backscattering echo ground-truthing was performed with exploratory fishing using semi-pelagic trawls, and they were used to calculate the Spanish sardine

relative abundance index (sAsardine) from the total pelagic acoustic data. For each cruise, the different proportions of Spanish sardine obtained from all trawls were averaged within three areas. Exploratory fishing was not possible for some acoustic survey areas, and the factors used were an average obtained from the other VECEP surveys. Those Spanish sardine factors varied from 0.1 to 1 with an average of 0.54 (Cárdenas and Achury 2002). Spanish sardine factors were calculated within three delimited areas (a) The Gulf of Cariaco which features upwelling focus in its southeastern extreme (Figure 3.3a); this area is considered an important nursery for the species (Freón *et al.* 1997). (b) The South Area, from 10.6°N to 11°N (Figure 3.1), and which shows important upwelling foci along the northern coasts of the Paria and Araya peninsulas and upwelling plumes extending toward the NW. This area is affected by the Orinoco River discharge on a seasonal basis (Figure 3.3a) and it presents variable depth, especially around the western area with the presence of islands and other topographic features. (c) The North Area, from 11° N to 11.4° N, with deeper waters off northern Margarita Island. This area has two local upwelling foci situated northeast of Margarita Island (Figure 3.3a). Open waters to the east of this area receive the input of the upwelling plumes from the South Area and also the Orinoco River discharge (Figure 3.3b).

3.3.3 Satellite Sea Surface Temperature and Chlorophyll:

Several satellite-derived products were extracted for the study area window (Figure 3.3). High resolution sea surface temperature (SST) imagery (~1 km^2 per pixel) from the Advanced Very High Resolution Radiometer (AVHRR, National Oceanic and

Atmospheric Administration), were collected using a ground-based L-band antenna located at the University of South Florida (St. Petersburg, Florida, U.S.A.). SST was derived using the Multi-Channel Sea Surface Temperature (MCSST) split-window techniques (Walton 1988; Strong and McClain 1984; McClain *et al.* 1983). The nominal accuracy of AVHRR SST retrievals is in the range of ±0.3 to ±1.0 °C (see also Brown *et al.* 1985, Minnett 1991). AVHRR imagery contains false cold pixels caused by cloud contamination; to improve data quality, a cloud filter similar to that of Hu *et al.* (2009) was implemented. The filtered daily images were used to calculate weekly averages and a long-term weekly SST climatology (1994-2009). Figure 3.4 shows the SST averaged over the duration of each acoustic survey cruise (V1 to V8) compared to the weekly SST climatology (1994-2009). Most survey samples were collected well within the expected range of temperatures for each area and season.

In order to assess whether Spanish sardine has a tendency to aggregate close to upwelling/thermal fronts or not, SST gradients (SST-gradient) from the SST imagery covering each acoustic survey were calculated. This was done using the following equation, where '*i*' denotes the latitudinal pixel position, and '*j*', the longitudinal pixel position:

$$SST\,gradient(i,j) = \sqrt{(SST(i+1,j) - SST(i-1,j))^2 + (SST(i,j+1) - SST(i,j-1))^2}$$

High resolution (~1 km^2 per pixel) satellite Chlorophyll-a (Chl) imagery was used, produced with the default NASA OC4 chlorophyll algorithm (O'Reilly *et al.* 2000), from images collected with the Sea-viewing Wide Field-of-view Sensor. Level 2 images (with derived geophysical variables at full resolution) were downloaded for the study area from the Ocean Color web page http://oceancolor.gsfc.nasa.gov/ (Sep 1997 to Dec 2009)

and mapped to a uniform space grid scale using Matlab routines provided by NASA. Weekly Chl time series composites and weekly long term means (1998-2009) were calculated. Correlations between SST and Chl were used to delimit the area influenced by upwelling from the area influenced by the Orinoco plume. SeaWiFS Chl was concurrent only for two acoustic surveys, VECEP 7 and 8, which were carried out during weak and strong upwelling conditions, respectively.

3.3.4 Data analysis:

For this work the following variables obtained for each VECEP acoustic survey were used: survey number, sampling time, latitude, longitude, sAsardine, number of small pelagics schools (Schools) and area of sampling (Area, see section 2.2). At each nautical mile along the acoustic tracks the following parameters were extracted from the satellite images: SST, SST-gradient, distance to the nearest upwelling focus (upw-foci, see location of the upwelling foci in Figure 3.3a), and Chl (for VECEP 7 and 8).

Due to the intrinsic aggregation behavior of sardines, the analysis of the relationships between sardine biomass and environmental variables is challenging. This behavior has caused a patchy spatial distribution off South Africa , with a significant portion (90%) of sardine (*Sardinops sagax*) biomass located in a small fraction of acoustic transects (~10%, Barange and Hampton,1997, Barange *et al.* 2005). For the VECEP surveys, Cárdenas and Achury (2000) did not find a clear correlation between Spanish sardine biomass with *in situ* sea temperature or chlorophyll-*a* data. This was likely related to the high proportion of data points with low sAsardine values caused by their aggregation behavior (see for example Figure 3.5). In order to overcome this

104

problem and visualize the distribution of sAsardine related to the seasonal spatial and intensity variations in upwelling (SST), histograms of SST and averaged sAsardine and Schools for each SST bin (0.3°C, Figure 3.6) were used. sAsardine follows a log-normal distribution; therefore, all analyses were made with its log-transformation.

Generalized Additive Models (GAM) were used to explore the relationship between sAsardine and different variables. The GAMs analysis were performed using the ''mgcv'' library (Wood 2006) in the free "R" statistical software (R Development Core Team 2011). GAMs find predictor-responses relationships without using a specific model (non-parametric model), allowing the data to reveal possible functional forms. The GAMs use a link function to establish a relationship between the mean of the response variable and a ''smoothed'' function of the explanatory variable(s). They are especially useful when the relationship between variables is expected to be complex, not easily fit to standard linear or non-linear models (Hastie and Tibshirani 1990).

The GAM analyses were performed with a Gaussian distribution; this was appropriate because sAsardine is a continuous variable with a log-normal distribution. Output plots from GAMs illustrate the non-linear relationship between the response variable and each predictor. For example, in Figure 3.7b the y-axis represents a relative scale with zero as the mean effect of the independent variable or predictor (Time) on the response variable (log[sAsardine]), and positive/negative y-values indicates a positive/negative effect on the response. The range of the function in the y-axis indicates the relative importance of each predictor. The black lines at the bottom of the x-axis (the rugplot) indicate where the data values lie. GAM graphs also show the 95% confidence limits, which tend to diverge near the extreme of the range for continuous predictors as a

consequence of fewer observations (e. g. Figure 3.8). In order to account for the geographical distribution of sAsardine (e. g. Figure 3.8), a two dimensional smoother (Guisan *et al.* 2002) was implemented using the two geographic coordinates as a variable (Lon, Lat).

3.3.5 Upwelling and phytoplankton biomass 2004-2005:

Spatial averages of SST and Chl were produced for 2004-2005 and compared to long-term SST and Chl climatologies. Annual spatial averages of SST were then contrasted with *Sardinella aurita* annual catch data from INSOPESCA (2012) with the objective of assessing whether there are long-term associations between particular SST or Chl regimes and sardine populations (Figure 3.2).

3.4 Results

3.4.1 Orinoco River effects:

The area dominated by the Orinoco River discharge had very high SST (Figure 3.3a) and a strong signal in the Chl product (Figure 3.3b) as a result of high concentrations of CDOM (Colored Dissolved Organic Matter). The SeaWiFS default Chl algorithm fails in turbid coastal waters with high concentrations of CDOM, producing erroneous high estimates of pigment concentration (Carder *et al.* 1999). The strength and boundary of the upwelling plume and of the Orinoco plume into the Caribbean Sea alternate seasonally (Varela *et al.* 2003). The lower salinity and warmer waters of the Orinoco plume overlap the dense, cold and high salinity water from the upwelling area. Correlation coefficients between weekly time series of SST and Chl show a

negative/positive relationship in the areas influenced by upwelling/Orinoco plume (Figure 3.3c). The boundary between these two phenomena was determined as the area with no significant correlation (p> 0.05) between weekly SST and Chl time series (1998-2009, Figure 3.3c). The upwelling plume area presented a negative correlation between SST and Chl; lower SSTs due to upwelling are related with higher Chl concentrations, as expected. The Orinoco plume, with higher SSTs from the warmer riverine discharge, had positive correlation with Chl caused by high CDOM and chlorophyll-*a* concentrations within the riverine waters. The area with no correlation (Figure 3.3c) is the boundary where those two phenomena interact in the southeastern Caribbean Sea along the course of the year. For this work the area covered by the Orinoco plume was masked and this region was not include in the analyses in order to obtain the spatial SST/Chl averages related solely to upwelling dynamics (e.g. Figure 3.2, Figure 3.4, Figure 3.10).

3.4.2 Acoustic cruises:

The spatially-averaged SSTs covering the acoustic surveys were very close to the long-term weekly SST spatial average for the study area (Figure 3.4), although VECEP 1 was warmer than average. Consequently, although the surveys were done during different years, we think that it is reasonable to analyze them as being part of a typical annual upwelling cycle (Figure 3.5). The SST histograms show seasonal differences in the distribution of sAsardine in relation with SST (Figure 3.6). During upwelling, sAsardine was distributed along all the SSTs bins, which imply a wide spatial distribution in the broader study area. During months of weaker upwelling (September and October surveys) sAsardine was concentrated in those fewer pixels showing the coolest SSTs
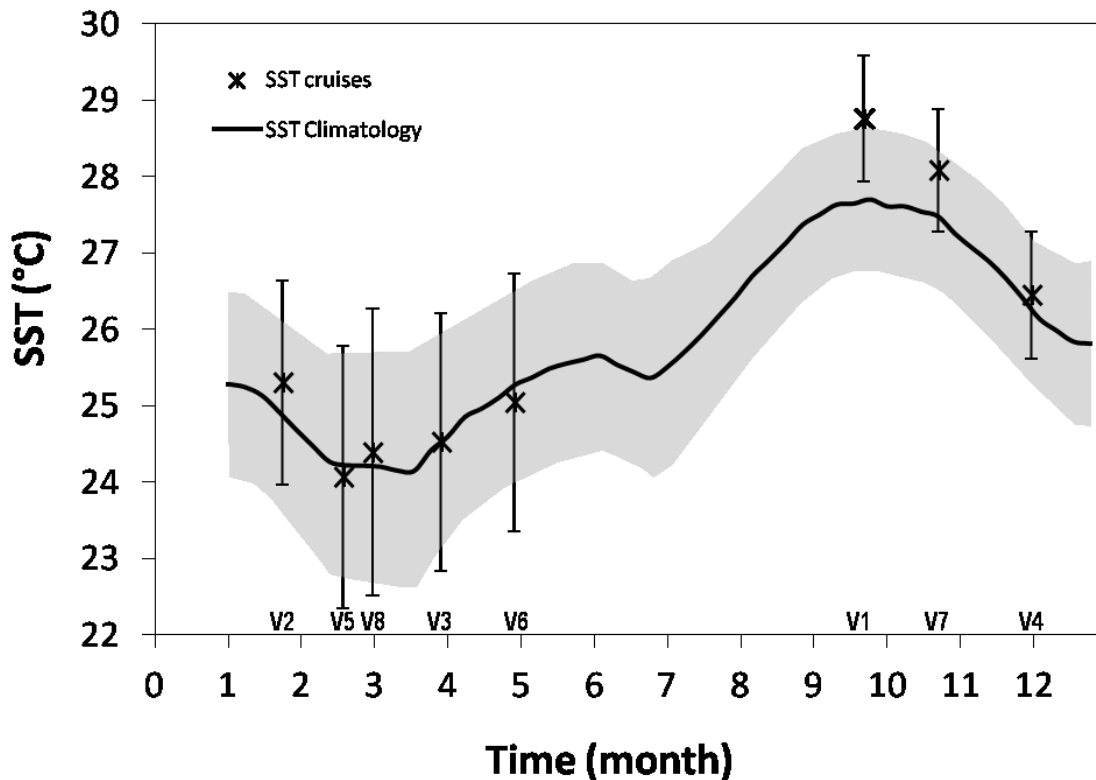
Figure 3.4. Averaged SST for each VECEP acoustic cruise (V1 to V8) compared to the weekly SST climatology (1994-2009). Spatial SST averages were calculated for the study area excluding the Orinoco mask (see Figure 3.3). Twice standard deviations are shown for the SST cruises (bars) and the SST climatology (gray shadowed).

(Figure 3.6). These months had cooler SSTs very close to the coast, particularly off the coasts of the Araya and Paria peninsulas and in the Gulf of Cariaco (Figure 3.5), and sAsardine was highest in these areas. On the other hand, the number of small pelagics schools did not show clear seasonal differences; the numbers of schools was always higher in areas with cooler SSTs (Figure 3.6). The GAM analysis was performed only with sAsardine because of its seasonal response.
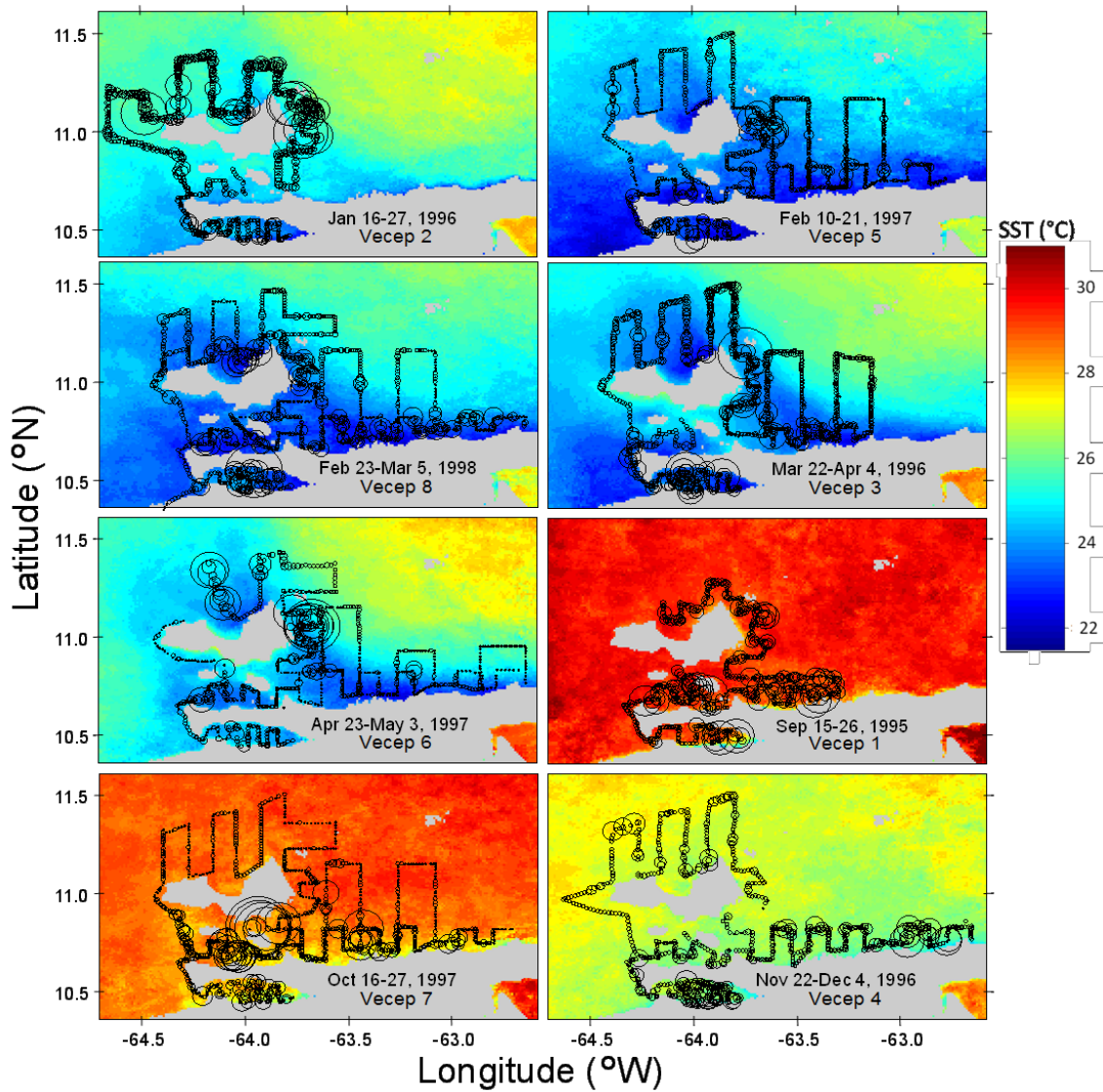
Figure 3.5 Spanish sardine relative abundance index (sAsardine, proportional to circle size) along the tracks of each VECEP acoustic survey, superimposed on average SST for each survey period (color coded).
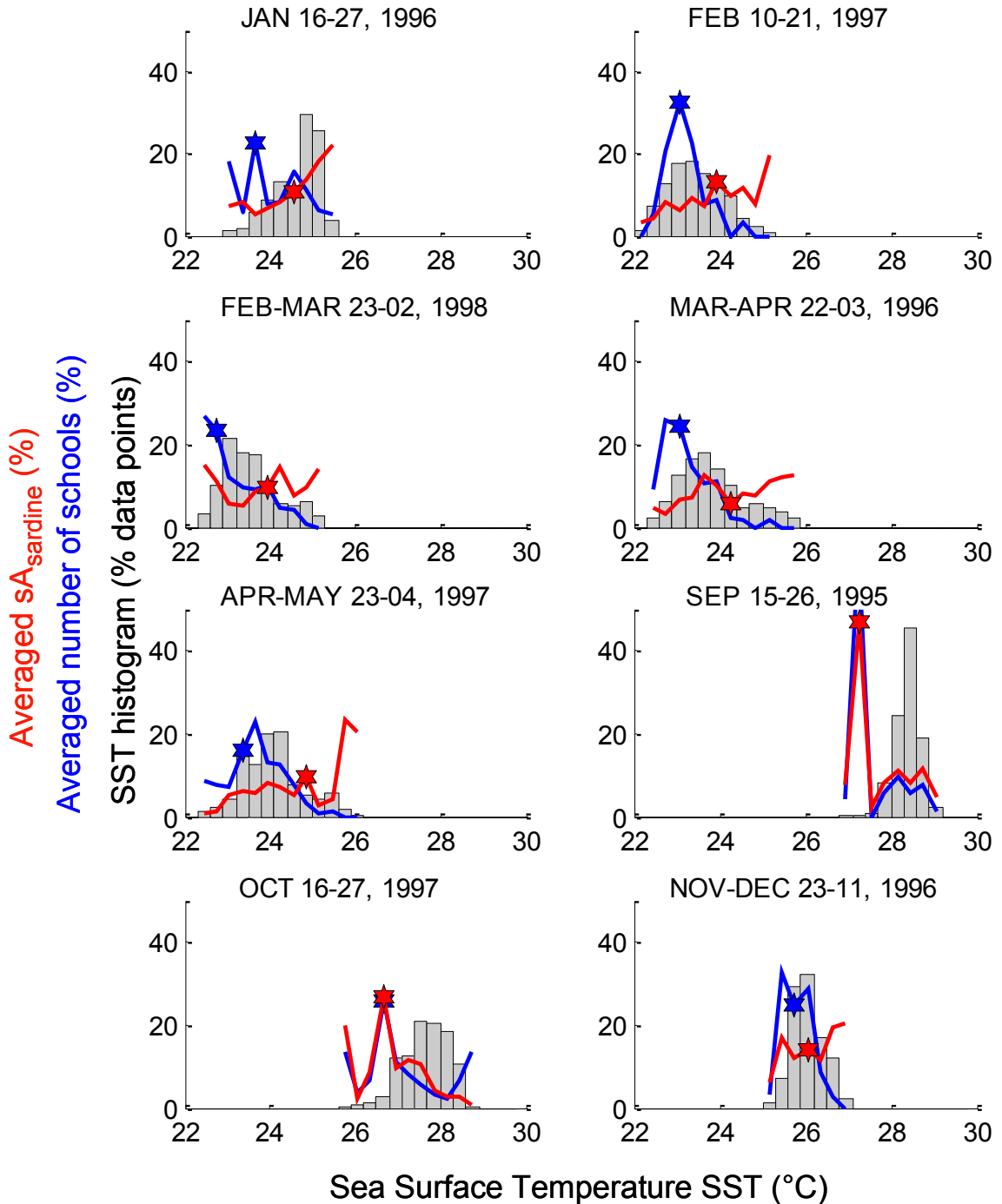
Figure 3.6. SST histograms calculated from the SSTs extracted along each cruise track. For each SST-bin, average log-sAsardine (red line) and the average number of small pelagic schools (blue line) were calculated and both were scaled to percent. Stars indicate the SST-bin where 50% of the average sAsardine and school number occurred.

There were differences among the acoustic surveys with regard to the mean density of sAsardine along the tracks (Figure 3.7a). The first 4 surveys had significantly higher averages (ANOVA, p<0.01) and lower variances than the last four surveys. Both groups of surveys were performed at different phases of the upwelling cycle. This indicates that the reason was not the seasonal nature of the upwelling but other factors, including inter-annual variations in upwelling strength, or logistical differences between surveys or even differences in surveys tracks.

The backscattering strength of sAsardine changed during the day for all the surveys. Higher backscatter was recorded during night-time (5:30 pm to 5:30 am, Figure 3.7b). This is further corroborated with day vs. night ANOVA analysis for each survey (p<0.01). This also shows that night-time data present lower variances than day-time data. The number of schools also changed during the day, in exactly the opposite pattern as backscatter, showing higher degree of aggregation during daytime (data not shown). To account for the differences on sAsardine within surveys and along the day, the data was normalized adding 'survey number' and 'sampling time' as factors in the GAM analyses. The 'area' was also added as a factor to account for errors in the sharp latitudinal delimitation of the three areas used to average the sardine biomass conversion factors obtained from the exploratory fishing samples (see section 2.2).

GAM analyses can be applied to several independent variables at the same time (multivariate model) to obtain the best model that explain the variations of the dependent variable. However, concurvity (the non-linear multicollinearity) could lead GAMs to produce unstable or even wrong estimates of the covariates' functional effects (Peng *et al.* 2006, Gu *et al.* 2010). Concurvity occurs when some smooth term in a model could be
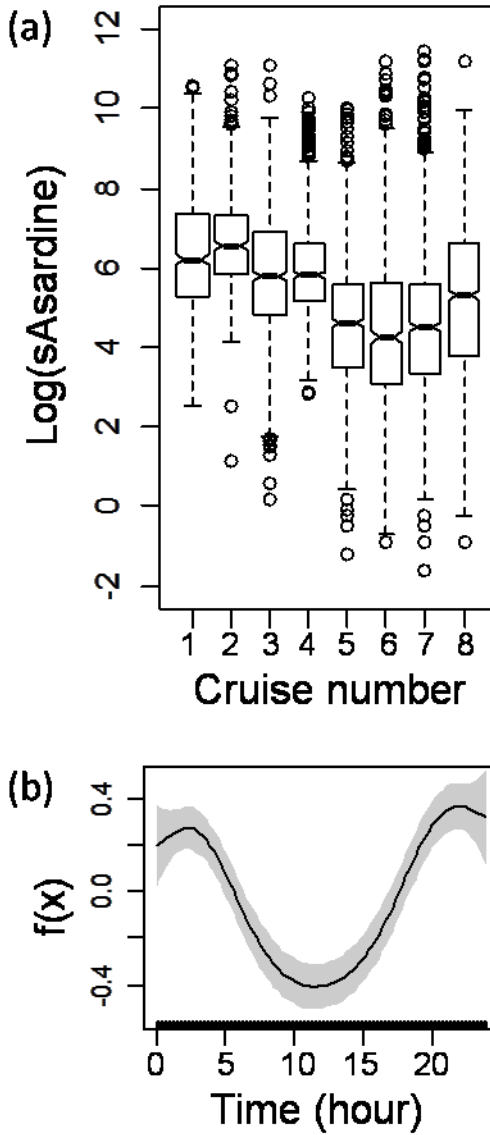
Figure 3.7. (a) Boxplot of sAsardine for each cruise showing that, regardless of the season, the four first cruises have higher averages than the rest. (b) GAM analysis of log(sAsardine) vs. hour of measurement (with cruise number as a factor, $p<0.001$, deviance explained 19.2%), showing a daily cycle in the backscattered strength of sAsardine recorded along the day, as a result of diel changes in aggregation patterns and vertical migrations.

approximated by one or more of the other smooth terms in the model. The level of

concurvity between the predictors was calculated, giving the 'estimate' index (values

between 0 and 1, with 0 indicating no problem, and 1 indicating total lack of

identifiability, Wood 2012). The data used in this work had high levels of concurvity with the geographic coordinates (Lon, Lat): SST (0.78), Chl (0.79), upw-foci (0.91); and from low to moderate concurvity levels with upw-foci: SST (0.32), Chl (0.20), and with SST: Chl (0.27). Concurvity in our data set was caused by the spatial stability of the upwelling foci, the spatial pattern of the upwelling plume dispersion, and by the correlation between upwelling and phytoplankton biomass.

There were no important differences (Table 3.1) between the GAM 'deviance explained' (analogous to variance in a linear regression) using a univariate model (i.e. comparing sAsardine with each predictor separated) or using a bivariate model (i.e. comparing sAsardine with a pair of predictors). In addition, the shape of some predictor had important changes when analyzed together, as it has been found in other works. For example, Jablonski and Legey (2004) found an optimal window dome shape relationship between recruitment with Ekman Transport and with SST when used separated, but the dome shape was lost when both terms were together. Since the objective was to understand the relationship of sAsardine with the different variables, and in order to avoid the problems produced by concurvity, GAM models were calculated for every parameter separated (see for example Bertrand *et al.* 2004) and including as factors the survey number, sampling time and area. An example of the GAM formula for SST is given below:

gam(log(sAsardine) ~ as.factor (hour) + as.factor (survey) + as.factor (area) + s(SST), data=Veceps

To contrast the differences in sAsardine distribution in the upwelling cycle, three parts of the cycle were analyzed (see Figure 3.4). (a) The strongest upwelling season ('Cool' conditions, when the seasonal SST minimum occurs between February-March) was analyzed using VECEP 5 and 8. (b) The weakest upwelling season ('Warm'

conditions, when a seasonal SST maximum is reached between September-October) was

analyzed using VECEP 1 and 7. During the local SST maximum there is still some level

of coastal upwelling, and SST is around 1°C lower than in the central-eastern Caribbean

Sea (i.e. Figure 2.5, Rueda-Roa and Muller-Karger, second chapter in this dissertation).

And (c), the upwelling transition period ('Transition' conditions, that occurs during

August and November) was analyzed using VECEP 4 (see Figure 3.4 and Figure 3.5).

Table 3.1. Comparison of the GAM '% deviance explained' (analogous to variance in a linear regression) for the univariate models (i.e. comparing sAsardine with each predictor separated, in bold and shadowed) and for bivariate models (i.e. comparing sAsardine with the pair of predictors placed in the column and row). For both cases 'sampling time' and 'Area' are included as factors. Predictors used were: location (Lon, Lat), phytoplankton biomass (Chl), Sea Surface Temperature (SST), and distance to upwelling foci (Foci). VECEP cruises 8 and 7 are presented because they have Chl data and represent the cool and warm upwelling conditions, respectively.

Vecep 8	Lon-Lat	Chl	Foci	SST	*Vecep 7*	Lon-Lat	Chl	Foci	SST
Lon-Lat	**29.0**				**Lon-Lat**	**27.5**			
Chl	31.0	**19.2**			**Chl**	29.1	**18.9**		
Foci	31.1	19.8	**19.0**		**Foci**	30.0	21.6	**17.4**	
SST	30.2	23.3	21.7	**19.5**	**SST**	28.6	19.0	19.4	**16.7**

During 'Cool' conditions (range of temperature of 22-25.5°C; Figure 3.8a) high

sAsardine was widely distributed (Figure 3.8c), especially north of 11°N. There was

slight lower sAsardine in the Gulf of Cariaco and between the Margarita Island and the

Araya Peninsula. The sAsardine was distributed evenly across the temperature range but

avoided SST < 22.5°C (Figure 3.8a). For VECEP 8, Chl was related to SST linear and

inversely between 22°C and 24°C; at SST > 24°C, Chl had the lowest values and did not

show any correlation with SST (GAM deviance explained 30.4%; data not shown). This

indicates that there was no shortage of phytoplankton in the freshly upwelled waters.

During VECEP 8, upwelled waters (Figure 3.5) and Chl (Figure 3.9a) were widely spread over the continental shelf. The highest Chl was found between 20-35 km from the upwelling foci (Figure 3.9c). Biomass of sAsardine had two peaks, around 1.1 and 4 mg m^{-3} (0.05 and 0.6 log[Chl], Figure 3.9b).

During 'Transitional' conditions (range of temperature of 25.4-26.1°C; Figure 3.8d) the highest sAsardine was found inside the Gulf of Cariaco (Figure 3.8f); high biomasses were also found in the entire study area but with some avoidance of waters around Margarita Island. There was preference for intermediate SST (25.4-26.1°C, Figure 3.8d). Below and above this preferred temperatures range the effect of SST was not significant (confidence intervals covered both positive and negative values). For both 'Cool' and 'Transitional' conditions, sAsardine was widely dispersed throughout the distance range from upwelling foci (Figures 8b and Figure 3.8e).

During 'Warm' conditions (range of temperature of 25.7-29.1°C; Figure 3.8g) sAsardine showed a strong avoidance of the northeast region with a south-east/north-west orientation (Figure 3.8i). This region coincides with the seasonal extension of the Orinoco plume (Figure 3.3c). sAsardine was concentrated close to the coast of the mainland and the islands of Cubagua and Coche (between ~63.2-64.2°W) and shoreward of Margarita Island. sAsardine had high avoidance of areas farther than 32 km from the upwelling foci (Figure 3.8h). There was a high sAsardine between 25.7-27.7°C. The range of SST with higher sAsardine coincides with the highest Chl (for VECEP 7) at the SST interval 26.5-27.7°C (and very low at warmer SST; GAM deviance explained 23.6%, data not shown). During VECEP 7 there was indeed some upwelling with cooler waters and higher Chl very close to the coast (compare SST and Chl on Figure 3.5 and

Figure 3.9a). sAsardine was larger at existing high Chl concentrations (1-2.2 mg m^{-3}, or 0-0.35 log[Chl] Figure 3.9b) and the highest Chl was found within the first 10 km of the upwelling foci (Figure 3.9c).

The percentage of sAsardine deviance explained for the three upwelling cases was always higher for the spatial location (Lon, Lat) than for SST, Chl and upw-foci (ranging from 12% to 89% higher than the next highest deviance, e.g. Table 3.1, Figure 3.8 and Figure 3.9). Explained deviances of SST and upw-foci were highest during 'Warm' upwelling conditions (~60% higher than during cool conditions), indicating that during the absence of strong upwelling, these variables exert a higher influence on the Spanish sardine distribution. SST-gradient was not significant for any of the upwelling conditions (data not shown). Analyzing each survey separately, SST-gradient was significant only for VECEP 3 and 6, when there was avoidance of areas with high gradients (> 0.3 and > 0.4 °C km^{-1}, respectively).

Caption for figure on next page

Figure 3.8. Univariate GAM analysis of log(sAsardine) vs. SST, distance from upwelling foci, and location (longitude, latitude) for: Cool (top, VECEP 5 and 8), Transition (middle, VECEP 4) and weak or "Warm" (bottom, VECEP 1 and 7) upwelling conditions. The y-axes (and the isolines in the map) show relative changes, so that a y-value of zero is the mean effect of the environmental variable on sAsardine; for [Longitude, Latitude] positive values are highlighted in red. Each parameter has the same y-axis scale (isolines for Lat-Lon) for comparing the importance of the fitted terms between the different upwelling conditions. A rugplot is displayed for SST and foci distance along the base of each plot (x-axes), where the data values lie; this was omitted in the maps for clarity. The 95% confidence intervals are grey shaded for SST and foci distance. All terms were significant (p<0.001) and the percentage of sAsardine 'deviance explained' (analogous to variance in a linear regression) is showed for each term.
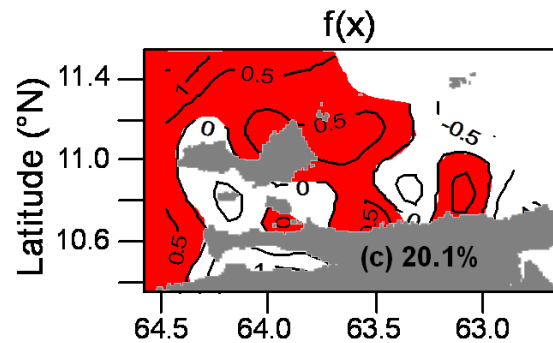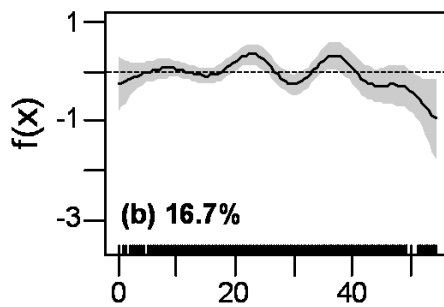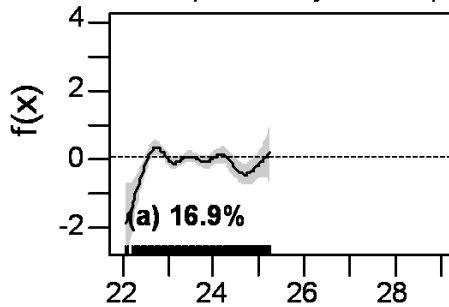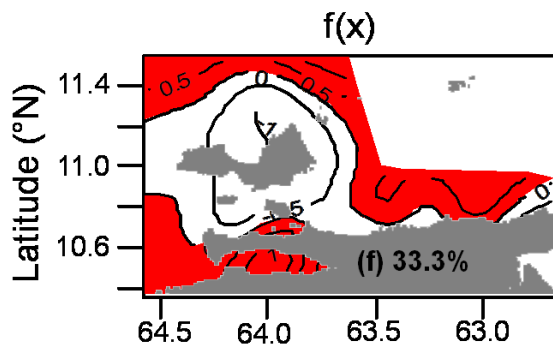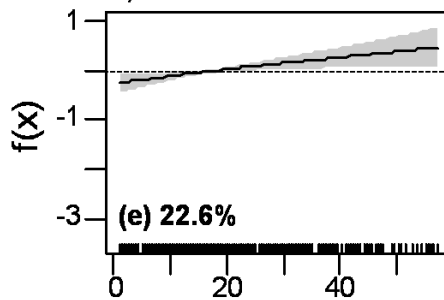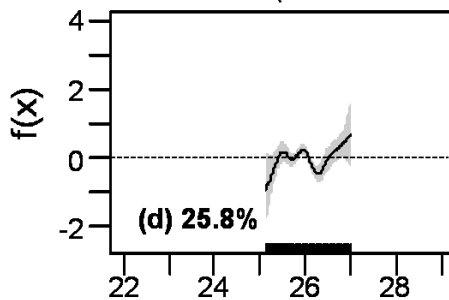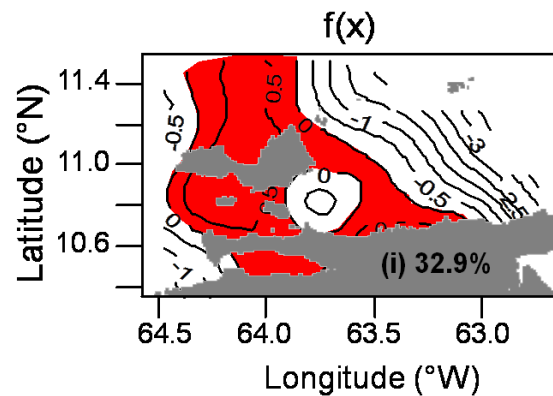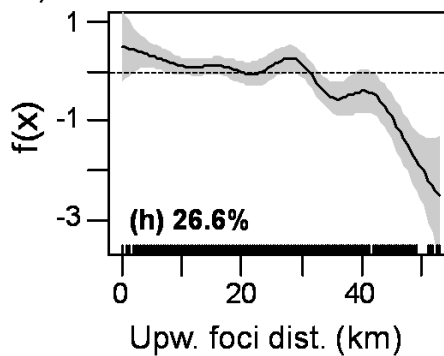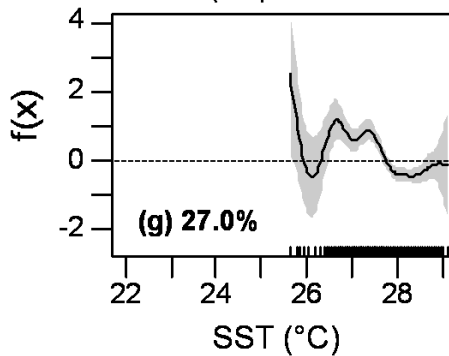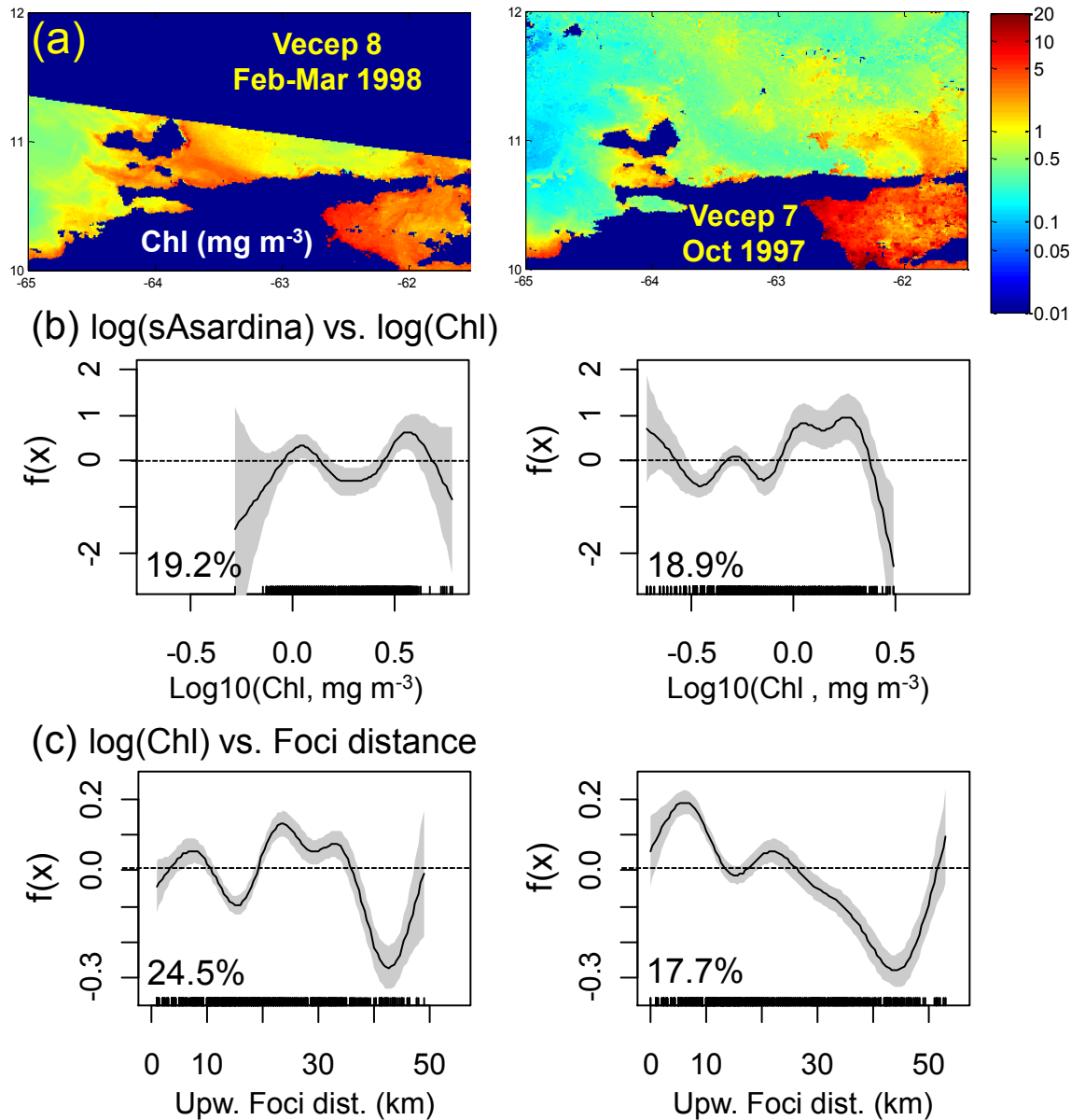
Figure 3.9. Comparison between strong upwelling (left column) and weak upwelling (right column) for: (a) Satellite Chlorophyll-a (Chl); (b) GAM analysis of log(sAsardine) vs. log10(Chl); and (c) GAM analysis of log10(Chl) vs. distance from upwelling foci. The GAM 95% confidence intervals are grey shaded; all the terms were significant ($p < 0.001$) and the percentage of deviance explained is showed for each term.

3.4.3 Upwelling and phytoplankton biomass 2004-2005:

Spanish sardine landings off northeastern Venezuela had steep increases in two years of

weak upwelling, namely 1998 and 2004 (high annual SSTs in Figure 3.2), followed by an

abrupt decline the year after. For 1998, the next upwelling season was a little cooler, and the period after that (2000-2003) had intense upwelling with SST values lower than the long term SST average (25.9°C). After two years of low catch, landings started to increase in 2001, one year after the first intense upwelling (2000). For the 2004 case, the next year (2005) was even warmer (Figure 3.2 and Figure 3.10), and the warm trend continued for several years (Figure 3.2) with annual SST above the long term SST average. Catches declined abruptly in 2005 and as of 2011 had still not recovered.
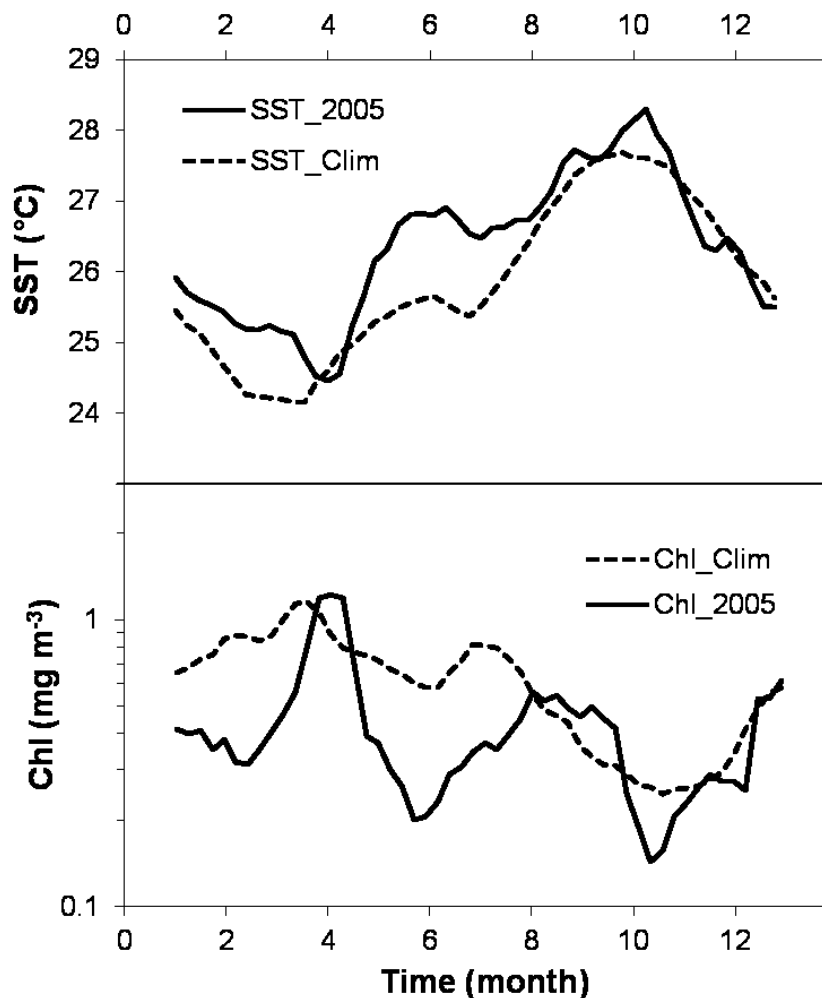
Figure 3.10. Long term (1994-2009) averages of SST and Chl compared to 2005 values. Spatial averages for the study area was calculated excluding the Orinoco mask (see Figure 3.3).

The upwelling season of 2005 was irregular and shorter (Figure 3.10). The principal upwelling had a short peak two months later (April) than average SST climatology. The mid-year upwelling (Rueda-Roa *et al.*, first chapter in this dissertation) was much weaker (1.7°C warmer). Very low levels of phytoplankton were present from December 2004 until March 2005 (Figure 3.10). There was a short Chl peak in April 2005 followed by low Chl during May-June that reached lower values (0.20 mg m^{-3}) than the Chl climatology annual minimum (0.25 mg m^{-3} during October). The lowest annual Chl was found in October 2005 (0.14 mg m^{-3}). Conditions during 2004 were warm and with low phytoplankton, but departures from the SST and Chl climatologies were not as marked as for 2005 (data not shown).

3.5 Discussion

3.5.1 Diel variations:

The sAsardine backscattering strength (Figure 3.7b) and the number of schools show diel variations caused by daily vertical migrations and aggregation patterns that are typical in most small pelagics. The fish school at depth during the day and disaggregate and ascend to the surface during the night (Mais, 1974). This behavior often results in "invisible" fish biomass during nigh-time surveys if they are conducted using narrow beam, downward-projecting hull-mounted echosounder transducers (Cutter and Demer, 2008). However, the VECEP acoustic series used a split-beam echo sounder SIMRAD EK500 that was able to detect higher and less variable relative densities during night time (Figure 3.7b). The VECEP results are consistent with those from previous acoustic surveys in the same study area (Fréon *et al.* 1993; Cárdenas 2003).

3.5.2 SST gradients:

Several small pelagics prefer areas with low SST gradients, keeping away from thermal fronts (Lanz *et al.* 2009) and there is little or no tendency to aggregate near fronts (Agenbag *et al.* 2003). On the other hand, off northern Chile, *Sardinops sagax* was mainly located on the offshore side of thermal fronts and their distribution became wider towards the ocean (Castillo 1996). Also, in Chile *Sardinops sagax* prefer oceanic waters and the frontal zone between these waters and more coastal waters (Castillo *et al.* 1996), while the same species is reported to have its main spawning and nursery areas in frontal zones off Perú (Gutierrez *et al.* 2007). No significant relationship was found between sAsardine with SST gradients. Only two surveys, carried out during the upwelling season, showed some avoidance of elevated gradients, however, this was not evident in the other three surveys done during the same season. The reasons behind this apparent lack of thermal front avoidance need to be explored. High food availability at fronts attracts predators (e.g. fish, squids, etc.) and their presence/absence could be a factor that influences the distribution of Spanish sardine in this area around thermal fronts.

3.5.3 Spatial distribution related to upwelling:

Our results indicate that from the start of the upwelling season as pulses during the transition period studied here (VECEP 4, November 23-December 11) to the fully developed upwelling case, Spanish sardine was broadly distributed in the study area, with some avoidance of the (cooler) waters closer to the coast. However, its spatial distribution was completely different during the season of weakest upwelling

(September-October). During this time, Spanish sardine was concentrated in the first 10 km from the upwelling foci and avoided areas farther than 30 km from the upwelling foci (Figure 3.6 and Figure 3.8). These seasonal differences seem related mainly to the level of spatial dispersion of upwelled waters, and therefore, to phytoplankton biomass along the seasonal upwelling cycle. During upwelling, cool upwelled waters are widely spread over the continental shelf (e.g. January to May, Figure 3.5) with its associated abundance of plankton (e.g. Figure 3.9a); therefore, Spanish sardine can find food in a broad area. The evasion of the coolest waters with the highest Chl near the coast has been documented for small pelagics in other areas. In South Africa, *Sardinops sagax* tends to concentrate in upwelled waters which have been warmed to14–19 °C (Agenbag *et al.* 2003). In the Gulf of California, *S. sagax* (and other small pelagics) prefer moderate Chl (1.0 to 3.0 mg m^{-3}) and moderate SST (17–22°C, Lanz *et al.* 2009). A habitat model for *S. sagax* (Zwolinski *et al.* 20011) indicates that the pacific sardine avoids areas with higher Chl and lower SST, indicative of freshly upwelled waters, and most often resides in water with Chl values between 0.3 and 1 mg m m^{-3}. Zwolinski *et al.* (2011) suggest that the reason for the apparent preference for mid-range SST could be inadequate food for adults in freshly upwelled, cooler, coastal waters and in warmer, oligotrophic, oceanic waters. During VECEP 8 there was high Chl at the lowest SSTs. The Mediterranean *S. aurita* feeds principally on zooplankton (Tsikliras *et al.* 2005); but in northeastern Venezuela *S. aurita* adults feeds largely on phytoplankton (Cellamare and Gomez 2007, and references therein). Therefore, the evasion of the coolest waters of this stock was not attributable to shortage of food and may be related to other factors, such as physiological

preferences (*S. aurita* is considered a tropical stenothermic species, Tsikliras and Antonopoulou 2006).

During the low upwelling season (September-October) coastal waters off northeastern Venezuela are ~1°C cooler than in the central-eastern Caribbean Sea (Muller-Karger and Aparicio-Castro 1994); some level of upwelling can be seen very close to the coast (Figure 3.5) with relatively high phytoplankton biomass (e.g. October in Figure 3.9a and Figure 3.9c). sAsardine was concentrated in those areas with higher phytoplankton (Figure 3.9b) and close to the upwelling foci (Figure 3.8h and Figure 3.9c). A seasonal difference in the offshore distance has been reported for other small pelagics. During warm events the Namibian pilchard (*Sardinops sagax*) shrinks to small areas adjacent to the coast where some localized upwelling is maintained (Thomas and Boyd 1985, as cited in Cole and McGlade 1998). In Perú, the pacific sardine (*Sardinops sagax*) is found farther offshore during winter/upwelling (Gutierrez *et al.* 2007); and, in the primary stages of El Niño (warm) events, *S. sagax* migrate towards the coast off Perú (Ñiquen and Bouchon 2004). In California, *S. sagax* is compressed along the coast during summer (non-upwelling), while it is located offshore during upwelling (Demer *et al.* 2012). When the range of the species shrinks, increased competition for food and higher levels of cannibalism of eggs and larvae also occurs (Cole and McGlade 1998). In the southeastern Caribbean, the coastal concentrations of Spanish sardine during warm conditions increases its availability (and likely also increases its catchability) to the artisanal fishery that operates within 10 km offshore. This behavior increases sardine availability during unfavorable environmental conditions (e.g. anomalous lower upwelling). Thus, it is possible that anomalous years with low upwelling intensities

would affect Spanish sardine in two strong ways: affect abundance due to food scarcity and at the same time increase catchability due to horizontal migrations toward cooler waters closer to the coast. Understanding when this condition occurs is crucial for proper fishery management of this small pelagic.

Eggs of *S. aurita* had been found in the study area between September and April (Huq 2003) with a maximum during November-January (Ramirez and Huq 1986). This stock has an unusual reproductive strategy, with the reproductive period uncoupled to the condition factor (Freón *et al.* 1997). This stock accumulates energy during the upwelling season, reaching a maximum in the condition factor during August (Freón *et al.* 1997), at the end of the mid-year upwelling (Rueda *et al.*, first chapter in this dissertation). On the other hand, the reproductive index starts to increase between September-October, peaking during December-February. This implies that during the low upwelling period a growing proportion of Spanish sardine with mature gonads are more susceptible to be fished.

The spatial distribution of *S. aurita* during September-October seemed also strongly affected by the position of the Orinoco River plume. The maximum discharge of the Orinoco occurs from July to October (Aparicio-Castro 2003). The seasonal effect of the Orinoco plume off northeastern Venezuela is delimited by the area of positive or no significant correlations between SST and Chl (Figure 3.3c). Spanish sardine strongly avoid this area during September-October (Figure 3.8). It has been previously noted that this stock has an eastern limit with the western haline front of the Orinoco plume; area that corresponds also to changes in plankton composition and in plankton biomass (Varela *et al.* 2003). Very low numbers of eggs and larvae have been found to the east (fresher and warmer waters) of this haline front (López 1972). *Sardinella aurita* is a

124

stenohaline species that avoids low salinity waters (Longhurst 1971). Therefore, there is a positive correlation between the availability of the species and water cooling, and a negative correlation with river inflow (Binet 1982). Consequently, during the lowest upwelling season there are two mechanisms that influence the contraction of *S. aurita* to a smaller area: (a) the wider haline front caused by the seasonal higher discharge of the Orinoco River during this period, that causes a horizontal migration of the stock away from the haline front and towards the western side of the study area; and (b) localized cells of upwelling very close to the coast, that produce Spanish sardine concentration closer to shore. A completely different scenario would occur during July, when the maximum freshwater extension (Aparicio-Castro 2003) coincides with the mid-year upwelling pulse (Rueda-Roa *et al.* first chapter in this dissertation). However, the acoustic VECEP series did not have cruises during this time frame. Analysis of acoustic surveys made during this period with concomitant oceanographic satellite products would help us to understand the distribution of Spanish sardine under two simultaneous, strong environmental forces with opposite effects: the upwelling, that produces the spread of Spanish sardine biomass over the continental shelf; and a wider haline front, that would produce the retreat of the stock to the west of the study area.

The location variable (Lon, Lat) always explained the largest deviance for every survey in the upwelling cycle (Figure 3.8, Table 3.1). The same has been found for herring and sprat in the Gulf of Finland (Peltonen *et al.* 2007). This is the result of several geographic factors that lead to enhanced upwelling and chlorophyll and that ultimately influence the distribution of Spanish sardine. Depth could be an important parameter in the distribution of *S. aurita* in the southeastern Caribbean Sea, as found for the Japanese

anchovy (*Engraulis japonicus*, Murase *et al.* 2009), for small pelagic fish in the Mediterranean (Brown *et al* 2006; Schismenou *et al.* 2008), and sardine (*Sardinops sagax*) in South Africa (Agenbag 2003). Seabed type could also be important, as found for the Atlantic herring (Maravelias 1999). In upwelling areas, diet composition of *S. aurita* varies with the intensity of upwelling (Tsikliras *et al.* 2005), and during cessation of upwelling sardines can feed on detritus (Nieland 1982, as cited in Tsikliras *et al.* 2005). *Sardinella aurita* off northeastern Venezuela show benthic feeding during the 'Warm' upwelling season (Cellamare and Gomez-Gaspar 2007). Both, bathymetry and seabed type are spatially distributed factors and they are connected with coastal dynamics (e.g. circulation); and their inclusion is advisable in future analysis. The discharge of the Orinoco River caused changes in *S. aurita* spatial distribution (e.g. Figure 3.3b and 2c) attributable to the salinity effect on this stenohaline organism (Binet 1982). Therefore, salinity is another spatially distributed factor important to include in future analysis.

3.5.4 Distribution of Schools:

Without regard of the upwelling season, all surveys had higher numbers of small pelagic schools in the cooler water range of the surveyed waters closer to the coast (Figure 3.6). This coastal schooling behavior is not related to the abundance of the Spanish sardine (sAsardine) close to the coast, and occurred even during the surveys with the lower sAsardine at cooler coastal SSTs. This nearshore enhanced schooling was also observed in other 6 acoustic surveys made in the study area during 1985-1989 (Cárdenas 2003). However, no references were found of this schooling behavior in other upwelling regions. It is now accepted that schooling has a multi-purpose function related to survival

to predator attacks, effectiveness of feeding, hydrodynamic advantages, migration, reproduction, and learning (Fréon *et al.* 2005 and references therein). An average of Spanish sardine factor > 0.5 (from exploratory fishing) indicates that more than half of those schools were *S. aurita*. In the study area, the schooling preference of Spanish sardine for the cooler waters available (and hence, in waters with higher levels of phytoplankton) suggests that schooling is strongly related to food availability. Waters with high levels of plankton would ensure low levels of intraschool food competition, and individuals located in the posterior margin of schools would be less affected by plankton scarcity due to other fishes feeding before them (Fréon and Mendoza 2003). This coastal schooling behavior also increases catchability of the stock to the artisanal fishery along the entire year.

For the *S. aurita* stock in northeastern Venezuela the weakness of the relation between effort and catch-per-unit-of-effort in tons per set suggests a lack of relationship between the size of the schools and stock abundance (Freón *et al.* 2003). In a review about sustainable exploitation of small pelagic fish, Fréon *et al.* (2005) explained that when sardine abundance decreases, it might decrease their area of distribution, which results in small changes in density within the reduced spatial range. They may continue to form schools of the same magnitude, although fewer schools would be present. In northeastern Venezuela, the schools are within the reach of the artisanal fishery year-round, regardless of actual total biomass. Because the ability of fishers to locate these schools remains high, catches and catch rates are maintained despite reduced abundance. As a result, the catchability of the stock increases and catch rates do not decrease dramatically when the stock declines, until the reduced abundance of schools begins to

127

impact fishing success or the stock even collapses (Fréon *et al.* 2005). Because higher (or more concentrated) Spanish sardine biomasses does not necessarily translate into higher number/size of schools, and because the local fishery is based on the detection and catch of schools, more studies are necessary to find out if higher coastal availability of Spanish sardine during lowest upwelling is really translated into higher catchability.

3.5.6 Case 2004-2005:

During adverse conditions, the Peruvian anchoveta experiences drastic declines and may collapse completely, partly through reduced food supply, and partly through enhanced vulnerability to fishing pressure caused by aggregation of the fish in the remaining foraging areas (Overland *et al.* 2010). We hypothesize that during 1998 and 2004, *S. aurita* was intensively fished as a result of the high market demand and increased catchability. As for 1998, catches in the following two years were lower, but catches started to increase in 2001 following favorable upwelling conditions during 2000 that enhanced recruitment. However, after the historical peak in landings in 2004, the extremely warm and irregular 2005 upwelling may have exerted added negative pressure over the population in several ways. Specifically: (1) An extreme shortage of plankton prey for larvae, postlarvae (from the November-January spawning maxima) and for juveniles from the 2004 year-class, and this probably caused cohort failure. (2) Shortage of food for energy storage and posterior gametogenesis in adults. (3) High levels of catchability throughout 2004 and 2005 (because of the weak upwelling and the presence of schools close to the coast) and increased fishing pressure caused overfishing of the environmentally stressed stock. (4) Relatively higher predation pressure due to reduced

abundance. (5) Subsequent years of weak upwelling haven't allowed the population to recover from the environmental and fishery pressure.

3.6 Conclusions

Correlations of Chl vs. SST were useful to delimit the area of influence of the seasonal Orinoco river discharge, because of the positive (negative) correlations of Chl with SST within the warm (cool) waters of the river discharge (upwelling waters).

Seasonal differences were found in the spatial distribution of *Sardinella aurita* in relation with the upwelling cycle. During strong upwelling conditions, when cool waters with high phytoplankton biomass are extensively spread, *S. aurita* biomass was widely distributed over the continental shelf. Spanish sardine was broadly distributed in the study area with higher biomass in the northwest region. The causes of avoidance of cooler waters (SST < 22.5°C) with higher Chl immediately next to the upwelling foci are still unclear. During the season of weakest upwelling (September-October), Spanish sardine biomass was concentrated close to the mainland and islands and tended to be in the first 30 km from the upwelling foci and higher in the first 10 km. The range of temperature was 25.7-29.1°C and highest biomass was found below 27.7°C. There was a very strong evasion of the northeast area that coincides with the seasonal extension of the Orinoco plume front. During this season there was some level of upwelling with cooler waters and higher Chl very close to the coast. Spanish sardine densities were larger at the higher Chl concentrations available (1-3 mg m^{-3}) located within the first 10 km of the upwelling foci. During this season, two mechanisms influence the spatial distribution of Spanish sardine: (a) localized cells of upwelling very close to the coast induce Spanish

sardine concentration closer to shore, increasing availability and likely increasing its catchability for the artisanal fishery that operates up to 10 km offshore; and (b) the seasonal high discharge of the Orinoco River causes horizontal migration of the stock toward higher salinity waters west of the haline front. Because the disconnection between Spanish sardine biomasses and the number/size of schools, more studies are necessary to find if the higher coastal concentration of Spanish sardine during lowest upwelling is really translated into higher catchability.

All surveys registered higher numbers of small pelagic schools in the cooler waters close to the coast, a schooling behavior that seems mainly related to feeding purposes. This coastal schooling behavior increases catchability of the stock to the artisanal fishery along the entire year, regardless of the total stock biomass.

Regarding the correlations of Spanish sardine biomass with the different variables, the percentage of deviance explained for the three upwelling periods was always higher with location (Lon, Lat). This suggests that there is a strong geographic control on population dynamics attributable to other factors (beside upwelling and chlorophyll) such as bathymetry, seabed, salinity, and circulation.

We hypothesize that during 2004 *S. aurita* was intensively fished in northeastern Venezuela owing to high market demand and increased catchability. In addition, the extremely warm and irregular 2005 upwelling exerted added pressure on the population, and the increased catchability facilitated the overfishing of the environmentally stressed stock. Following years with weak upwelling hindered the recovery of the stock.

3.7 Recommendations

It is important to include spatially-explicit indices of upwelling, such as synoptic and frequent SST maps from satellite imagery, in fishery management strategies that require prediction of habitat of *Sardinella aurita*. Analysis of acoustic surveys jointly with oceanographic satellite products would helps to understand the distribution of Spanish sardine. Satellite chlorophyll-*a* maps would improve our understanding of the spatial distribution of Spanish sardine related to seasonal food availability and freshwater input. Small pelagic fish catches seem to have stronger correlations with Chl than with SST (Lanz *et al.* 2009).

As for 2011, there has only been one acoustic survey since the last VECEP survey in 1998. Routinely acoustic surveys along all the upwelling cycle are essential to understand *S. aurita* variations in biomass and spatial distribution and their relations with interannual upwelling variations.

Because of *S. aurita* coastal schooling preference and their fishery occurring up to 10 km offshore, detailed catch/landing records are essential to understand the spatial and temporal variability of the number and size of *S. aurita* schools. The knowledge on the factors affecting the variability of the schools (related directly with catchability) and of the stock biomass and distribution would allow a reliable stock assessment and management.

3.8 Acknowledgements

Astor and Juán José Cárdenas (from the same institution) for discussions concerning that

data set. We warmly thank José Alió and Ramón Guzmán, from INIA (Instituto Nacional

de Investigaciones Agrícolas, Venezuela) for providing fishery data and also very

instructive conversations about the fisheries in Venezuela. The passion and hard work of,

Xiomara Gutierrez (from INSOPESCA, Instituto Socialista de Pesca y Acuicultura) was

an inspiration for this work. We are in debt with her for her efforts in providing detailed

data of Spanish sardine landing. We are also grateful to Luis Gerardo González and

Massimo Ortisi for information from the cannery industry perspective. This research was

carried out under the CARIACO Time-Series program, funded by: the National Science

Foundation (NSF, USA, Grants OCE- 0752139, OCE-9216626, OCE-9729284, OCE-

9401537, OCE-9729697, OCE-9415790, OCE-9711318, OCE-0326268 and OCE

0963028), the National Aeronautics and Space Administration (NASA, USA, Grants

NAG5-6448 and NAS5-97128), the Consejo Nacional de Investigaciones Cientificas y

Tecnológicas (CONICIT, VENEZUELA, Grant 96280221) and the Fondo Nacional de

Investigaciones Científicas y Tecnológicas (FONACIT, Venezuela, Grant 2000001703).

3.9 References

Aparicio-Castro R (2003) Review of the oceanographic characteristics on the continental shelf of northeastern Venezuela [*Revisión de las características oceanográficas de la plataforma nororiental de Venezuela*]. Pp. 171-200 *In*: Frèon P and Mendoza J (eds.) The sardine (*Sardinella aurita*), its environment and exploitation in Eastern Venezuela. IRD (Colloques et Séminaires), Paris.

Astor Y, Muller-Karger F, Scranton MI (2003) Seasonal and interannual variation in the hydrography of the Cariaco Basin: implications for basin ventilation. *Cont. Shelf Res.,* 23, 125-144.

Agenbag JJ, Richardson AJ, Demarcq H, Fréon P, Weeks S, Shillington FA (2003) Estimating environmental preferences of South African pelagic fish species using catch size- and remote sensing data. *Progr. Oceanogr.,* 59: 275–300

Bakun A (1996) Patterns in the Ocean: Ocean Processes and Marine Population Dynamics. University of California Sea Grant, San Diego, California, USA, in cooperation with Centro de Investigaciones Biologicas de Noroeste, La Paz, Baja California Sur, Mexico. 323 pp.

Barange M, Coetzee JC and Twatwa NM (2005) Strategies of space occupation in anchovy and sardine in the southern Benguela: the role of stock size and intra-species competition. *ICES J. Marine Science,* 62: 645-654.

Barange M and Hampton I (1997) Spatial structure of co-occurring anchovy and sardine populations from acoustic data: implications for survey design. *Fish. Oceanogr.,* 6: 94-108.

Bertrand A, Segura M, Gutiérrez M, and Vásquez L (2004) From small-scale habitat loopholes to decadal cycles: a habitat-based hypothesis explaining fluctuation in pelagic fish populations off Peru. *Fish and Fisheries,* 5:296-316

Binet D (1982) Climatic changes related to the *Sardinella aurita* fishery of the Ivory Coast and Ghana: A drought-overfishing relationship. *Oceanol. Acta,* 5(4): 443-452.

Brown OB, Brown JW, Evans RH (1985) Calibration of advanced very high resolution radiometer infrared observations. *J. Geophys. Res.,* 90:11667-11678.

Brown,AM, Bellido JM, Valavanis VD and Giráldez A (2006) Investigating the distribution of small pelagic fish in Spanish Mediterranean waters using environmental modeling and essential fish habitat mapping. ICES CM 2006/O:13. ICES ASC Sept 2005, Maastrich (Netherlands)

Cárdenas J (2003) Distribution and quantification of fish biomass on the continental shelf of Eastern Venezuela, with special emphasis on sardine, as observed using hydroacustic methods. [*Distribución y cuantificación de la biomasa íctica del mar nororiental venezolano, con énfasis especial en la sardina, determinadas por medios hidroacústicos*]. Pp. 401-423 *In*: Frèon P and Mendoza J (eds.) The sardine (*Sardinella aurita*), its environment and exploitation in Eastern Venezuela. IRD (Colloques et Séminaires), Paris.

Cárdenas J, and Achury A (2000) Acústica pesquera sobre los recursos marinos del nororiente de Venezuela: evaluación y seguimiento espacio-temporal del stock de sardina, *Sardinella aurita. Mem. Fundac. La Salle Cien. Nat.,* 154:39-54.

Carder KL, Chen FR, Lee ZP, Hawes SK, Kamykowski D (1999) Semianalytic Moderate Resolution Imaging Spectrometer algorithms for chlorophyll a and absorption with bio-optical domains based on nitrate-depletion temperatures. *J. Geophys. Res.*, 104(C3): 5403- 5421.

Castillo J, Barbieri MA, Espejo M, and Catasti V (2000) Evaluación acústica del reclutamiento de anchoveta y sardina común en la zona centro-sur de Chile. Fondo de Investigación Pesquera, Informe Final Proyecto FIP 99-13: 138 pp.

Cellamare M, and Gómez-Gaspar A (2007) Alimentación de la sardina *Sardinella aurita* (clupeidae) en el sureste de la isla de Margarita, Venezuela. *Bol. Inst. Oceanogr. Venezuela, Univ. Oriente,,* 46 (1): 23-36.

Cervigón F (1991) Los peces marinos de Venezuela.Vol. 1. Fundación Científica Los Roques. Caracas, Venezuela.

Cole J, and McGlade J (1998) Clupeoid population variability, the environment and satellite imagery in coastal upwelling systems. *Rev. Fish Biol. Fish.,* 8:445-471

Cury P, and Roy C (1989) Optimal environmental window and pelagic fish recruitment success in upwelling areas. *Canadian J. Fish. Aquat. Sci.*, 46(4): 670-680.

Cutter GR, Demer DA (2008) California current ecosystem survey 2006. Acoustic cruise reports for NOAA FSV Oscar Dyson and NOAA FRV David Starr Jordan. OAA Technical Memorandum NMFS-SWFSC-415, 98pp.

Demer DA, Zwolinski JP, Byers KA, Cutter GR, Renfree JS, Sessions TS, and Macewicz BJ (2012) Prediction and confirmation of seasonal migration of Pacific sardine (*Sardinops sagax*) in the California Current Ecosystem. *Fish. Bull.*, 110(1): 52-70.

El Nacional, 03/21/2009 Enlatadoras trabajan a media máquina porque no hay sardinas. http://www.guia.com.ve/noticias/?id=37593

FAO- FGIS - Fisheries Global Information System. http://www.fao.org/fishery/figis/en

Fréon P, Cury P, Shannon L, Roy C (2005) Sustainable exploitation of small pelagic fish stocks challenged by environmental and ecosystem changes: A review. *Bull. Mar. Sci.*, 76 (2), 385-462.

Fréon P, El Khattabi M, Mendoza J, Guzman R (1997) Unexpected reproductive strategy of *Sardinella aurita* off the coast of Venezuela. *Mar. Biol.,* 128, 363–372.

Fréon P, Guzmán R and Aparicio R (2003) Relationships between catch, fishing effort and coastal upwelling indices in the sardine fishery of Eastern Venezuela. [*Relaciones entre capturas, esfuerzo pesquero y surgencia costera en la pesquería de sardina del Oriente de Venezuela*]. Pp. 451-471 *In*: Fréon P and

Mendoza J (eds.) The sardine (*Sardinella aurita*), its environment and exploitation in Eastern Venezuela. IRD (Colloques et Séminaires), Paris.

Fréon P, and Mendoza J (Eds) (2003) The sardine (*Sardinella aurita*), its environment and exploitation in eastern Venezuela [*La sardina (Sardinella aurita), su medio ambiente y explotación en el oriente de Venezuela*]. Freón and Mendoza (scientific editors). Colloques et Séminaires. 549 p.

Fréon P, Soria M, Mullon C, and Gerlotto F (1993) Diurnal variation in fish density estimate during acoustic surveys in relation to spatial distribution and avoidance reaction. *Aquat. Living Resour.,* 6: 221-234.

Gómez A, Vicent P, Pérez J, and González LW (2006). Captura de sardina *Sardinella aurita* en Nueva Esparta (Venezuela) durante 2003. pp. 16-21. En S. Salas, M.A. Cabrera, J. Ramos, D. Flores y J. Sánchez. (eds). Memorias Primera Conferencia de Pesquerías Costeras en América Latina y el Caribe. Evaluando, Manejando y Balanceando Acciones. Mérida, Yucatán, 4-8 Octubre, 2004.

González LW, Salas S. and Eslava N (2005). Caracterización socio-económica de la pesquería artesanal de la sardina (*Sardinella aurita*) en el sureste de la Isla de Margarita, Venezuela. *Bol. Centro Invest. Biol*.: 39(3) 197 – 216

Gu H, Kenney T, and Zhu M (2010): Partial Generalized Additive Models: An Information-Theoretic Approach for Dealing With Concurvity and Selecting Variables. *J. Comput. Graph. Stat.*, 19:3, 531-551

Guisan A, Edwards Jr. TC, and Hastie T (2002) Generalized linear and generalized additive models in studies of species distributions: Setting the scene. *Ecol. Modell.*, 157, 89-100.

Gutierrez M, Swartzman G, Bertrand A, and Bertrand S (2007) Anchovy and sardine spatial dynamics and aggregation patterns in the Humboldt Current ecosystem, Peru, from 1983-2003. *Fish. Oceanogr.*, 16: 155-168.

Guzmán R, Freón P, and Mendoza J (2003) Spatial and temporal variability of the sardine fishery in Eastern Venezuela from 1959 to 1989. [*La Pesquería de sardina en el Oriente de Venezuela, su variabilidad espacio-temporal: Periodo 1959-1989*]. Pp. 427-450 *In*: Fréon P and Mendoza J (eds.) The sardine (*Sardinella aurita*), its environment and exploitation in Eastern Venezuela. IRD (Colloques et Séminaires), Paris.

Hastie TJ and Tibshirani RJ (1990) Generalized Additive Models. New York: Chapman and Hall.

Herrera LE and Febres-Ortega G (1975) Kinematics of the wind-generated velocity field in the surface waters off eastern Venezuela, Caribbean Sea. *Bol. Inst. Oceanogr. Venezuela, Univ. Oriente*, 14(2): 165-186.

Hu C, Muller-Karger F, Murch B, Myhre D, Taylor J, Luerssen R, Moses C, Zhang C, Gramer L, and Hendee J (2009) Building an Automated Integrated Observing System to Detect Sea Surface Temperature Anomaly Events in the Florida Keys. *IEEE Trans. Geosc. Remote Sens.,* 47(6):1607–1620.

Huq MF (2003) Review of the fishery biology of sardine (*Sardinella aurita* Valenciennes, 1847) in Eastern Venezuela [*Estado del conocimiento biológico pesquero de la sardina, (Sardinella aurita Valenciennes 1847) en el oriente de Venezuela*]. Pp. 331-356 *In*: Fréon P and Mendoza J (eds.) The sardine (*Sardinella aurita*), its environment and exploitation in Eastern Venezuela. IRD (Colloques et Séminaires), Paris.

INAPESCA (2001). Gaceta Oficial 37323, decreto No. 1524, artículo 21. Ley de Pesca y Acuicultura. *Official J. No. 37323, dated 11/13/2001. Law on Fisheries and Aquaculture.*

INSOPESCA (2012). Producción pesquera de Venezuela durante el período 1996-2011. Instituto Socialista de la Pesca y la Acuicultura, Ministerio de Agricultura y Tierras, Caracas.

Jablonski S, and Legey LFL (2004) Quantifying environmental effects on the recruitment of Brazilian sardine (*Sardinella brasiliensis*), 1977-1993. *Sci. Mar.*, 68: 385-398.

Lanz E, Nevárez-Martínez, López-Martínez J, and Dworak JA (2009) Small pelagic fish catches in the Gulf of California associated with sea surface temperature and chlorophyll. *Calif. Coop. Oceanic Fish. Invest. Rep.*, 50:134–146.

Lasker R (1975) Field criteria for survival of anchovy larvae: the relation between inshore chlorophyll maximum layers and successful first feeding. *Fish. Bull.*, 73: 453-462.

Longhurst AR (1971) The clupeoid resources of tropical seas. *Oceanogr. Mar. Biol. Ann. Rev.*, 9: 349-385

López H (1972) Distribución y abundancia estimada de huevos de la sardina *Sardinella anchovia* en la región Oriental de Venezuela,1968-1969. Proy. Invest. Des. Pesq. MACPNUD-FAO. *Ministerio de Agric. y Cría,Venezuela. Inf. Téc.*, 46: 1-27.

Mais KF (1974) Pelagic fish surveys in the California Current. State of California, Resources Agency, Dept. of Fish and Game, Sacramento.

Maravelias CD (1999) Habitat selection and clustering of a pelagic fish: effects of topography and bathymetry on species dynamics. *Canad. J. Fish. and Aquatic Sci.,* 56(3): 437-450.

Minnett PJ (1991) Consequences of sea surface temperature variability on the validation and applications of satellite measurements. *J. Geophys. Res.* 96(C10):18475-18489.

Muller-Karger, F. E., C. R. McClain, T. R. Fisher, W. E. Esaias, and R. Varela. 1989. Pigment distribution in the Caribbean Sea: Observations from Space. *Progr. Oceanogr..* 23: 23-69.

Muller-Karger and Aparicio-Castro (1994). Mesoscale processes affecting Phytoplankton abundance in the southern Caribbean Sea. *Cont. Shelf Res*., 14(2/3): 199-221

Murase H, Nagashima H, Yonezaki S, Matsukura R, and Kitakado T (2009) Application of a generalized additive model (GAM) to reveal relationships between environmental factors and distributions of pelagic fish and krill: a case study in Sendai Bay, Japan. *ICES J. Mar. Sci.*, 66: 1417–1424.

Ñiquen M, and Bouchon M (2004) Impact of El Niño events on pelagic fisheries in Peruvian waters. *Deep-Sea Res., II*, 51: 563-574.

O'Reilly JE, Maritorena S, Siegel D, O'Brien MC, Toole D, Mitchell BG, Kahru M, Chavez FP, Strutton P, Cota G, Hooker SB, McClain CR, Carder KL, Muller-Karger F, Harding L, Magnuson A, Phinney D, Moore GF, Aiken J, Arrigo KR, Letelier R, and Culver M (2000) Ocean color chlorophyll a algorithms for SeaWiFS, OC2, and OC4: Version 4. Pp: 9-23 *In*: Hooker SB and Firestone ER (eds.) SeaWiFS Postlaunch Technical Report Series, Volume 11, SeaWiFS Postlaunch Calibration and Validation Analyses, Part 3. NASA, Goddard Space Flight Center, Greenbelt, Maryland.

Overland JE, Alheit J, Bakun A, Hurrell JW, Mackas DL, and Miller AJ (2010) Climate controls on marine ecosystems and fish populations. *J. Mar. Syst*., 79(3-4): 305-315.

Peng RD, Dominici F, Louis TA (2006). Model choice in time series studies of air pollution and mortality. *J. Royal Statist. Soc., series A*, 169(2): 179–203.

Peltonen H, Luoto M, Pääkkönen JP, Karjalainen M. Tuomaala A, Pönni J and Viitasalo M (2007) Pelagic fish abundance in relation to regional environmental variation in the Gulf of Finland, northern Baltic Sea. *ICES J. Mar. Sci.*, 64: 487–495.

R Development Core Team (2011). R: A language and environment for statistical computing. R Foundation for Statistical Computing, Vienna, Austria. ISBN 3-900051-07-0, URL http://www.R-project.org/.`

Ramírez I, Huq MF (1986) Aspectos reproductivos de la sardina, *Sardinella aurita* Valeciennes, 1847 (Pisces: Clupeidae) del Golfo de Cariaco, estado Sucre, Venezuela. *Bol. Inst. Oceanogr. Venezuela. Univ. Oriente*, 25 (1-2): 3-20.

Richards FA (1960). Some chemical and hydrographic observations along the north coast of South America. I. Cabo Tres Puntas to Curacao including the Cariaco Trench and the Gulf of Cariaco. *Deep-Sea Res.*, 7(3): 163-182

Rueda-Roa D (2001) Variabilidad temporal de la distribución vertical de la biomasa fitoplanctónica en la Cuenca de Cariaco y sus relaciones con los aspectos hidrográficos del estrato superficial (1996-1998). Master Thesis, Programa de Ciencias Marinas, Univ. de Oriente, Venezuela. 190 pp.

Rueda-Roa D, Ezer T, Muller-Karger F (in preparation) Contribution of Ekman transport and pumping on the mid-year Southern Caribbean upwelling and on phytoplankton biomass. (First chapter on this dissertation).

Rueda-Roa and Muller-Karger (in preparation) Southern Caribbean Upwelling System: characterization of sea surface temperature, Ekman forcing and chlorophyll concentration. (Second chapter on this dissertation).

Schismenou E, Giannoulaki M, Valavanis VD, Somarakis S (2008). Modelling and predicting potential spawning habitat of anchovy (*Engraulis encrasicolus*) and round sardinella (*Sardinella aurita*) based on satellite environmental information. *Hydrobiologia,* 612: 201-214

Simmonds EJ, Williamson N, Gerlotto F and Aglen A (1992) Acoustic survey design and analysis procedure: a comprehensive review of current practice. *Rapp. Rech. Collectives Cons. Int. Explor. Mer*, 187: 131 p.

Strong AE, McClain E (1984) Improved ocean surface temperatures from space-comparisons with drifting buoys. *Bull. Am. Meteorol. Soc.*, 85, 138.

Stromme T, Saetersdal G (1989) Surveys of the fish resources in the shelf areas between Suriname and Colombia 1988. Reports on surveys with RV 'Dr. F. Nansen', Vol 1 Institute of Marine Research, Bergen.

Thomas RM and Boyd AJ (1985) Trends in the Namibian pilchard *Sardinops ocellata* fishery in 1984. *Colln Scient. Pap. Int. Commn SE Atl. Fish*. 12: 181-191.

Tsikliras AC, Antonopoulou E (2006) *Reproductive biology of round sardinella (Sardinella aurita) in the north-eastern Mediterranean. Scientia Marina*, 70: 281-290

Tsikliras AC, Torre M, Stergiou KI (2005) Feeding habits and trophic level of round sardinella (*Sardinella aurita*) in the northeastern Mediterranean (Aegean Sea, Greece). *J. Biolog. Res.*, 3: 67-75.

Varela R., Carvajal F., Muller-Karger F (2003). The phytoplankton of the continental shelf of northeastern Venezuela [*El fitoplancton en la plataforma nororiental de Venezuela*]. Pp. 263-294 *In*: Frèon P and Mendoza J (eds.) The sardine (*Sardinella aurita*), its environment and exploitation in Eastern Venezuela. IRD (Colloques et Séminaires), Paris.

Walton CC (1988) Nonlinear Multichannel Algorithms for Estimating Sea Surface Temperature with AVHRR Satellite Data. *J. Appl. Met.*, 27(2): 115-124

Wood SN (2006) Generalized Additive Models: an introduction with R. Chapman & Hall/CRC.

Wood SN (2012) The mgcv Package. Online documentation of R. http://cran.r-project.org/web/packages/mgcv/mgcv.pdf

Zwolinski, J. P., Emmett, R. L., and Demer, D. A. 2011. Predicting habitat to optimize sampling of Pacific sardine (*Sardinops sagax*). *ICES J. Mar. Sci.*, 68: 867–879.

CHAPTER FOUR

Conclusions

4.1 Overview of the motivations and Objectives:

The southern Caribbean upwelling system experiences a strong upwelling process along the coast (from about 61°W to 75.5°W, 10-13°N). This process had been characterized historically as following a simple seasonal cycle, with strong upwelling occurring between about December and April every year caused by the seasonal intensification of the alongshore Trade Winds (Richards 1960, Herrera and Febres-Ortega 1975, Muller-Karger and Aparicio 1994, Muller-Karger *et al.* 2004). The aim of this research was to study the dynamics and forcing of this upwelling and how it affects the seasonal cycle of phytoplankton biomass and the spatial distribution of the Spanish sardine (*Sardinella aurita*). This research used synoptic satellite-derived products of sea surface temperature (SST, as a proxy for upwelling), chlorophyll-*a* (Chl, as a proxy for phytoplankton biomass), and satellite wind products (to calculate upwelling due to wind forcing).

4.1.1 Mid-year upwelling:

Data from the CARIACO Oceanographic Time Series (1996-1998) located off northeastern Venezuela (10.50ºN, 64.66ºW) documents a mid-year upwelling between

June-August, at a time of the year when land-based meteorological stations typically show a decrease in wind speed (Rueda 2000, Astor *et al.* 2003). This phenomenon was acknowledged in some historical oceanography reports as an anomaly and not a regular and periodic feature of the upwelling cycle. The objectives of this study were to (a) establish whether the mid-year upwelling is part of the seasonal upwelling cycle of the southern Caribbean Sea; (b) characterize the mid-year upwelling effect on phytoplankton biomass; and (c) assess the relative contribution of along-shore winds and wind curl in forcing the upwelling process.

4.1.2 Upwelling dynamics along the southern Caribbean Sea

The study focuses on the zonal variations observed in the upwelling system of the southern Caribbean Sea. The strongest upwelling occurs in two separate areas: the eastern and western upwelling areas at 63-65°W and 70-73°W, respectively at a latitude of roughly 10-13°N. Both areas have very important fishery resources; however, fish biomass is more abundant in the eastern upwelling area than in the western area (78% and 18%, respectively, of the total small pelagic biomass from the southern Caribbean upwelling system, Stromme and Saetersdal 1989).

4.1.3 Influence of the upwelling cycle on the Spanish sardine:

One of the most important fisheries in the eastern upwelling area is the Spanish sardine (*Sardinella aurita*), with around 95% the catches of the whole Caribbean Sea region. Following two consecutive years of weak upwelling (2004-2005) the Venezuelan Spanish sardine fishery crashed and hasn't recovered to previous yields. The fast

response of small pelagics populations to environment changes, such as upwelling, led to the objective of help to understand the response of *S. aurita* distribution to changes in upwelling in the southeastern Caribbean Sea. This information is needed for competent fishery management.

4.2 Main Conclusions and implications?

4.2.1 Mid-year upwelling:

The analysis of historical data from northeastern Venezuela dating back to 1948 (section 1.4.1) established that the mid-year upwelling is not an anomaly but a normal feature of the upwelling cycle in this area. Fourteen years of synoptic satellite SST over the Caribbean Sea provided evidence that the mid-year upwelling is part of the annual upwelling cycle along the entire southern margin of the Caribbean Sea from 61°W to 75.5°W.

The mid-year upwelling is a short-lived event (~5 weeks) and not as cold as the principal upwelling event (~1.5°C warmer). However, in combination with the principal upwelling, this phenomenon result in the presence of cool waters (< 26°C) in the euphotic zone of the region for an extended period of time (~8 months). The mid-year upwelling stimulates phytoplankton growth, as documented in section 1.4.4. Together the principal and the mid-year upwelling events enhance phytoplankton biomass for up to 8-9.5 months (i.e. Chl averaged up to 100 km offshore averaged ≥ 0.35 mg m^{-3} for this period).

During the middle of the year, winds measured on land along the coast are starting a decline. However, satellite estimates of wind speeds ~25km offshore revealed high wind intensities during this period (section 1.4.3). June-July alongshore winds

produce high offshore Ekman Transport (ET) that lead to the mid-year upwelling (averages of 2.4 and 3.8 m^3 s^{-1} per meter for the east and west upwelling areas, respectively). The satellite wind data set shows that the mid-year coastal upwelling is driven mostly (~90%) by offshore ET due to alongshore winds. However, as a result of (a) the inherent coastal gap of satellite wind products (~25km, Hoffman and Leidner 2005), and (b) to the significant drop-off in coastal wind speed closer to shore (Capet *et al.* 2004), the direct contribution of coastal Ekman Pumping (EP) due to wind-curl could be significantly higher.

In the open-sea EP upwelling seems to enhance the mid-year upwelling by the shoaling of isopycnals on the waters feeding the coastal upwelling. During June there is an intensification of positive EP (open-sea upwelling) along a band from the southern Caribbean Sea coast throughout the tropical North Atlantic Ocean (section 1.4.2). This open-sea upwelling is evidenced by the good correlation between the annual cycles of EP (integrated up to 100 km offshore, EP100km) and of the depth of the 22°C isotherm along the southern Caribbean Sea. The relevance of EP on the upwelling cycle along the southern Caribbean Sea is supported by the higher correlations between the time series of Chl_100km and of SST with EP100km, compared with ET.

4.2.2 Upwelling dynamics along the southern Caribbean Sea:

The southern Caribbean upwelling system features 21 upwelling foci with a strong semiannual SST cycle: it has a principal upwelling season between December and April, a mid-year upwelling during June-August and the weakest upwelling during September-October. Foci adjacent to each other tend to have coherent upwelling cycles.

143

Seven groups of contiguous foci can be identified with different characteristics in their seasonal SST cycle. Two of those clusters encompass the largest number of foci in extensive sections of coast: the eastern upwelling area (between 63-65°W) and the western upwelling area (between 70-73°W). Those two areas experience the strongest SST decrease of the southern Caribbean upwelling system. Both host very important fish biomasses.

Nearshore satellite winds are upwelling favorable all year-round along the southern Caribbean upwelling system. There are three coastal areas with distinctive wind regimes: moderate wind speed east of 68°W (annual mean 6.3 m s^{-1}); stronger winds between 69-74°W all year round (annual mean 8.3 m s^{-1}); and, strongest wind speed and highest seasonal range occurs between 74-76°W (annual mean 8.7 m s^{-1}). Although the western upwelling area has the strongest winds, the upwelling process is less efficient compared to the eastern area as a result of the lower proportion of winds aligned alongshore (85 and 94%, for the western and eastern areas, respectively) and because the western area is located at a slightly higher latitude/coriolis parameter which causes ~10% less transference from wind stress to upwelling (see Table 2.2 in chapter 2). Nevertheless, offshore ET in the western upwelling area is ~1.5 higher than in the eastern area (annual means of 3 and 2 m^2 s^{-1}, respectively). Those three sub-regions also had differences in the seasonal variability of the core depth of Subtropical Underwater (using the 22°C isotherm as a proxy). Subtropical Underwater reaches the shallowest depths east of 68°W (85 m), it is deepest between 68-74°W (115 m), and has intermediate depths between 74-76°W (109 m). Coastal SST was better explained by a multiple parameter regression including nearshore wind speed and the depth of the 22°C isotherm, than with wind alone (Figure

2.9). The multiple parameter correlation improvement was especially marked for the western upwelling area, where the deeper position of the Subtropical Underwater core (~30 m deeper than in the eastern area) produced higher sensitivity of the SST to the 22°C isotherm depth.

Chl cycles are inversely related and coherent with SST cycles in both the eastern and the western upwelling areas, indicating that the increase in phytoplankton biomass is driven by upwelling. An exception of this is the mid-year Chl peak in the western upwelling area, which is disproportionately high compared to the SST during mid-year upwelling. The mid-year Chl peak is concurrent with the seasonal maximum in the wind in the western upwelling area in June-July (> 9 m s^{-1}). This midyear Chl maximum is enhanced by high wind stress turbulence which leads to additional entrainment of nutrients from the thermocline.

Upwelled waters in the eastern upwelling area feature higher phytoplankton biomass than in the western area. For example, using the correlation equations between coastal Chl and SST for each area (weekly time series 1998-2009, section 2.4.2), at SST=22°C Chl is about 4.0 and 2.4 mg m^{-3} for the eastern and western upwelling areas, respectively. A possible reason could be related to the wider continental shelf in the eastern upwelling area (~90km) compared to the western area (10-40km). The higher Chl in the eastern area could be attributable to the blooming of resuspended cells from the sediment (Muller-Karger and Aparicio 1994)

The eastern upwelling area featured the lowest SST (annual mean 25.2°C) and the highest Chl (annual mean 1.7 mg m^{-3}), moderate winds (annual mean 6.1 m s^{-1}), and shallower offshore isotherms (22°C isotherm annual mean at 85m depth). The western

145

upwelling area has stronger winds (annual mean 8.2 m s^{-1}) but deeper offshore isotherms (22°C isotherm annual mean at 115 m depth), which lead to upwelling SST similar or higher than in the eastern area (annual mean 25.5°C), and lower Chlorophyll concentrations (annual mean 1.1 mg m^{-3}).

The upwelling dynamics of the eastern upwelling area seems to fit the "optimal environmental window" for fish recruitment, which explains its higher fish biomasses. Possibly, the most important factors that quench fish biomass in the western area are the high degree of turbulence and strong offshore transport. This produces strong dispersion of plankton and larvae, which in turn would affect larvae feeding and mortality and export of nutrients, plankton and larvae from the coastal upwelling system.

4.2.3 Influence of the upwelling cycle on the Spanish sardine:

To understand the response of *Sardinella aurita* to changes in upwelling in the southeastern Caribbean Sea, capture statistics were examined. Capture data were provided by the fish cannery industry to the Venezuelan government agency INSOPESCA, which is responsible for the sustainable management of regional fishing resources. This information included the total weight of Spanish sardine bought, name of the provider, and place and date of the capture. These data in principle have adequate spatial and temporal resolution needed for the analysis. Much effort and time was devoted with INSOPESCA to the transcription of this information into digital media files. However, an important number of missing forms prevented a systematic study of fisheries patterns using these data. To avoid additional loss of information INSOPESCA is now digitizing the data as soon they obtain it.

Next we tried to determine whether the spatial patterns of Spanish sardine distribution was related to the upwelling annual cycle using historical acoustic biomass surveys. Fishing activities for *S. aurita* take place within ~10 km of the shore as this is a legally-protected artisanal fishery (Freón and Mendoza 2003, González *et al.* 2005). A goal was to clarify whether Spanish sardine catchability is influenced by the upwelling cycle. The data set used was the series of VECEP hydroacoustics surveys (8 surveys) that estimated stock abundance and distribution of *S. aurita* off northeastern Venezuela between 1995 and 1998. These surveys had previously been analyzed using *in situ* oceanographic data (Cárdenas and Achury 2000). Here, we augmented these data using synoptic coverage of environmental parameters offered by satellite. A *Sardinella aurita* relative abundance index (sAsardine) and number of small pelagics schools (Schools) were compared with SST, SST gradients, Chl (only available for the last two surveys), location (longitude and latitude) and distance to upwelling foci, using histograms and Generalized Additive Models. Spatially-averaged SSTs for the surveys were similar to long-term SST averages previously published for the study area. Therefore, surveys were grouped into strongest (February-March), weakest (September-October) and transition (November-December) upwelling periods.

There were differences in the spatial distribution of *S. aurita* in relation with the upwelling cycle. During the strongest upwelling conditions, sAsardine was widely distributed in the cooler, Chl rich upwelling plumes that spread over the ~70 km continental shelf. The distribution pattern was similar for transition conditions. During the weakest upwelling conditions, sAsardine was more abundant near upwelling foci where higher Chl (1-3 mg m^{-3}) was observed within the first 10 km of the coast. During

147

these weak upwelling conditions, the sardines avoided distances farther than 30 km from the upwelling foci. The weakest upwelling season also presented high riverine discharge. Spanish sardine avoided the southeast-northwest front between clear Caribbean Sea waters and the turbid Orinoco River plume (assessed with ocean color satellite images). When *Sardinella aurita* is so concentrated near the coast during weak upwelling periods, their availability to fisheries is increased to the local artisanal fishery, likely increasing the catchability. Thermal gradients and fronts didn't seem to have an effect in defining sAsardine or the distribution of schools. In general, the parameter pair describing location (longitude, latitude) always showed the highest percentage of sAsardine deviance explained for the three upwelling periods; this suggests a strong geographic control on population dynamics caused by other factors, beside upwelling and chlorophyll (e.g. bathymetry, seabed, salinity, and circulation).

Without regard of the upwelling season, higher numbers of small pelagics schools were always found in the cooler waters closer to the shore all year round. The same behavior was observed in previous acoustic surveys (6 surveys made between 1985-1989, Cárdenas 2003). The enhanced coastal schooling is not related to the density of Spanish sardine close to the coast, and occurred even for surveys with low sAsardine densities close to the coast. Because the Spanish sardine fishing operations are based in the localization and catch of schools, this coastal schooling behavior increases catchability throughout the year, regardless of total stock biomass.

There is therefore a disconnect between Spanish sardine biomass and the number/size of schools in the region close to the coast, confirming earlier studies by Freón *et al.* (2003). More studies are necessary to verify whether higher availability of Spanish

sardine closer to the coast during low upwelling conditions is translated into higher catchability or not. Two historic peaks in the landings of Spanish sardine off northeastern Venezuela were concurrent with years of weak upwelling (1998 and 2004, Chapter 3, Figure 3.2); this supports the idea that Spanish sardine concentration closer to the coast during low upwelling conditions does increase catchability.

We therefore hypothesize that the 2005 collapse of *S. aurita* fishery off northeastern Venezuela was caused by a combination of sustained stressful environmental conditions (weak upwelling and warmer water temperatures from 2004 to 2010) and overfishing due to the increased catchability of the stock caused by aggregation of the fish in the cooler coastal upwelling cells.

4.2.4 Implications:

This research presented here shows that the mid-year upwelling pulse in the southern Caribbean Sea causes a longer upwelling season (i.e. from December to August) and, therefore, a more prolonged nutrient supply in the upwelling system than considered previously (December- May). This explains the prolonged period of high phytoplankton biomass (8 and 9.5 months, for the western and eastern upwelling areas, respectively; chapters 1 and 2). This knowledge helps to have a better understanding of the ecology of the organisms living within the upwelling system. For instance, off northeastern Venezuela the 'condition factor' of *Sardinella aurita* increases steadily from January and peaks in August (Freón *et al.* 1997). The traditional view that the upwelling season ends in May did not explain the higher 'condition factor' for sardines several months after the upwelling season.

The phenomenon of upwelling in the southern Caribbean Sea caused by offshore Ekman Transport produced by the seasonal intensification of the Trade Winds is well known. Our study finds that Ekman Pumping due to changes in the curl of the wind also plays an important role in the southern Caribbean upwelling cycle. The higher correlations between open-sea Ekman Pumping upwelling and both coastal SST and Chl, compared to Ekman Transport (Chapter 1, Table 1.1), emphasizes the importance of this mechanism. That could be associated with the effect of open-sea upwelling (due to Ekman Pumping integrated up to 100 km offshore) in the depth of the core of Subtropical Underwater; which is supported by the similarity and timing in their annual cycles (i.e. Figure 1.10).

It is intriguing that upwelled waters with the same SST signature show higher phytoplankton biomass in the eastern upwelling area than in the western area. The water source for the upwelling is the same for both areas, namely Subtropical Underwater. Understanding the ecological dynamics that leads to lower phytoplankton concentrations in the western area requires further studies.

Along the southern Caribbean upwelling system there are differences in the upwelling forcing mechanisms of upwelling (i.e. wind field and depth of the Subtropical Underwater core) and in topography (coastline, geographical features, width of the continental platform, etc.). They cause the presence of seven groups of contiguous upwelling foci with similar upwelling characteristics. Therefore, although it is possible to extrapolate processes within foci from the same group, higher discretion must be exerted in extrapolation between different groups of foci.

Schools of *Sardinella aurita* off northeastern Venezuela are present throughout the year closer to the coast. Therefore they are always accessible to the artisanal fishery regardless of total stock biomass. During periods of weak upwelling *S. aurita* tends to further concentrate closer to the coast around upwelling foci. Understanding these behaviors is of importance for the management of this stock. During prolonged periods of low upwelling, Spanish sardine populations can be stressed as a result of lower than normal amount of food. If these stressed populations are then heavily harvested by the fishery, as a result of their higher concentration closer to the coast, this can lead to overfishing. Synoptic satellite products of sea surface temperature and chlorophyll-*a* are of great use and low cost to monitor upwelling conditions. These tools are helpful in the decision making process about protective measures for the stock. For example, if the first half of the year had low upwelling conditions, it is advisable to take precautionary actions on the Spanish sardine fishery during the second part of the year. Further studies are needed to find out the threshold values of SST and Chl (during certain interval of time) that identify environmental stress in the Spanish sardine population. It is also necessary to formulate the best precautionary regulations for the fishery taking in account the biology of *S. aurita* and its behavior during the different phases of the upwelling cycle.

GENERAL REFERENCES

Astor Y, Muller-Karger F, Scranton MI (2003) Seasonal and interannual variation in the hydrography of the Cariaco Basin: implications for basin ventilation. *Cont. Shelf Res.*, 23, 125-144.

Cárdenas J (2003) Distribution and quantification of fish biomass on the continental shelf of Eastern Venezuela, with special emphasis on sardine, as observed using hydroacustic methods. [*Distribución y cuantificación de la biomasa íctica del mar nororiental venezolano, con énfasis especial en la sardina, determinadas por medios hidroacústicos*]. Pp. 401-423 *In*: Frèon P and Mendoza J (eds.) The sardine (*Sardinella aurita*), its environment and exploitation in Eastern Venezuela. IRD (Colloques et Séminaires), Paris.

Cárdenas J, and Achury A (2000) Acústica pesquera sobre los recursos marinos del nororiente de Venezuela: evaluación y seguimiento espacio-temporal del stock de sardina, *Sardinella aurita*. *Mem. Soc. Cien. Nat. La Salle*, 154:39-54.

Capet XJ, Marchesiello P, McWilliams JC (2004) Upwelling response to coastal wind profiles. *Geophys. Res. Lett.*, 31: L13311.

FAO- FGIS - Fisheries Global Information System. http://www.fao.org/fishery/figis/en

Fréon P, El Khattabi M, Mendoza J, Guzman R (1997) Unexpected reproductive strategy of *Sardinella aurita* off the coast of Venezuela. *Mar. Biol.*, 128, 363–372.

Fréon P, Guzmán R and Aparicio R (2003) Relationships between catch, fishing effort and coastal upwelling indices in the sardine fishery of Eastern Venezuela. [*Relaciones entre capturas, esfuerzo pesquero y surgencia costera en la pesquería de sardina del Oriente de Venezuela*]. Pp. 451-471 *In*: Fréon P and Mendoza J (eds.) The sardine (*Sardinella aurita*), its environment and exploitation in Eastern Venezuela. IRD (Colloques et Séminaires), Paris.

Fréon P, and Mendoza J (Eds) (2003) The sardine (*Sardinella aurita*), its environment and exploitation in eastern Venezuela [La sardina (*Sardinella aurita*), su medio ambiente y explotación en el oriente de Venezuela]. Colloques et Séminaires, Paris 549 p.

González LW, Salas S. and Eslava N (2005). Caracterización socio-económica de la pesquería artesanal de la sardina (*Sardinella aurita*) en el sureste de la Isla de Margarita, Venezuela. *Bol. Centro Invest. Biol.*: 39(3) 197 – 216

INAPESCA (2001) Gaceta Oficial 37323, decreto No. 1524, artículo 21. Ley de Pesca y Acuicultura. *Official J. No. 37323, dated 11/13/2001. Law on Fisheries and Aquaculture.*

Hoffman RN, Leidner SM (2005) An introduction to the near-real-time QuikSCAT data. *Weather and Forecasting*, 20: 476-493

Muller-Karger FE, Aparicio R (1994) Mesoscale Processes Affecting Phytoplankton Abundance in the Southern Caribbean Sea. *Cont. Shelf Res.*. 14(2-3): 199-221.

Muller-Karger FE, Varela R, Thunell R, Astor Y, Zhang H, Luerssen R, Hu C (2004) Processes of coastal upwelling and carbon flux in the Cariaco Basin. *Deep-Sea Res. II*, 51: 927–943

Richards F (1960) Some chemical and hydrographic observations along the north coast of South America, *Deep-Sea Res.*, 7: 163-182.

Rueda-Roa D (2001) Variabilidad temporal de la distribución vertical de la biomasa fitoplanctónica en la Cuenca de Cariaco y sus relaciones con los aspectos hidrográficos del estrato superficial (1996-1998). Master Thesis to obtain the title of M.Sc. in Marine Sciences, Univ. De Oriente, 190 pp.